Bioactive surfaces by atomic layer deposition

Julie Nitsche Kvalvik

Master's thesis in Materials Science and Nanotechnology

60 credits

Department of Physics

Faculty of Mathematics and Natural Sciences

UNIVERSITY OF OSLO

June 1st, 2015

2015

Bioactive surfaces by atomic layer deposition

Julie Nitsche Kvalvik

http://www.duo.uio.no/

The University Print Centre, University of Oslo

Acknowledgements

This work was performed at the Department of Chemistry, University of Oslo and the Laboratory for tissue culture, Oslo University Hospital, between August 2013 and May 2015.

First I would like to thank my main supervisor, Ola Nilsen. You are always enthusiastic and cheerful, and you make me feel that what I am doing is actually worth something. A big thank you goes to both of my co-supervisors also. Henrik Hovde Sønsteby, you are very patient when it comes to all my stupid and perhaps not so stupid questions. And Jon Roger Eidet, thank you for sharing all your knowledge about cells. Karina Barnholt Klepper, thanks a lot for all your time, tea and sharp analysis. A lot of people have helped me in various labs also and proof read, thank you to you too! Special thanks go to Leva Momtazi, Michael Norderhaug-Getz, John André Louison, Amund Ruud, Jon Einar Bratvold, Øystein Slagtern Fjellvåg, Sjur Reppe and Ketil Nagel Støren.

I have also been blessed to be surrounded by a lot of nice people during my time here at NAFUMA, especially in the thin film group. My current and previous office mates have all been awesome; either you have spent a shorter or a longer time here with me. I have enjoyed sharing office with you all! Special thanks go to Ingunn, Marte, Ingvild, Kristian and Aninna for always listening to me and making every day a bit brighter. You rock!

Finally, I would like to thank the people closest to me. Thank you to my parents, you have always believed in me, helped me and you are excellent baby-sitters. The same goes for my wonderful mother-in-law. The hugest thank you goes to the two people in the world I have the dearest; my husband and my daughter. As C.S. Lewis said *"affection is responsible for nine-tenths of whatever solid and durable happiness there is in our lives".* Thank you for making me happy, and Martin, thank you for being the world's most patient man. I love you.

I will end this with a Ricky Lake quote; *"motherhood is the greatest thing and the hardest thing".* It is way harder than finishing a master's thesis, but I think I managed to do pretty well on both.

Julie Nitsche Kvalvik

Oslo, June 1st 2015

Abstract

The overall goal of this work has been to make bioactive surfaces with atomic layer deposition (ALD). To do this, a new ALD system with titanium tetraisopropoxide (TTIP) and lysine as precursors was developed with emphasis on studying the effects of pulsing times and deposition temperatures. TTIP was chosen as titanium is regarded to be biocompatible and lysine was chosen as poly-L-lysine is a part of the extra-cellular matrix (ECM) and hence affects cell adhesion. The effect of a water pulse in the system has also been investigated. An imagined application for bioactive ALD coatings is on 3D cell growth scaffolds such as electrospun membranes, and coating of cellulose membranes was therefore also attempted. As the last part of this work, cell growth experiments were performed on various TTIP/lysine films and the proliferation of the cells was studied.

Quartz crystal microbalance (QCM) experiments at 225 ^{o}C proved that self-limiting growth was taking place for both the TTIP/lysine and TTIP/lysine/water systems. QCM experiments also found that 1s/1s/2s/1s/2s/3s were adequate pulsing and purging parameters for TTIP, lysine and water respectively. Using these parameters at 225 ^{o}C, a growth rate of 0.09 Å/cycle was obtained for the TTIP/lysine system and a growth rate of 0.53 Å/cycle was obtained for the TTIP/lysine/water system.

These films were further characterized with fourier transform infrared spectroscopy (FTIR) which showed that both systems indeed gave films with various organic functional groups, meaning that the films had an inorganic-organic hybrid character. Gracing incidence x-ray diffraction (GIXRD) revealed that both systems gave amorphous films, and atomic force microscopy (AFM) showed that they were smooth with a roughness, Rq, of about 0.3 nm.

Spectroscopic ellipsometry showed that the films were stable over time, apart from a slight decrease in refractive index over time for the TTIP/lysine system. Moreover, the films did not dissolve in either water or cell culture medium.

Retinal pigment epithelium (RPE) cells were seeded on the substrates. They proliferated equally well on the TTIP/lysine and TTIP/lysine/water coated substrates as on the reference glass plate. However, the cells seeded on titanium oxide films did not proliferate.

Abbreviations

ALD	Atomic layer deposition
AFM	Atomic force microscopy
ATR	Attenuated total reflection
BME	Basal medium Eagle's
BSA	Bovine serum albumin
BSC	Biological safety cabinet
BSE	Backscattered electrons
CVD	Chemical vapor deposition
DMEM	Dulbecco's modified Eagle's medium
ECM	Extra cellular matrix
EDTA	Ethylene-diamine-tetraacetic acid
FA	Focal adhesion
FBS	Fetal bovine serum
FTIR	Fourier transform infrared spectroscopy
GIXRD	Gracing incidence x-ray diffraction
GLP	Good laboratory practice
HA	Hydroxyapatite
HEPA	High efficiency particulate air (filter)
hOB	Human osteoblast
Hq	Hydroquinone
iPSCs	Induced pluripotent stem cells
MLD	Molecular layer deposition
MS	Mass spectroscopy
NAFUMA	Nanostructures and functional materials
NCHR	Non contact high resolution
NMR	Nuclear magnetic resonance
PEG	Poly-ethylene glycol
PEEK	Poly-ether-ether-ketone
PHBV8	Poly-hydroxybutyrate-co-hydroxyvalerate
Phl	Phloroglucinol

PI	Propidium iodine
PIPAAm	Poly(*N*-isopropylacrylamide)
PLA	Poly-D/L-lactic acid
PLGA	Polylactic-glycolic acid
PS	Penicillin/streptomycin
RGD	Arginine-glycine-aspartic acid
SAM	Self-assembly monolayer
SE	Secondary electrons
SEM	Scanning electron microscopy
SFM	Serum free media
TDMAT	Tetrakis-dimethyl-amido titanium
TEM	Transmission electron microscopy
TFEL	Thin film electroluminiscent (display)
TMA	Trimethyl aluminium
TTIP	Titanium tetraisopropoxide
UV	Ultraviolet
XRD	X-ray diffraction
XRR	X-ray reflectivity

Contents

1. Introduction

Ever since the time of the old Egyptians mankind has attempted to repair damages to our bodies by adding implants[1]. Although implants run the risk of being rejected by the body's immune system and can be the source of both allergies and inflammations, they are still in many cases the only possible treatment. A more sophisticated type of implant which could circumvent issues like organ rejection is the produces through by regenerative medicine. In regenerative medicine organs are grown in the lab and then implanted into the patient. This is opposed to synthetic implants, and organs from organ donors which are not made of the patient's own cells.

As good as regenerative medicine sounds; making it possible is a very difficult task. One of the major hurdles to overcome is to find a good surface for the cells to grow on in the lab. A suitable surface must first and foremost be bio-compatible and not harmful or toxic on any time scale. If achievable, it could even be bio-active, which means facilitating increased cell growth in comparison to inactive substrates. An additional criterion is substrate transparency, so the cells can be studied in a microscope. It would also be advantageous to achieve some kind of surface structure, making it easier for the cells to adhere to it.

This thesis seeks to find a new way of obtaining active surfaces for cell growth, utilizing Atomic Layer Deposition (ALD)-technology. This chapter will be used as an introduction to important techniques and prior work in the field, while placing this work into a broader picture. General history and prior art of ALD and cell growth for regenerative medicine will be summarized, and used to clearly define the scope of the research. The chapter will lastly define how these very diverse fields will be brought together and concretize what the work seeks to do.

1.1 Regenerative medicine

This subchapter will present a general overview of the historical scientific development leading to what we today call regenerative medicine, and also the state of the art for the research fields closest to this study.

1.1.1 History of regenerative medicine

In 1907, cells growing *in vitro* were first reported by Ross Harrison[2], an American biologist working at Yale University. *In vitro* is latin and means “in glass”, and that is exactly were Harrison grew his neural frog cells. This was the first time on record mankind was able to make cells proliferate *ex vivo*; outside the body. Looking at the factors that need to be controlled in order for cells to thrive, this achievement was truly extraordinary. First, the cells need to be stored at an appropriate temperature. Second and more difficult, the concentrations of oxygen and carbon dioxide in the atmosphere around the cells must be absolutely right. If they are not, the pH of the fluid surrounding the cells, hereby known as the culture medium, will be altered. The culture media is also difficult to design, as its task is to provide the cells with everything they need regarding nutrition. Harrison used what was already available from nature’s side; the lymph of the frog. As will be elaborated on later, this is not so far from what is being done today.

After Harrison grew the frog cells, the scientific community was eager to do the same with mammalian cells. Alexis Carrel, who would later receive the Nobel Prize in Medicine for his efforts, published a paper in 1910 were the goal was to explore a general way of growing mammalian cells in the laboratory[3]. The study concluded that growing mammalian cells in laboratory environments was possible, but it also showed that different kinds of cells proliferated to various extents. We now know that different cells have different requirements regarding the composition of the culture media and the substrate they grow on, so it is not surprising that the cells reacted differently when given the same treatment!

Harry Eagle revolutionized the way we look at culture media[4]. In 1955 he formulated the first cell culture medium where all the components were defined. It is known as Eagle’s medium or basal medium Eagle’s (BME) and is still used in cell culture labs worldwide. BME, or any other basal medium, is a balanced salt solution that contains all the energy sources, the essential amino acids and vitamins the cells need. Basal media also contains buffers to control the pH in addition to a pH indicator, normally phenol red.

What Eagle and his colleagues soon realized, was that even if the cells were provided with all components thought necessary, they still did not grow very well. An additional component from another living organism was required, what we today refer to as a *serum*. Serum is

taken from living animals, such as a frog in Harrison's case. It is therefore also difficult to quality check and reproduce. Serums can also be a source of contamination in the lab, as the donating animals may carry infections. Today, fetal bovine serum (FBS) is the most widely used serum. It contains many beneficial growth factors, as it is extracted from an embryo[5]. FBS is also a bi-product of the cattle industry, making it a sustainable route of obtaining high quality serum. The complete contents of the serums are not known and they are hence not fully reproducible. Great efforts have been made to make serum free media (SFM) to avoid the reproducibility issue, but a general SFM suitable for all kinds of cells has not yet been achieved. It is important to notice, however, that SFMs have been obtained for several specific cell types.

Even though it has been possible to grow human cells in the lab for the past 100 years, the first successful attempt to make artificial organs to be implanted was not made until the 1960s[6]. Then artificial skin was made in the lab and implanted into burn victims. Making two-dimensional skin is one thing, making three-dimensional organs is much more difficult. It is therefore not surprising that the greatest advancements in regenerative medicine have been made with urine bladders, a hollow organ. These achievements are the work of Anthony Atala at Wake Forest Institute for Regenerative Medicine, an urologist and one of the most prominent researcher within regenerative medicine today[7]. Atala claimed in his 2009 TED Talk Lesson that regenerative medicine can solve the problem with organ-donor queues[8], a problem that will only become larger as the population grows older.

However, there is still quite a long way to go for Atala's vision to become true. A major difficulty with growing organs that are not hollow, such as lungs, kidneys or hearts, is that these organs consist of several types of cells that all have to be in the right place and interact perfectly for the organ to function[9]. For example, the surfaces of the organs are usually composed of cells that should cover and protect the organ, in opposition to the interior of an organ, which will usually carry out the organ's main function. One way of creating a complex organ is to grow the organ with embryonic stem cells in a 3D scaffold[10]. The scaffold mimics the natural surrounding for the cells when the organ is made in the womb, which may make the cells differentiate into just the right organ with the various types of cells. As it is known that the surface of the scaffold affects the cell growth[11], and that the interfaces

between scaffolds or implants and biological tissue is where most of these attempts fail[12], efforts are now being made to functionalize the scaffolds with coatings.

1.1.2 Prior art of regenerative medicine

As regenerative medicine may overcome issues like inflammations, allergies and people dying while waiting for a new organ, major research efforts are put into the field. The field is truly transdisciplinary – including medicine, biology as well as chemistry, materials science and nanotechnology[11]. This subchapter will therefore elaborate on the state of the art of the research within regenerative medicine and cell growth with emphasis on surface chemistry of the scaffolds or implants, especially for the materials used in this work. The cell type used in this work will also be described.

There are two major ways one can alter a surface for cell growth – it can either be by changing the structure or the chemistry of the surface. The structure implies the topography, but surface chemistry concerns both charge, affinity for attaching water (hydrophobicity), how many and which functional groups are available and the homogeneity of the surface[11]. A common way to functionalize a surface is to simply dip the substrate in a solution containing components from the extra cellular matrix (ECM), which is what surrounds the cells in a tissue. Typically the substrate is dipped in the ECM-solution and then rinsed with water and left to dry. This method has for example been used to coat tantalum, a bio-compatible metal, with collagen[13], the most abundant component of the ECM[14]. It was shown that even though the coating of tantalum with collagen made the surface hydrophobic, cells did indeed proliferate on them. A similar method has been used to coat the polymer PEEK (poly-ether-ether ketone) which is normally biointert with fibronectin, another component in the ECM[15]. Poly-lysine, the polymer form of the essential amino acid lysine and a part of the ECM, is also a commonly used coating. Poly-lysine improves cell adhesion and it also affects cell differentiation[16] which is essential when it comes to usage within regenerative medicine. Today coverslips pre-coated with collagen, poly-L/D-lysine and fibronectin are available commercially[17]. Other examples of pre-coated coverslips include the ones with gelatin[17, 18], a collagen-derivative, laminin[19] which is a part of the ECM affecting cell differentiation and vitronectin[20], also an ECM component.

Besides coating the substrates with parts of the ECM, there are several signal molecules that cells prefer to attach to. For the cells they work as a sign saying “hello cell, this is a good spot for you to adhere to”. The most well-known of these is RGD, a peptide consisting of L-arginine, glycine, and L-aspartic acid[11, 21, 22]. There are also other components in the serum that function in a similar manner[11]. This effect can be utilized for example by coating bone implants made of polylactic-glycolic acid (PLGA) with RGD. This will enhance cell growth and integration of the natural bone in the graft, a process called osteointegration[21].

Coatings to promote osteointegration are probably the most common coatings used today. Osteointegration is important both when implants and grafts are used, and is also essential within the field of odontology. When it comes to osteointegration a material can be bio-active in two ways, either osteoconductive or osteoproductive[23]. Osteoconductive materials bind directly to the hard bone whereas osteoproductive materials induce cell growth around the implant[23].

Well-known osteoproductive materials are titanium and titanium alloys such as Ti-Al-V[11], as they increase the growth of bone forming cells. Naturally occurring titanium will have an oxide layer on the surface, which implies that it is actually the oxide layer and not the metal itself which is bio-active. One disadvantage with using titanium as medical implants is that the pure metal is thrombogenic[24], in other words that it may lead to blood clots. A way to circumvent this is to increase the thickness of the surface oxide layer[25], so that the blood and the pure metal are shielded from each other. Another option for a coating material which enhances the osteoproductive properties is titanium nitride, which may be sputtered onto the implant[26].

Hydroxyapatite (HA) is the major mineral part of the ECM in bone[27] and is consequently osteoconductive[23]. A search for “hydroxyapatite” + “cell” in the search engine oria.no generates more than 50.000 hits, indicating that major research has been done on the field and that the material is well studied. HA-powder is available commercially[28], and this powder is a good precursor for a variety of coating methods. The materials being subject to coating are often titanium alloys, as these are popular materials to make implants of[28]. The simplest way to coat with HA is still dip-coating, but many other methods have been

used. This includes plasma spray deposition[29], magnetron sputtering[30], sol-gel based methods[31], pulsed laser deposition[32] and electrophoretic deposition[33]. Furthermore organic self-assembly monolayers (SAMs) are used to coat titanium alloys with HA[34]. The SAM has then served as a template for HA, which is dip-coated on the already existing self-assembled layer. One advantage of utilizing SAMs for HA-coating is that HA will bind wherever there is a SAM, also inside porous structures. These HA-coatings also show a higher degree of crystallinity than HA obtained from other methods, such as plasma spraying. A high degree of crystallinity is necessary for the material to be osteoconductive[34].

Retinal pigment epithelia (RPE) cells are the cell-type used in this study, and several efforts have been made to regenerate this epithelial layer in the lab. The RPE cells comprise the outermost part of the retina, and damages to this layer are known to be pathogenic as the cells are vital for the photoreceptors[35]. Several studies using various polymers like poly-hydroxybutyrate-co-hydroxyvalerate (PHBV8)[36], PLGA[37] and PLGA combined with either poly(L-lactic acid)(PLLA)[38] or the diblock polymer poly(ethylene glycol) and poly(DL-lactic acid) (PEG/PLA)[39, 40] to grow RPE cells on have been conducted. The aim has then been to make a biodegradable surface so that it can dissolve after the cell layer attached to the scaffold is implanted. Also, the studies utilizing PLGA combined with PEG/PLA[39, 40] aimed to control the cell differentiation by patterning the surface. Glass combined with regions of non-adhesive octadecyltrichlorosilane SAMs have been used in a similar manner[41].

Various ECM-based coatings have also been used to aid the culture of RPE cells. A study comparing various types of collagen, fibronectin, laminin, gelatin, RGD, vitronectin and poly-L-lysine showed that only fibronectin enhanced the cell growth compared to the reference plastic substrate[42]. In fact did the cells adhere less to poly-L-lysine than the reference.

Another approach used to make implantable RPE cells, is to culture the cells on the temperature responsive polymer poly(*N*-isopropylacrylamide) (PIPAAm). The cell sheet is then removed from the polymer before implantation[43]. When the temperature of the substrate and the attached cells is decreased to 20^{o}C, the substrate changes its structure, making the sheet gently fall of. It is also possible to release cells chemically, by adding an enzyme that breaks the intercellular bonds, but this will harm the sheet structure needed for implantation[44].

Implantation of lab-made sheets of RPE cells has already been done. In September last year an old Japanese lady was cured from blindness after getting implanted a new RPE layer, made from her own skin cells[45]. However, already in 2009 it was demonstrated by the same research group that made the RPE sheet for implantation, that it was indeed possible to make the sheets from the patient's own cells[46], which overcomes issues like rejections. After extraction from the patient the cells are modified to become stem cells, and then differentiated into RPE cells. The process of differentiation is also affected by the substrate the cells are grown on, and in case of the preliminary study the substrate used was poly-D-lysine/laminin/fibronectin-coated plastic wells. Adult non-stem cells, e.g. differentiated cells from the skin "pushed" to become stem cells by specific factors, are called induced pluripotent stem cells (iPSCs), and Shinya Yamanaka was awarded the Nobel Prize in Physiology or Medicine in 2012 for developing this method[47].

1.2 Atomic layer deposition

This subchapter will firstly present a general overview of the historical development of ALD, and subsequently the state of the art research on inorganic-organic hybrid materials and various options for titanium precursors.

1.2.1 History of atomic layer deposition

ALD is a method to deposit thin films on substrates. The method was reported used in the 1970s[48] by T.Suntola and J.Antson, where a system producing ZnS-films was constructed. T.Suntola is considered to be the "inventor" of ALD, but it has been revealed that a group in the Soviet Union led by Professor Aleskovskii used the technique as early as the 1960s. This group used the $TiCl_4/H_2O$ process to make TiO_2, which is similar to the model system used in this thesis[49]. It was, however, only after the millennium that the research on ALD really exploded, with over 5000 articles published between 2002 and 2012[50].

The first application of ALD was Thin Film Electroluminiscent (TFEL) displays. A display of this kind was installed in Helsinki's airport in 1980, stating the country's import role in the ALD-community[48]. TFEL displays require a uniform film with a high dielectric constant and few pinholes to work, and ALD enables this with its extraordinary conformity. Its abilities to coat any three dimensional structure uniformly and its thickness control at the nanometer scale

are also increasingly used by the IT-industry. In 2007, ALD found its way into Intel's 45 nm CMOS process technology, where the gate made of hafnium oxide is deposited with ALD[50]. It is also used in thin film magnetic reading heads and in various types of coatings such as anti-corrosion, optical, water repellent and hardening coatings.

The applications now mentioned are primarily concerned with inorganics, whereas this thesis focuses on organic-inorganic hybrid materials. This field of ALD is still in its infancy and has few, if any, applications today. One imagined application is to use them into a ceramic ALD-matrix in order to make them less prone to damage when bending[50]. This thesis, however, seeks to bring the ALD-films into the cell culture lab.

1.2.2 Prior art of atomic layer deposition

As this thesis is concerned with inorganic-organic hybrid materials, this sub-chapter will also focus on this class of material, especially where titanium forms the inorganic part. Since titanium oxide is used as reference material in this study, this will also be treated here.

The idea of combining inorganic and organic precursors in one ALD-run is a rather new one. Even if pure organic ALD, also called molecular layer deposition (MLD), has been around since the early 1990s[51], the idea of combining the two is about ten years old. A patent describing the entire field combining ALD and MLD was filed by NAFUMA (research group for nanostructures and functional materials) researchers Ola Nilsen and Helmer Fjellvåg in 2004 and approved in 2006[52]. The patent was based on research about aluminium benzene oxides, using trimethyl aluminium (TMA) combined with hydroquinone (Hq) or phloroglucinol (PhI).

In 2008 hybrid films with TMA and ethylene glycol as precursors, so called alucones, were synthesized[53]. The year after alkyl films with zinc, zincones, were also reported, using diethylzinc and ethylene glycol as precursors[54]. Besides these alkyls, a paper about thin films with $TiCl_4$ and ethylenediamine or 4-aminobenzoic acid was published in 2009 from the NAFUMA group[55]. The latter precursor contains both an amine group and a carboxyl group, just as the amino acids.

Various organic precursors have been used together with $TiCl_4$, in addition to ethylenediamine and 4-aminobenzoic acid. The most extensively studied class of organic

precursors used in hybrid films is the alcohols and phenols[56]. Alcohols and phenols used with $TiCl_4$ include hydrokinon[57], ethylene glycol[58], glyserol[58], 8-hydroxyquinoline[59], polydiacetylene[60], 4-aminophenol[61] and 2-aminoethanol + propanediyol dichloride[62]. In the last example the pulsing of the two organic precursors was alternated, leading to an ABCB-type of process. It should also be noted that 4-aminophenol and 2-aminoethanol contain amine groups. Another organic precursor containing amine groups that has been used with $TiCl_4$ is 4,4'-oxydianiline[63].

Even though there have been made hybrid films with TMA and carboxylic acids varying in length such as oxalic acid (2C), glutaric acid (5C) and sebacic acid (10C)[64], there have not been reported materials of this kind with titanium as the inorganic part[56].

However, there has been conducted research with $TiCl_4$ and amino acids, which contain a carboxyl group, at NAFUMA previously. The amino acids used have been serine[65], lysine[66] and glycine[67]. All of the films were amorphous, very smooth with roughnesses in the range of a few Å and somewhat hydrophilic. From Figure 1 it can be seen that the growth rate per cycle for the $TiCl_4$/lysine system seems to be stable in a range between about 250°C to 350°C, but that the growth rate per cycle increases with temperatures below this range.

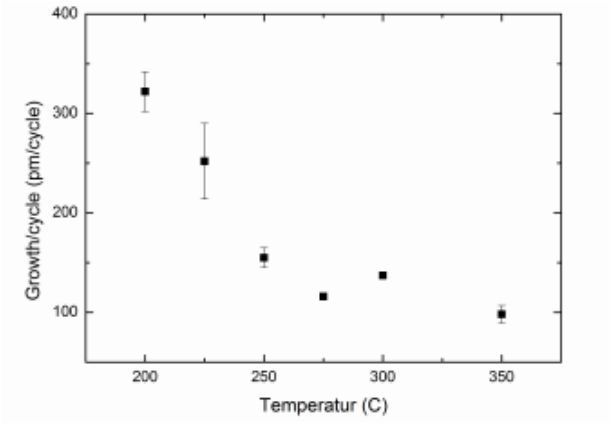

Figure 1[66]. Growth rate per cycle as a function of temperature for the $TiCl_4$/lysine process.

Even if $TiCl_4$ has been used as a precursor for several hybrid systems, it is not always the best choice. $TiCl_4$ is highly volatile and produces hydrogen chloride gas when it reacts with water which is dangerous to inhale[68] for the operator, and if it is the by-product of the ALD

reaction it may cause damage to the reactors. Additionally, using $TiCl_4$ may lead to chlorine in the synthesized films, which is undesirable when the films are to be used in the cell laboratory. Therefore this work will use titanium tetraisopropoxide (TTIP) as a titanium precursor. The use of the TTIP/H_2O process to make TiO_2 was first reported in the beginning of the 1990s, and a study comparing the TTIP/H_2O process with the $TiCl_4$/H_2O process was conducted[69]. From Figure 2 it can be seen that the TTIP/H_2O process exhibited ALD growth in temperatures ranging from a bit above 200°C to around 325°C, whereas the $TiCl_4$/H_2O process shows self-limiting growth up to 600°C. Furthermore, the $TiCl_4$/H_2O process had a growth rate of 0.56 Å/ cycle, which is almost the double of the TTIP/ H_2O process that only had about 0.30 Å/ cycle. This may be due to the fact that TTIP is significantly larger than $TiCl_4$, which may lead to steric hindrance. However, both processes lead to the same crystal structure of TiO_2, namely anatase. It must further be noted that the signal-to-noise ratios for the diffractograms reported were low, and only two of the peaks seemed clear. This might imply the presence of some amorphous TiO_2. Also, the article reported that the crystallinity increased with temperature.

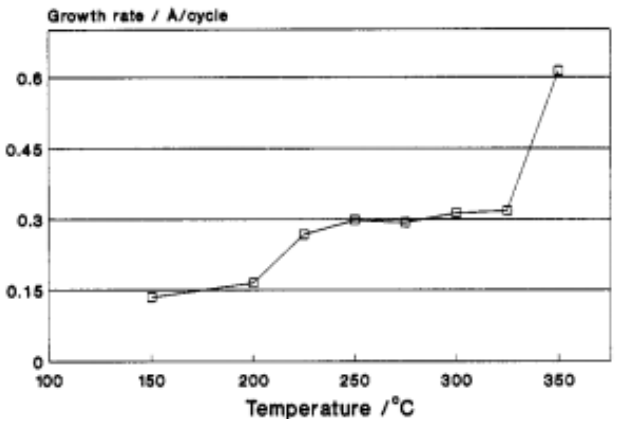

Figure 2[69]. Growth rate versus temperature for the TTIP/H_2O process to synthesize TiO_2.

There has been reported one rather complex hybrid ALD-process where TTIP is the inorganic precursor[56]. The organic precursor is 7-octenyltrichlorosilane, and it is pulsed with water and ozone in the following order; 7-octenyltrichlorosilane + H_2O + O_3 + TTIP + H_2O[70]. A mechanism for the growth is proposed in figure 3.

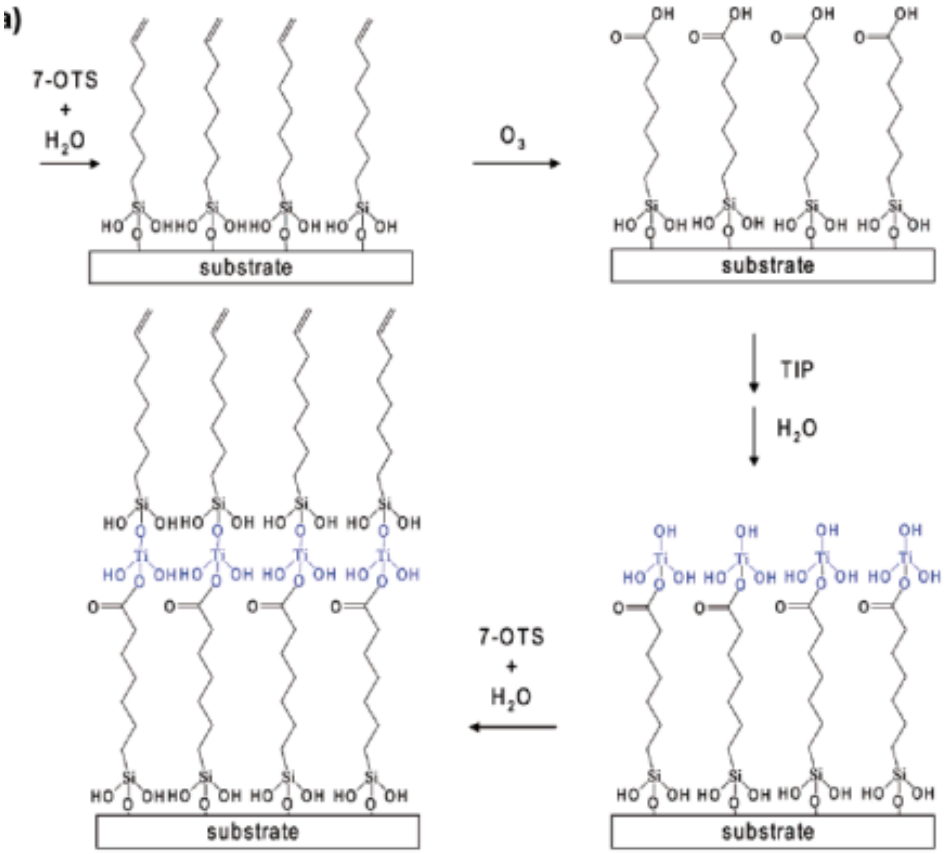

Figure 3[70]. A growth mechanism for the 7-octenyltrichlorosilane + H_2O + O_3 + TTIP + H_2O process.

Another precursor commonly used for producing TiO_2 and TiN is tetrakis-dimethyl-amido titanium (TDMAT). In 2007 a study comparing TTIP and TDMAT to make TiO_2 was conducted[71]. It was found that TDMAT required longer pulsing times compared to TTIP for the surface to be saturated. The strongest argument for not using TDMAT is, however, that it is very air sensitive[72].

1.3 Definition of the thesis

The first goal of this thesis is to synthesize organic-inorganic hybrid thin films with ALD, using titanium as the central atom and various amino acids. Possible Ti-precursors are $TiCl_4$ and TTIP. It is known that hybrid films with $TiCl_4$ as a precursor often contain chlorine. Since chlorine is not beneficial to cells, TTIP will be the primary choice. The amino acid used will primarily be lysine. Serine and glysine are other possibilities that may be investigated if time permits. All three amino acids are hoped to be easy to be put into the gas phase, and especially lysine is reported to enhance cell growth. As part of this study the optimal

parameters with regards to pulsing times and reaction temperatures for these ALD-systems will be investigated.

Secondly, the films obtained are to be characterized using various techniques. Spectroscopic ellipsometry, Fourier transform infrared spectroscopy (FTIR), gracing incident X-ray diffraction (GIXRD), X-ray reflectivity (XRR), scanning electron microscopy (SEM) and atomic force microscopy (AFM) will all be used. Since affinity to water is related to cell growth, goniometry will also be used.

The last part of the thesis is to seed out cells on the films and study how well the cells grow and proliferate on them. The number of cells on the substrates will be quantified using fluorescence microscopy.

2. Methods and theory

This chapter is organized so that the theoretical aspects and methodology related to cell growth is presented first, then some theory about ALD before the various characterization techniques are presented.

2.1 Cell growth

2.1.1 The cell culture laboratory

The cell culture laboratory aims to be a place where cell cultures can be managed and grown in a sterile environment[2]. The term “sterile” refers to “without life”, and there are several reasons why the environment should be as sterile as possible. Firstly, if the environment is not kept sterile, one cannot know whether the cells growing are the ones that are desired to study or cells from elsewhere, perhaps from the operator himself. Furthermore, the cells that are supposed to be studied may be harmed from biological contaminations. This can for example be a viral or bacterial infection. Thirdly, everything in the laboratory must be kept as sterile as possible to avoid cross-contaminations with the rest of the lab. In the worst case scenario the entire cell culture laboratory must be fumigated[73].

For the laboratory to remain sterile, it is obvious that various sterilization methods must be used. However, the methods have variable effects on different parasites, and some of the methods are harmful to the operator. Also, the objects that are being sterilized may be damaged. This is an important factor in this study where the structure and chemistry of the substrates must remain intact after sterilization.

A standard sterilization-technique is to use heat over a period of time. This may be done in two ways; either by heating in a wet environment, wet heating, or in a dry environment, dry heating. A general limitation for both of the heating techniques is that heat sensitive materials cannot be sterilized in this manner. This includes poly-styrene which deteriorates before 121 ^{o}C, which is the standard wet-heating sterilization temperature.

Wet heating is probably the most common sterilization technique of them all. It may be performed at temperatures below or above 100 ^{o}C, and the degree of sterilization is dependent of both the temperature and the time the objects are exposed to it. For many micro-organisms such as viruses and bacteria temperatures as low as 55 ^{o}C will be enough to

inactivate them. However, other micro-organisms such as prions may be more resistant. The inactivation is usually due to denaturation or coagulation of protein in the micro-organisms.

Pasteurization, i.e. wet heating at around 60-80 ^{o}C, is vastly used by the food industry, but it is rare in the cell culture laboratory. Here wet heating above 100 ^{o}C, autoclaving, is much more common to use. This is in practice steam under pressure. Typical conditions are 121 ^{o}C for a quarter of an hour. Only very few micro-organisms, such as prions, will require harsher conditions than this. Many different types of autoclaves are available, from simple table-top models to machines that can take larger loads[74]. There are also autoclaves able to sterilize culture media. It is important to quality check if the autoclave is actually hot enough on a regular basis. This can be done by performing a so-called Bowie-Dick test, which is a sheet of temperature sensitive paper placed into a stack of towels in the autoclave[73].

Dry heating has a clear advantage over wet heating due to the simple fact that the objects do not get wet. However, it is not nearly as efficient and is therefore much less used. One application of dry heating is to “flame” openings of glass bottles and other containers or metal objects, a technique which is called incineration. Another application for dry heating sterilization is hot-air ovens which are routinely used for glassware and metal objects. This is in contrast to wet heating a rather slow process, where timespans of more than an hour are required when the temperature is 170 ^{o}C.

Irradiation is another way to sterilize objects in the cell culture lab. Normally ultraviolet (UV) light is used, but gamma-rays are also utilized in industrial applications. Both of the irradiation types attacks the nucleic acids, making the strands break or cross-link. The largest limitation of this technique is poor penetrating power. It is often used to sterilize air in cabinets and even whole rooms, but it is dependent on a clear line of sight to the objects being sterilized, i.e. no shadowing effects. It can also be used to sterilize small, transparent objects such as coverslips. A typical time frame is around twenty minutes, so it is relatively fast.

Chemical sterilization is a third way to sterilize objects in the cell culture laboratory. It may either be performed by fumigation, which is used to sterilize whole rooms or cabinets, or by liquid disinfectants, which is used for surfaces. Ethylene oxide and formaldehyde gas are common in use for fumigation, whereas liquid disinfectants often involve alcohols,

aldehydes or hypochlorite. A general limitation when using chemicals is the dangers to the operator. Measures should therefore be taken to at least make fumigation unnecessary. One standard method to keep surfaces sterile and prevent the spreading of undesirable micro-organisms is to wipe off all surfaces with ethanol before and after use.

A final sterilization method worth mentioning is filtering. Filtering is used to sterilize culture media, sera and other cell culture supplements. However, the most important filters are probably the high efficiency particulate air (HEPA) filters. Outside the cell culture laboratory they are found in vacuum cleaners[75], but it is an essential part of the laminar flow hood, which is the primary spot to manage the cell cultures.

A laboratory is not a proper cell culture laboratory without a laminar flow hood. For all cell cultures where there is a risk for pathogens passing on to the operator, a so-called class II (micro)-biological safety cabinets (BSC), shown in figure 4, are required[2]. Cell cultures involving severe risks for the operators are for example human cells, as human cell lines catch the same diseases as the human operators. In the class II BSC air is drawn in where the operator sits, contrary to the regular laminar flow hoods. This implies that there is no air blowing directly from the work surface of the BSC which potentially contains infected cells, to the operator. The air in the BSC is circulated and taken through a HEPA filter to become sterilized. This has an important implication when it comes to usage of chemicals dangerous for the operator, such as methanol for fixating the cells. Since most of the air is circulated, dangerous fumes are not let out and it can therefore not be used as a regular fume hood. Proper cell culture laboratories must therefore also have a fume hood for dealing with chemicals.

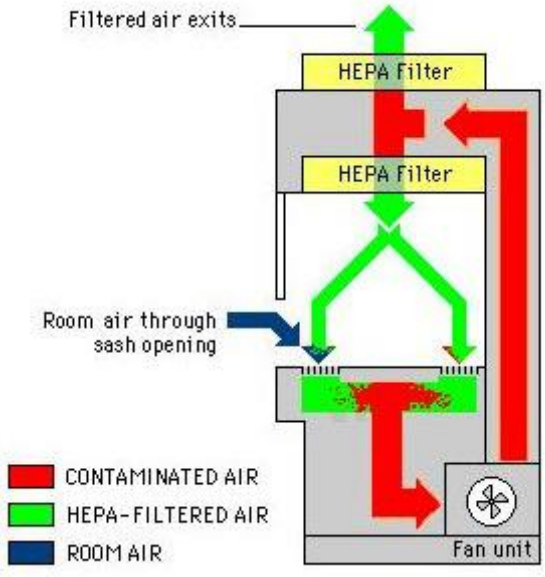

Figure 4[76]. A schematic drawing of the airflow in the class II microbiological safety cabinet. Room air is drawn from the sash opening when the bench is in use and fanned into the HEPA filters. The HEPA filters make the air in the cabinet sterile. Also, since there is no air flow from the work space to through the sash opening, this is very safe for the operator.

When working with a BSC there are several considerations which must be taken to ensure a good laboratory practice (GLP). Firstly, the bench must be wiped off with ethanol before and after usage. Also, everything that is taken into the cabinet, such as containers with media, must be wiped off before it is taken in. In order to prevent contamination into the various containers of media, sera or even the multi-welled plates for cell growth, the lids must be put on as soon as possible after opening. One of the most common sources of contamination is human arms that are stretched over opened containers, and this should therefore never be done. Lastly, good hand hygiene is essential. This is ensured by washing and sterilizing hands before entering the lab and usage of gloves.

Besides the BSC and a fume hood, several other pieces of equipment are essential in the cell culture lab. An incubator is needed to keep the cells at the right temperature and to regulate the atmosphere surrounding the growing cells. The air in the incubator is CO_2-rich, which makes the cell media more acidic. This also means that the lids of the various flasks and multi-welled plates to grow cells in are not air-tight. In fact, they also contain HEPA-filters to hinder contamination of the samples. Other necessary components of the cell culture laboratories include a centrifuge, an optical microscope, freezers and refrigerators, a water bath for toughing, automatic pipettes of various sizes and something to easily quantify cells with, such as the hemacytometer described in chapter 2.2.

How these various pieces of equipment are distributed around in the laboratory is also of great importance. They should be distributed to obtain a sterility gradient as shown in figure 5, so that the part of the laboratory where sterility is most vital is kept as far away from the "dirty" parts as possible. Furthermore some equipment and facilities should be kept outside of the laboratory in separate rooms. This includes washing and sterilization facilities, further storage areas, water baths and fume hoods.

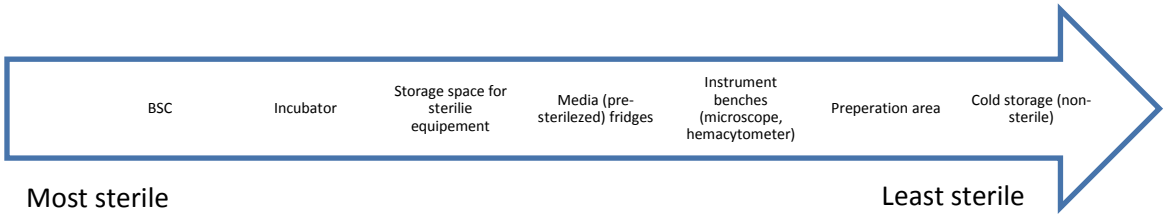

Figure 5[2]. The sterility gradient, where the most sterile components are to the left. The most important instruments in the cell culture laboratory are places according to how important sterility is for its function and how sterile the instrument normally is.

2.1.2 Cell adhesion and proliferation

The mammalian cells cultured in the laboratory can be divided into two categories after their need of attachment[77]. The first category is the cells in suspension, for example red and white blood cells[78]. Their growth mechanisms and requirements differ substantially from the need of the other category, attached or anchoring dependent cells. Attached cells are all cells in tissue, including the RPE cells. Since the cells studied in the present thesis falls into the category of attached cells, only these cells will be described in this subchapter.

As the attached cells also sometimes are referred to as anchoring dependent cells, it is clear that these cells truly depend on a substrate to thrive. Various types of substrates have been described earlier in this thesis, but this subchapter seeks to look into what actually happens when cells are attaching to a surface.

Figure is a schematic drawing of the cell attachment and proliferation process where the initial adhesion part is in a dotted box. Below the very first picture it is stated that the adsorption of proteins must happen before the cell contacts the surface. These proteins come from the biological fluid surrounding the substrate, in other words the medium and

serum. A fact worthwhile reflection is therefore that the cell's initial response and attachment on the surface largely depends on the proteins attached to it, rather than the surface itself[79].

However, what Figure does not say is that the proteins in serums, such as bovine serum albumin (BSA) from FBS also may inhibit the cell attachment[80]. This is another reason to develop SFMs. It should be noted that these kinds of interactions are substrate-dependent.

It is also seen that ECM assembly happens just after initial cell contact with the surface. This is part of the reason why coating with ECM proteins enhances the cell growth. Further, the integrins are mentioned in the next stage in figure 6. Integrins are trans-membrane receptors involved in the cell-ECM interactions through their extra-cellular domains[79]. They also interact with the cytoskeleton whose prime task is to keep the cell's shape and resist mechanical stress. The ECM and cytoskeleton interactions make integrins able to regulate many of the cellular functions, such as adhesion, motility (movement), shape, growth and differentiation[81]. Moreover, the integrins are programmed to attach to certain amino acid sequences, such as RGD[81].

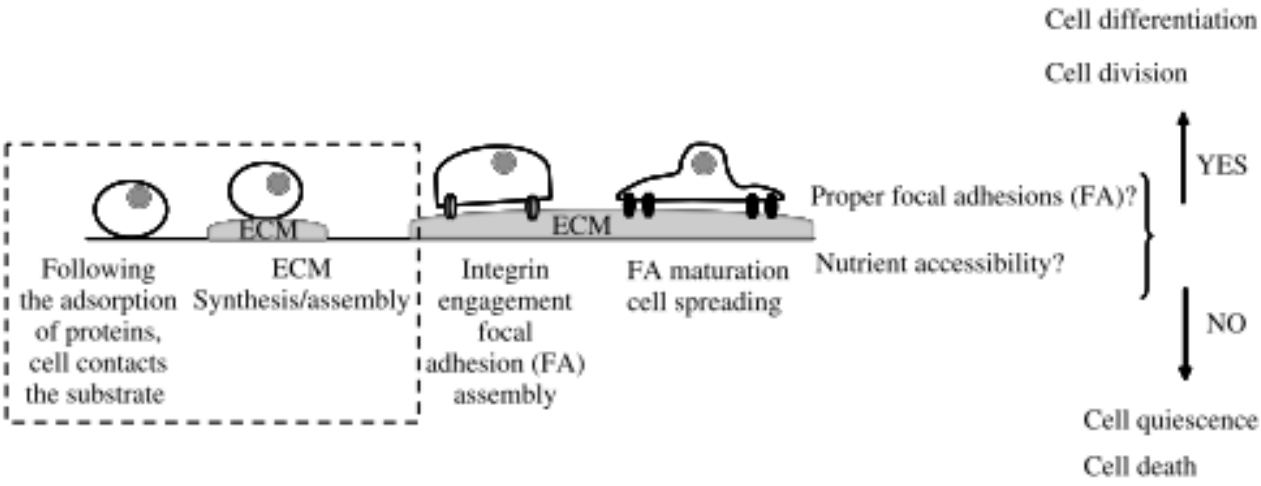

Figure 6[80]. Illustration of how anchoring-dependent mammalian cells attach and proliferate onto a surface. The attachment precedes the further division and differentiation meaning that good attachment is crucial for the cells to thrive.

Furthermore, the focal adhesion (FA) sites are described as a part of the cell attachment process. These sites are the places where the cell comes closest to the actual substrate, as close as 10-15 nm from the substrate[11], and are comparable or equal to the sites where cells connect to ECM *in vivo*[82]. The FAs consists of clustered, extended[83] intergrins and

other proteins from inside the cell[11], and function as huge transmembrane junctions[82]. With time the FAs will mature and the cell will spread out. The maturation process includes more attachment to the cytoskeleton. As shown in Figure this step is vital for the further proliferation of the cells.

Considering the previous discussion, it is no surprise that the cell attachment is affected by the chemical surface properties, the protein properties and the surface topography (in order of importance)[11]. In addition to altering the surface chemistry of the substrate, numerous examples of which are mentioned earlier in this thesis, changing the surface topography may lead to better facilitation of cell attachment and growth. The latter has also been studied, but as there is no consensus for topography characterization, comparing the studies is hard[79]. Also, it is difficult to know whether it is the surface topography or the chemistry that is being studied, as many techniques will alter both. The size magnitudes must also be considered when looking at cellular responses to altered topography. For example, it has been shown that human osteoblasts (hOB) prefer smoother topography below the cell size range (<50 µm), but over this range hOB appreciated a rather rough topography with bowl-like cavities[84]. It is also shown that human osteoprogenitor cells from bone marrow prefer to grow on the peaks when they are exposed to surfaces with topographies smaller than their own size[79]. The sizes of the cells themselves also matter when it comes to their responses to a substrate's topography. Human cells range from larger ones like primary bone cells (50 µm) to platelets which are only around 2 µm[79]. For comparison the RPEs are 10-15 µm *in vivo.*

2.1.3 Choice of cell line

There are two major types of cell lines, namely limited lifespan cultures and continuous cell lines[85]. The key characteristics of them both are summarized in Table 1. The terms *phenotype* and *karyotype* refers to an organisms observable traits and its number and appearance of chromosomes, respectively[86]. To show aneuploidy implies that both the phenotypes and karyotypes will be altered, as aneuploidy is to have another number of chromosomes than the species normally has. In humans this may be a cause of abnormal development, the most well-known being Down's syndrome[87].

Table 1[85]. Key characteristics of limited lifespan cultures versus continuous cell lines.

Limited lifespan cultures	Continuous cell lines
	Established spontaneously, chemically or virally
Normal phenotypes and karyotypes	May show aneuploidy
Homogeneous cell cultures	Heterogeneous cell cultures
More sensitive to growth conditions	Less sensitive to growth conditions
	No tissue-specific genes
	May be tumorigenic *in vivo*
Can be split and reseeded only a limited number of times	In theory it can be split and reseeded an infinite number of times

As can be seen from the table above several factors are different between the limited lifespan cultures and the continuous cell lines. Firstly, if cell differentiation is the subject of investigation, a continuous cell line is a bad choice as they do not differentiate normally. The same goes if the ECM or properties of a lab-grown tissue are to be studied. However, the continuous cell lines are less sensitive to the growth conditions, meaning that they are easier to handle. Lastly, they can be split an infinite number of times which means that many experiments may be performed with the same cells.

2.1.4 Sub-culturing cells

Since the cell lines used in this work are attached cells, they need to be detached before being sub-cultured, in other words before they are split and moved. As attached cells need to adhere both to the substrate and to the surrounding tissue to thrive, the method for sub-culturing them involves breaking the bonds involved in the adhesion. The most common chemical used for this is *trypsin*, which is an enzyme cleaving peptide bonds. This will make the adherent tissue become a cell suspension, as the peptide bonds holding the tissue together are subject to cleaving. The method of using trypsin to sub-culture cells is referred to as *trypsination*[77].

Trypsination is the standard way to sub-culture attached cells; however, there is one very important precaution to be made when choosing to do this. Since trypsin catalyzes reactions cleaving peptides in general, it will also start to break down the peptide bonds within the cells themselves. This implies that the cells should be exposed to trypsin only for a very

limited period of time, and the cells should be monitored extremely carfully using light microscopy within this timeframe. In general, trypsination is regarded to be a harsh method on the cells. There exist alternatives to trypsin, for example ethylene diamine tetra-acetic acid (EDTA). EDTA is a chelating agent, and binds up metal ions of calcium and magnesium which the cells use in their FAs. Using only EDTA is in this way a milder method[88], but much less effective. EDTA is also routinely used together with trypsin. Alternatively, manual scraping off the cells may be done[77].

A standard method to sub-culture attached cells using trypsin is as follows;

1. The light microscope should be focused on the cells in the cell culture flask, so valuable time is not wasted on this step later on.
2. The medium needs to be rinsed off the cells. If the cells are not properly rinsed the trypsin will start to cleave the peptides from the medium and serum, instead of working on breaking down the ECM. The rinsing process is performed by firstly aspirating (removing with the use of suction) the culture medium and then rinsing the cell sheet with a balanced salt solution. The balanced salt solution must be aspirated before proceeding with addition of the trypsin.
3. Enough trypsin to cover the entire surface of the bottom of the cell culture flask is added to the flask. The flask is then placed in the incubator and a stopclock should be started to measure the time.
4. The cells should be examined after approximately five minutes. If it appears like most of the cells are “floating around” instead of being attached, the trypsination process is done. If not, the flask should be put back into the incubator for some additional time. The cells should then be checked every two minutes.
5. When the cells are mostly in suspension, cell medium should be added. The amount of medium depends on the size of the flask. The trypsin will then start to cleave the peptides in the cell medium, and no longer be harmful to the cells.
6. The fluid from the flask should be transported into a centrifuge tube, using a pipette.
7. The tube containing the cell suspension must be centrifuged. The cells which are denser than the surrounding medium will then fall into the bottom of the tube.
8. Using a pipette the medium must be aspirated, leaving the cells. Approximately 5 mm of medium should remain above the cells, so no cells are aspirated.

9. New medium should be added to the tube. The total amount of fluid should be a round number, which makes it easier to calculate the concentration of cells in a later stage.
10. The fluid in the tube should be drawn up and ejected by a pipette several times to ensure that the cells are evenly distributed in the medium.
11. Shortly after the previous stage, the cells should be seeded out on the desired substrates placed into welled plates. When seeding out the cells a micro-pipette must be used, to ensure that the same amount of cells are seeded out in each well. Also, the pipette should be placed in the middle of the tube and certainly not in the bottom whilst taking up the cells. This is to ensure as even as possible distribution of cells between the studied well. The seeding process must also be quick, so the cells do not all fall into the bottom of the tube. The remaining fluid should be put into a cell culture flask for further cultivation.
12. The cell concentration of each well is calculated by first finding the total amount of cells using the hemacytometer. The number of cells seeded out in one well is then calculated by using Equation 1 shown below.

Equation 1

$$\frac{total\ number\ of\ cells\ \cdot volume\ of\ cell\ containing\ medium\ seeded\ out\ in\ a\ single\ well}{total\ volume\ of\ cell\ containing\ medium\ in\ the\ tube} = number\ of\ cells\ seeded\ in\ one\ well$$

13. More medium must then be added to the wells with the newly ceded cells. The lids are then put on the welled plates and the plates are placed into the incubator.

Another factor to consider before choosing to sub-culture is the confluence of the cells, which refers to how large proportion of the well bottom that is covered by the cells. The cells used in this study create a monolayer of cells, which implies that when the cells are 100 % confluent they cannot actually split into larger numbers anymore. The confluence of the cells is related to in which phase of cell growth the culture is in, as shown in figure 7. In the third and stationary phase the cells are completely confluent.

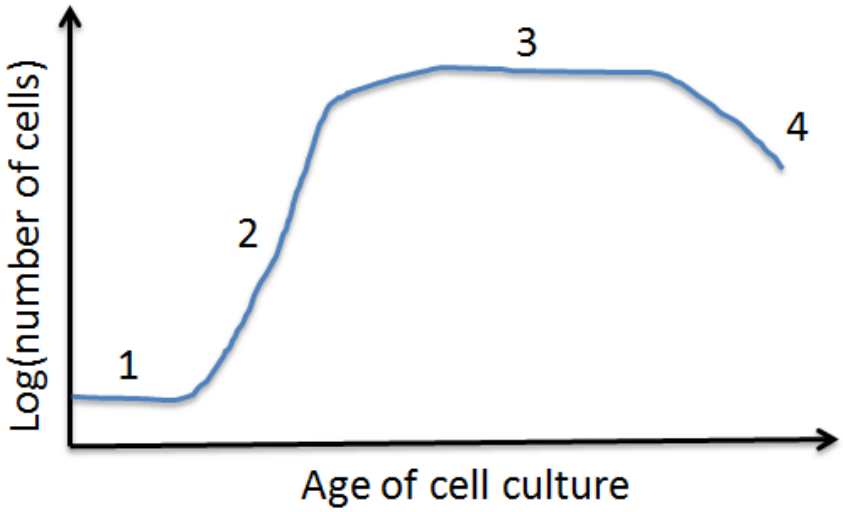

Figure 7. A graph showing the four different phase of cell growth. 1 is the lag phase just after the cells are seeded out. The cells do not divide in the lag phase, but rather attach to the substrate. 2 is the phase of exponential growth in which much more cells divide than die. In 3, the stationary phase, the division and death of the cells even out. Finally, in the fourth phase, the cells deaths are more than the division and the number of cells decline.

It is in the second phase, the phase of exponential growth, that the cell population is considered to be the healthiest. It is therefore within this phase it is best to sub-culture the cells[77]. A good rule of thumb is to sub-culture the cells when they are around 75 % confluent. In relation to the graph showing the growth phases, this is towards the end of the second phase. How long this is in actual time varies from cell culture to cell culture, and is affected by several parameters. A rough estimation is two to three days. However, it may take longer if the seeding density is low, the cells are old/ passaged many times or the sub-culture is cultured from unhealthy cells (e.g. phase four cells).

2.2 Cell-counting

In this work the Neubauer-ruled hemacytometer is used for cell counting before the cells are seeded out. It is a cheap and fast technique to count cells in suspension. The hemacytometer is a microscope slide that has been modified with grids for counting the cells. Approximately 10 µL of cell-containing medium is loaded into the hemacytometer using a micro-pipette. A cover glass is then put on top and the droplet spreads over the gridded counting area. The gridded area has nine primary squares, and these are surrounded by easily identified tripled lines, as shown in figure 9. The cells are then counted as described in the enlarged part of figure 8.

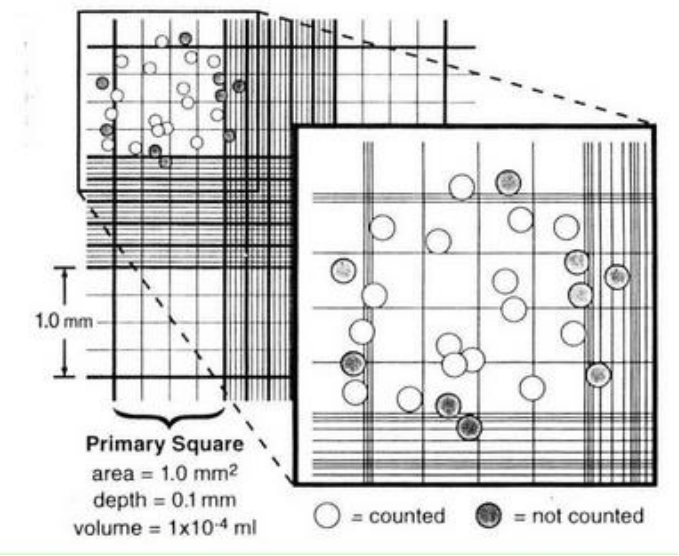

Figure 8[77]. An illustration of the counting squares of the Neubauer modified hemacytometer. The illustration also shows which cells should and should not be counted. This is determined by the tripled lines. Cells that are within the square are counted, and also those which touch the upper or left boundary. However, cells that touch the lower or right boundary are not counted.

The number of cells within one counting square multiplied by 1000 is the number of cells in one milliliter. However, for a more accurate cell count several squares should be counted and the average of those should be taken before multiplying with 1000. When calculating the total number of cells in a tube the total volume of the cell-containing medium must also be taken into consideration, as the hemacytometer only gives the values for one milliliter.

2.3 Fluorescence microscopy

In fluorescence microscopy a fluorescent-dyed sample is illuminated with high-intensity light of a single wavelength. The sample then re-emits light of a longer wavelength[89]. This is due to the sample exhibiting fluorescence, which is to emit light after the sample is subject to electromagnetic radiation. The importance of fluorescence microscopy was emphasized last year when Eric Betzig, William Moerner and Stefan Hell won the Nobel Prize in Chemistry for improving the technique to be applicable even for nano-dimensions[90].

In the cell culture lab, however, the dimensions are much larger, but the fluorescence microscopy still has a huge advantage over any other technique. Dyes, called fluorochromes, binding specifically to only one organelle, are available. This means that fluorescence microscopy can be used to view only certain parts of the cells. Different organelles can also be stained with different fluorochromes, meaning that one cell will re-emit several different

wavelengths. The specific binding to organelles may be done through the use of antibodies, which are specifically binding molecules used by the immune system. Usually a specific primary antibody is applied first, followed by a fluorochrome-conjugated secondary antibody which binds to the first one[91]. Another way to stain the cell's DNA is to use compounds that intercalate into the base strands, such as Propidium Iodine (PI)[92].

2.4 Atomic layer deposition

Atomic layer deposition (ALD) is a method for depositing thin films. It is related to chemical vapor deposition (CVD), but uses self-limiting sequential reactions between precursors in gas phase and a substrate. This implies that the thickness of the film depends linearly on how many repetitions, or cycles, are performed. Since the reactions are self-limiting, at least two precursors are required. Typically, an ALD-run progresses like this:

Step 1: Precursor 1 is pulsed in the chamber.

Step 2: The chamber is purged with an inert gas.

Step 3: Precursor 2 is pulsed in the chamber.

Step 4: The chamber is purged with an inter gas.

The process is repeated for the required number in order to reach the desired film thickness, for example 1000 times. After the first step the entire surface is saturated with precursor 1. The purging step, often utilizing nitrogen, will flush out the surplus precursor in order to ensure that there will be no reaction between the remaining gas molecules and the next precursor. If this happens, a powder is formed in the gas phase. The third step of the ALD-cycle is to pulse in precursor 2. This will react with the surface already saturated with precursor 1 and produce a new by-product. Thereafter the surplus is removed by purging, and the cycle can be repeated. One example of a well-studied ALD-process is the production of alumina films with trimethylaluminium (TMA) and H_2O[48]. As seen in figure 9 ALD is truly a cyclic process[49]. One exception is perhaps the first few cycles were lower growth rates are to be expected due to differences in surface chemistry of the native substrate and a growing Al_2O_3 surface.

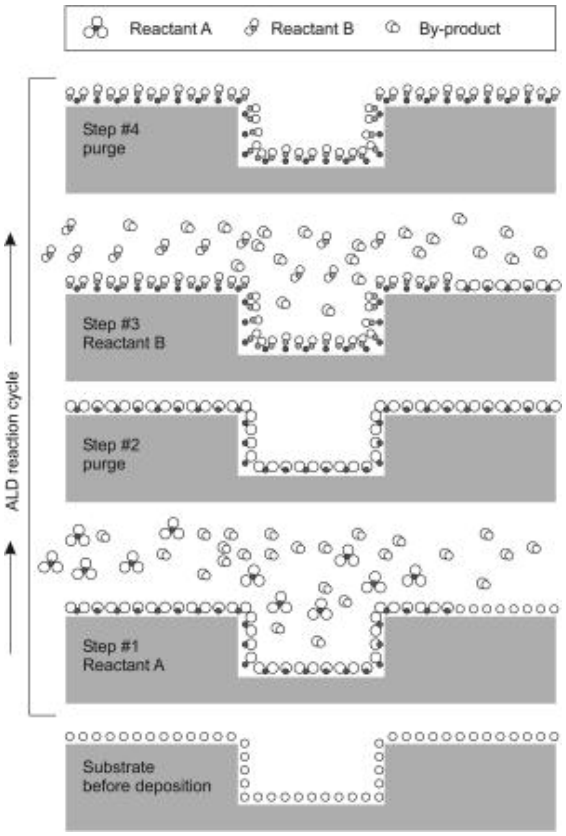

Figure 9[49]. This is a schematic drawing of a binary ALD process. Reactant A is TMA, reactant B is water and the waste product is methane.

Several factors are important to run an ALD process, firstly, the choice of precursor. The precursor must not react with itself or decompose during application. Furthermore, the precursors must be in the gas phase, it must have a sufficient vapor pressure (typically 0.01 mBar) or be heated to a sufficient pressure. The vapor pressure, and its sticking properties, will affect the pulsing times used, and a short pulsing time is desired for practical reasons.

Secondly, the right temperature is vital for the reaction to continue. It needs to be within the so-called ALD-window, as shown in figure 10. If the temperature is outside of the ALD-window other growth mechanisms will dominate and the self-saturating principle may be hampered. At too high temperatures, decomposition or desorption may occur, giving too high or too low growth rates respectively. Similarly, too low temperatures may result in too high or too low growth rates, probably due to limited kinetics or condensation of precursor, respectively. Within the ALD window, the growth rate should be relatively insensitive to the deposition temperature.

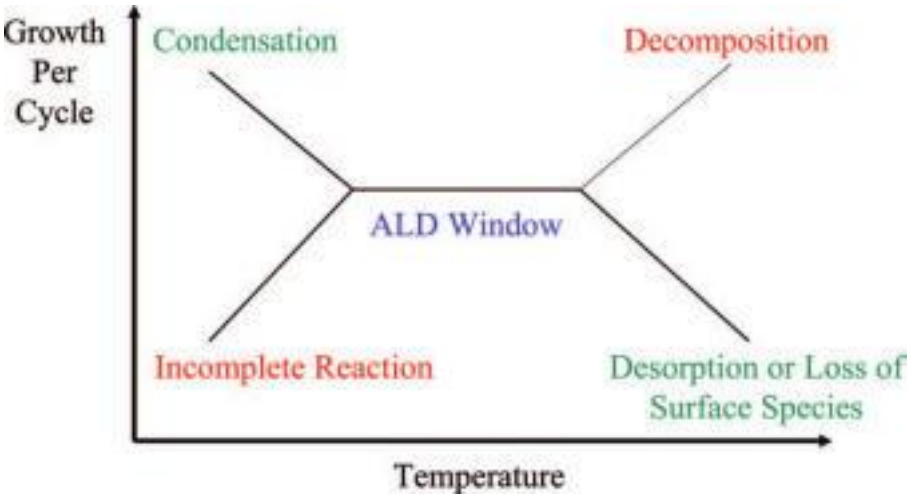

Figure 10[48]. This a plot of the growth per cycle versus the temperature for the ALD process. The figure indicates that for too low temperature there can be two different growth regimes. Either the precursor can condensate so that the growth rate becomes too high or the growth rate gets very low due to poor kinetics. Also, for high temperatures the growth rate can become high due to decomposition or it can get low due to desorption of the surface species.

2.4.1 Quartz crystal microbalance

Using a quartz crystal microbalance (QCM) is a way to characterize the growth of ALD thin films. It is based on a piezoelectric quartz crystal that will resonate at certain frequencies when an oscillating bias is applied across it. The resonance frequency is a function of the mass deposited on the quartz crystal, and can be expressed by the Sauerbrey's equation, Equation 2, below[93]:

Equation 2

$$\Delta f = \frac{2f_0^2 \Delta m}{A\sqrt{\mu\rho}} = C\Delta m$$

where f is the resonance frequency of the quartz crystal, f_0 is the resonance frequency of the unloaded crystal, A is the surface area between the electrodes, μ is the shear modulus of the crystal, ρ is the density of the crystal and m is the mass of the crystal. It can also be seen from the equation that the change in frequency is directly proportional to the change in mass. The QCM is placed directly into the reaction chamber as a substrate and used to measure *in situ* the mass changes connected to growth of the film. For example the growth rate versus pulsing times can be studied to give information about the required pulsing times to saturate the surface.

Even though Equation 2 states that the change in frequency is directly proportional with the change of mass, a calibration relation is needed to relate the frequency change with actual mass changes. The real surface area of the quartz crystal is fact uncertain due to variations in surface roughness. In order calibrate the crystal a film of known density and growth rate is first deposited. This film is deposited sequentially during the QCM acquisition to account for variations of the QCM crystal during growth. This procedure use Equation 3 as basis for the calibration factor:

Equation 3

$$\Delta m = \frac{r_{growth} \cdot \rho}{\frac{f_{ref}}{s} \cdot t} \cdot \Delta f = k \cdot \Delta f$$

where r_{growth} is the growth rate of the reference film, ρ its density, $\frac{f_{ref}}{s}$ the change of frequency per second when the reference film is deposited, t is the time for an ALD cycle of the reference film, k is the derived conversion factor and m is the mass.

2.4.2 Precursor tester

The precursor tester is an installation used for exactly what it sounds like, namely testing precursors. In the precursor tester a small amount of the precursor is placed inside a chamber which is put under vacuum to simulate actual conditions when the precursor is used. A QCM unit is also installed in the chamber, alongside with a time-laps camera monitoring the precursor and a temperature sensor. The precursor is then heated, and both pictures, frequency of the QCM unit and the temperature are logged as functions of time. This gives information about the sublimation temperature and possible decomposition processes, which is vital when choosing the suitability of an ALD precursor.

2.5 Fourier transform infrared spectroscopy

Infrared spectroscopy utilizes infrared radiation from the electromagnetic spectrum. When the radiation is shone upon the sample, some of the radiation will be absorbed. A recording of this absorbed radiation give rise to an absorption spectrum[94]. The absorption is due to transitions between quantized vibrational energy states of the bonds[95]. The vibration of a molecular bond depends on both the length of it and the mass of the atoms involved, and

can be either stretching a bond between two atoms or bending between three atoms. The infrared spectrum can consequently give information about the bonds, for example which organic functional groups are present in the sample. For infrared spectra, it has become common to plot the transmittance in percent versus the frequencies in cm^{-1}. The peak positions for various organic functional groups are given in databases[95]. However, the hybrid materials produced in this work are largely missing in these databases, making identification a bit more cumbersome.

The main advantage of Fourier transform infrared spectroscopy (FTIR) versus traditional infrared spectroscopy is the time it takes to measure a sample[94]. An FTIR-spectrometer radiates all wavelengths at the sample simultaneously, and does therefore not use a monochromator. However, it needs a Michelson interferometer, as shown in Figure to split the incoming beam in two and make it superimpose as a function of the position of the moving mirror[96].The Michelson interferometer is setup-wise the largest difference between the FTIR spectrometer and the traditional one.

There are different kinds of FTIR instruments. They can be in a transmission mode where the beam is passed through the sample before being measured. This poses some challenges when working with thin films, as the substrates the films are deposited on usually are much thicker than the films themselves. It therefore requires measuring a blank substrate first and the sample itself afterwards. The signal from the film itself is found by dividing the signal from the real sample by the signal from the blank substrate. This method may lead to errors due to differences between the substrates, and it is therefore important to ensure that the blank substrate is equal to the substrate the film is deposited on. Ensuring this may be difficult, as one “mother substrate” may have local differences when it comes to things like doping levels and thickness of oxide layers. To circumvent the importance of the substrate, an attenuated total reflection mode (ATR) may be used. This requires an IR-neutral crystal, often germanium, clamped to the solid sample to ensure proper contact. The beam will be totally reflected at the crystal-sample interface, but is internally reflected within the crystal, so that the beam is reflected from the sample several times.

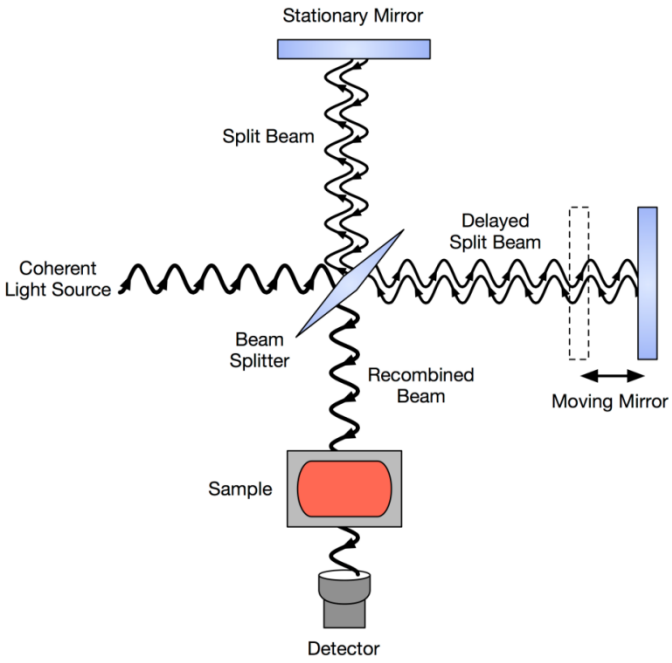

Figure 11. Setup of the Michelson interferometer for FTIR[97]. The coherent beam is split into two parts through the beam splitter. The beam is recombined and will superimpose as a function of the position of the movable mirror.

2.6 X-ray characterization

2.6.1 Grazing incident X-ray diffraction

X-ray diffraction (XRD) is a routine method to characterize the structure of crystalline materials. It is based on the fact that a crystalline lattice will diffract X-rays, since the distance between the lattice planes in crystalline materials are in the same size range as the wavelengths of X-rays. When the wavelengths are such that they satisfy Bragg's equation[98], written in equation 4 and illustrated in figure 12 , the waves will interfere constructively and create a signal.

Equation 4

$$n\lambda = 2dsin\theta$$

where n is an integer, λ is the wavelength of the X-rays, d is the distance between the planes and θ is the angle between the incoming beam and lattice plane.

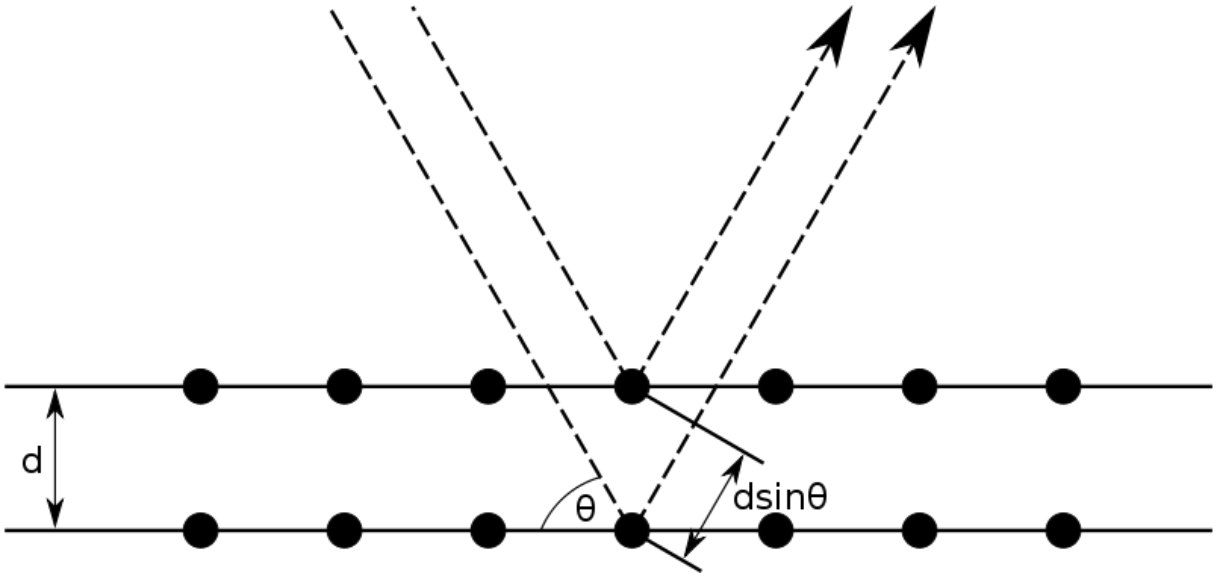

Figure 12. This figure illustrates Bragg's law. The beam reflected from the bottom plane traverses the distance 2dsinθ longer than the other one, and out of the sample both beams will interfere constructively and create a signal[99].

The most common setup for XRD in polycrystalline samples is the so-called θ/2θ scan as shown in figure 13. Here the x-ray source and detector are moved simultaneously to maintain the relationship ω=θ and a diffracting angle of 2θ. This is a good method to scan powders and thicker films (>100 nm), but for thin films, most of the signal will come from the substrate and not the film.

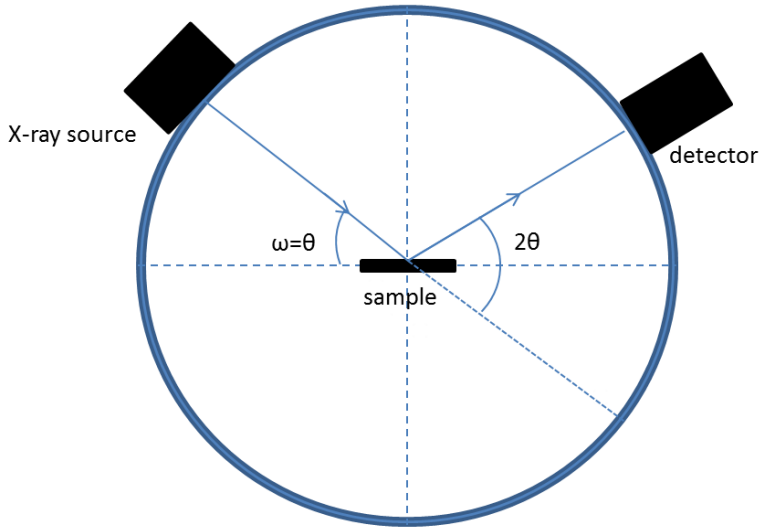

Figure 13. This figure shows the setup for the θ/2θ scan. The x-ray source and the detector are moved simultaneously so that if the angle between the incident beam and the detector is 2θ, the angle between the incident beam and the sample is ω=θ.

Another setup called grazing incident x-ray diffraction (GIXRD) shown in figure 14 is therefore adopted for measurements on thin films. Here the angle between the x-ray source and the substrate, ω, is kept constant on a low value just above the critical angle, θ_c, whilst

the detector is moving. This means that the beam's path in the actual sample will be longer, giving a better signal to noise ratio.

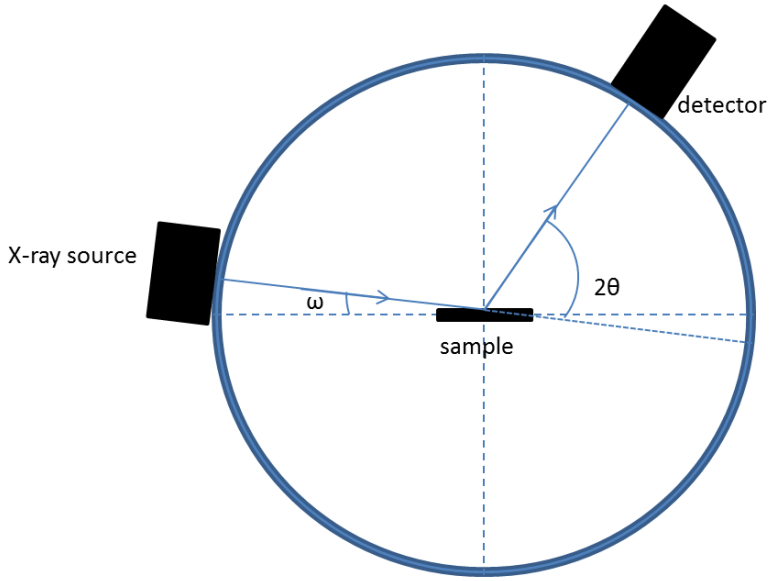

Figure 14. This figure shows the setup for GIXRD. The angle between the x-ray source and the sample is kept constant at a low angle whilst the detector is moving.

2.6.2 X-ray reflectivity

X-ray reflectometry (XRR) is a technique that gives information about the density, roughness and film thickness. It also utilizes x-rays, and is therefore coupled with the XRD-measurements. The angle of the incoming beam and the detector is varied according to $\theta/2\theta$, however, at rather small angles. If the incident beam is below the critical angle, θ_c, the beam will be fully reflected within the sample. As θ_c is directly proportional to the electron density at the surface[100], this gives information about the density of the film. Also, in thin films, an incoming beam can be reflected at intersections between the film and the substrate. These reflections will interfere with the specular reflection and make the refleced beam oscillate in intensity as function of θ. These oscillations are called "Kiessing fringes"[101]. The film thickness can be calculated from the periodicity of these oscillations. Furthermore, how fast these oscillations wane when the angle between the incoming beam and the sample increases will give a measure on the roughness of the sample. To calculate the density, roughness and film thickness from XRR-data, a model must be made from information about the sample and fitted to the measured data. An example of a recorded graph and a fitted model is shown in figure 15.

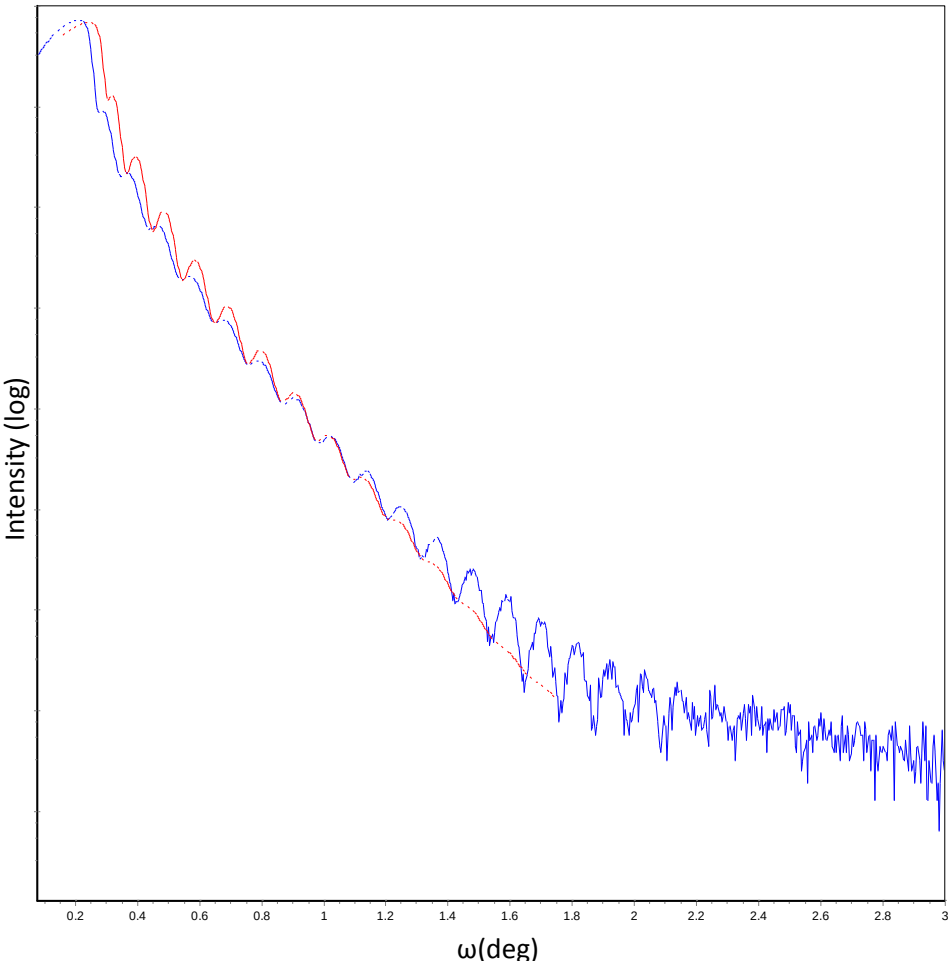

Figure 15. A graph from a XRR-measurement of a TiO_2-sample. The blue line is the recorded data, whereas the red line is the fitted data.

2.7 Ellipsometry

Spectroscopic ellipsometry, usually referred to as just ellipsometry, is an optical technique to characterize thin films. It can be used to determine the film thickness, index of refraction, roughness, the concentration of a dopant and conductivity. For transparent films, it can measure film thicknesses ranging from 0.1 nm up to 200 µm, but absorbing films must be very thin to be possible to measure.

A simple setup for the ellipsometer is shown in figure 16 As can be seen, photons are radiated onto the sample and reflected from it with an angle, θ, between the film and the reflected beam. The incoming beam is polarized and contains radiation with a spectrum of various wavelengths. When the photons in the beam interact with the sample the polarization will change and this change of polarization is what the detector actually measures.

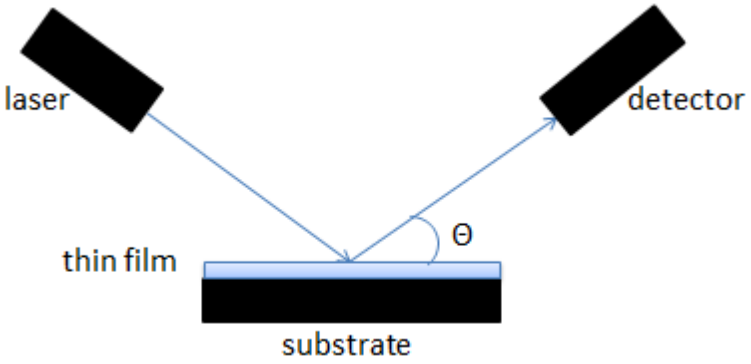

Figure 16. This figure shows a setup for the ellipsometer. A laser shines polarized light at a sample and the detector is measuring the change of polarization due to interactions with the thin film sample.

In order to get something useful out of the results, the data must be fit into a model. In this study, where all of the samples have been non-absorbing, the Cauchy-function as written in equation 5 has been used.

Equation 5

$$n(\lambda) = n_0 + \frac{n_1}{\lambda^2} + \frac{n_2}{\lambda^4}$$

where n is the refractive index, n_0, n_1 and n_2 are Cauchy-constants and λ is the wavelength of the photons. More about the various mathematical models and the technique itself can be read in ref. [102].

2.8 Atomic force microscopy

Atomic force microscopy (AFM) is a method to analyze the topography of a sample. It both gives a measurement for the roughness of the sample in addition to reveal any larger features. A cantilever with a sharp tip is scanned over the surface, and when the tip is close to the surface the cantilever will bend due to the force experienced from the sample. A laser pointing at the cantilever will reflect differently when it bends, which is registered by a photodiode. This is shown in figure 16. The resolution of the AFM pictures is limited by the sharpness or size of the tip used. This also means that shapes appear rounder on the AFM images than they really are.

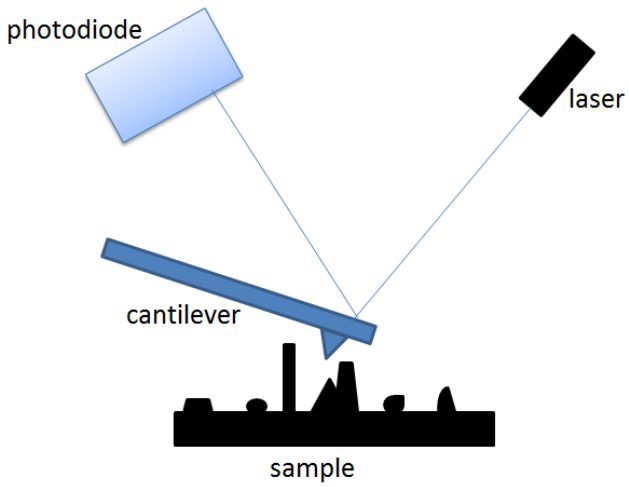

Figure 16. This figure shows the setup for the atomic force microscope. A cantilever with a tip is scanned very close to the surface. When the tip on the cantilever gets near the surface the cantilever bends. This alters the position the laser light hits the photodiode, which in turn gives the signal.

Various modes can be used, including the non-contact mode used in this study. Here the tip is quite far away from the sample, and the tip will therefore only experience attractive forces.

2.9 Goniometry

Goniometry is a method to measure the contact angle between an applied droplet of liquid, usually water, and a surface. These measurements may be used to calculate the surface tensions of the samples. As cell adhesion is connected to the surface's affinity to water, this is an important measurement for materials used for biological applications. In order to measure the contact angle, a camera, a sample stage and something that produces small droplets are required.

2.10 Scanning electron microscopy

The scanning electron microscope (SEM) is scanning the sample with an electron beam to obtain information about the topography and composition of the sample. The setup is comparable to the optical microscope, but uses electromagnetic lenses and an electron beam instead. When the electrons hit the surface, they may be spread either elastically or in-elastically, which gives rise to two types of signal. The various types of interactions between the electron beam and sample is shown in figure 18. The elastically spread electrons are called backscattered electrons (BSE). These are sensitive to the mass of the elements in the sample, and heavier elements will deflect more electrons and appear lighter in the SEM micrograph. The in-elastically spread electrons are the secondary electrons (SE). They are called secondary electrons because they do not come from the electron beam itself;

they are rather electrons from the samples kicked out from their orbitals by the incoming beam. As these have very low kinetic energies, they must be close to the surface to escape the sample. The SE are therefore very sensitive to the topography of the sample, and give a good visualization of this.

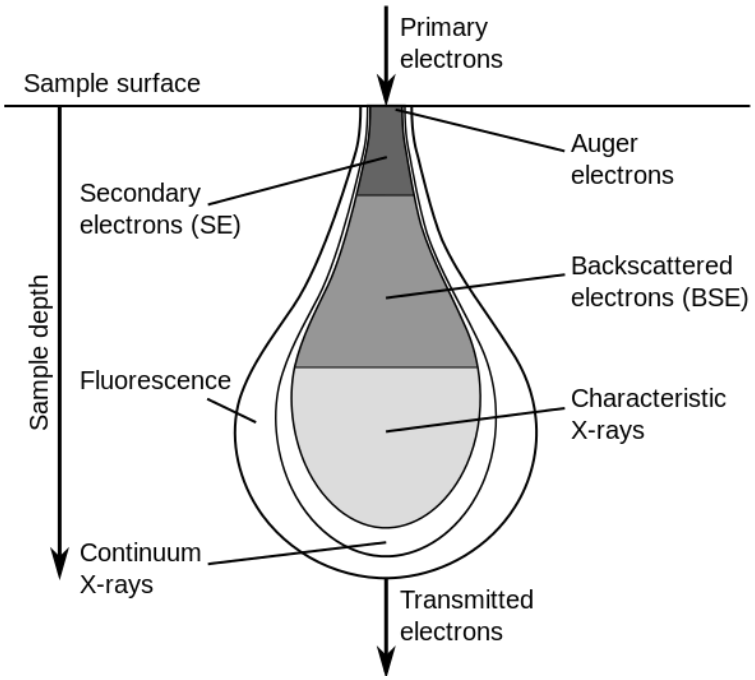

Figure 18[103]. An illustration of the various interactions between the electron beam and the surface of the sample in a SEM.

As can be seen from figure 18 the sample and the beam have a pear-shaped interaction volume. The size of this depends on the acceleration voltage, but is usually around 100 nm deep. Hence will analyzing very thin films mostly lead give signal from the substrate, especially for the BSE.

3. Experimental

This subchapter is divided into three parts, where the first is concerned about the synthesis of thin films, the second about characterizing them and the third about the experiments performed on cells.

3.1 Synthesis of thin films

3.1.1 The atomic layer deposition reactor

The reactor used in this work is an ASM Microchemistry F-120 Sat reactor . It has five zones for temperature regulation, and is *hot wall* meaning that theentire reaction chamber is heated. This results in good temperature control at the substrate and limited temperature gradients. This also implies that all surfaces in the reactor chamber will be exposed for film deposition. Figure 19 shows the gas flow in the reactor and the placement of the precursors. Four of the temperature zones are located along the pyrex glass tube where the precursor boat is inside. This gives room to have a temperature gradient within the reactor and hence have different temperatures at the precursors and at the reaction chambers. Another possibility, if the precursor has sufficient vapor pressure at room temperature, is to place the precursors outside of the reactor in a flask and then connect the flaks to the reactor through one of the valves shown at the left side in figure 19.

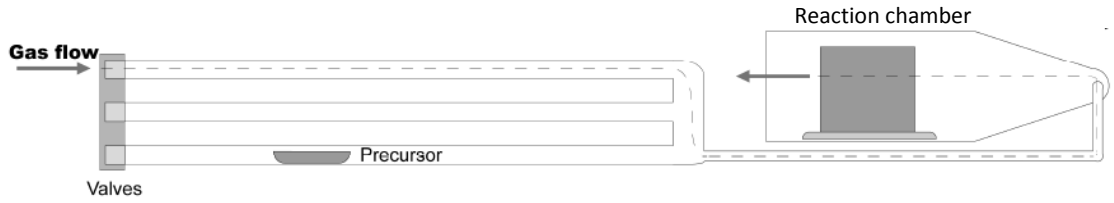

Figure 19[104]. A sketch showing the gas flow and the placement of the precursors in a F-120 Sat ALD-reactor.

The precursors are pulsed by opening and closing magnetic valves placed as shown in Figure . When the valves are closed the carrying gas, in this case nitrogen (<99.999 %) from a Schmidelin-Sirroco 5 generator, will divert the precursor towards the valves and not the reaction chamber. In the other case, when a valve is open, the nitrogen will carry the precursor to the reaction chamber. To ensure the purity of the nitrogen gas it is passed through a Mykrolis O_2 filter. In the reaction chamber, the precursor reacts with the all available surfaces, including the substrates. After the desired pulsing time, the valves to the precursor are closed and the chamber is rinsed with nitrogen gas.

3.1.2 Precursors

Three different ALD precursors have been used in this thesis as shown in Table 2. In this work the TTIP and water have been placed externally as they both have sufficient vapor pressures at room temperature. The lysine, however, has been placed inside the reactor in a precursor boat.

Table 2. List of precursors used in the ALD reactions.

Name	Structural formula	Abbreviation	Appearance	Purity	Supplier	CAS
Titanium tetraisopropoxide	$Ti[OCH(CH_3)_2]_4$	TTIP	Clear liquid	≥ 97 %	Sigma Aldrich	546-68-9
L-Lysine	$H_2N(CH_2)_4CH(NH_2)CO_2H$	Lys	White powder	≥ 97 %	Sigma Aldrich	56-87-1
Deionized water	H_2O	-	Clear liquid	Type 2	Deionized at University of Oslo	-

3.1.3 Substrates

Generally the substrates used have been 1x1 cm^2 pieces of silicon wafers. These wafers have a layer of native oxide on top, which was measured before use to be typically 2 nm. Usually, five substrates were used in each run, one in each corner of a glass plate and one in the middle. The glass plates used were 5.1 x 7.6 cm^2, had a thickness of 1 mm and were purchased from Glaswarenfabrik Karl Hecht. Looking for coloring at the edge of the glass has been an easy way to check if the depositions have been successful. Special un-doped silicon substrates with one rough side have been used for FTIR measurements. All of the substrates were purchased from University Wafer.

For cell growth applications thin films have been deposited on glass cover slips. These cover slips are 15 mm in diameter and purchased from VWR. As the deposited films are almost completely transparent and hence close to invisible, it was desirable to coat both sides of the cover slip before they were taken to the cell culture laboratory where it is important that the “up-side” is coated. This was done by putting the cover slips on top of a curled copper band, as shown in figure 20.

Figure 20. A picture of the curled copper band used to balance the cover slips. Its maximum capacity is eight cover slips at a time.

Some depositions were done on electrospun cellulose membranes. As these are very light, they were secured with small clips to ensure that they did not move around, as shown in figure 21.

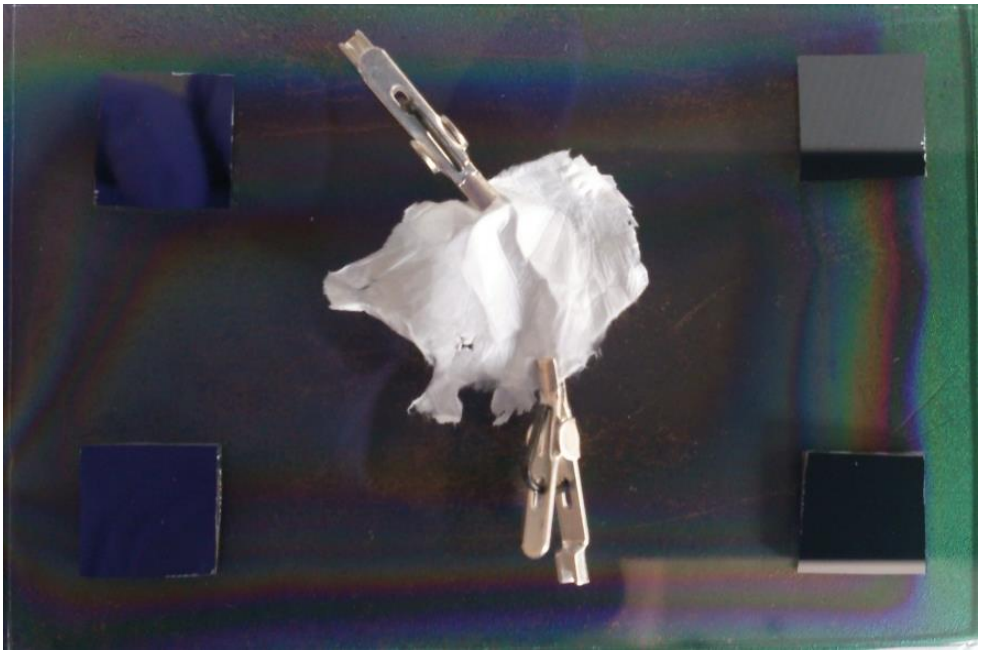

Figure 21. A picture of the clamped cellulose membrane and four normal substrates on the 7.6 mm long glass plate before deposition.

3.1.4 Reaction times and temperatures

If nothing else is specified, the timeframe described in table 3 for pulsing/ purging has been used. These values were obtained from the QCM measurements described in chapter 4.1.2.

Table 3. This table shows the pulsing and purging times for the TTIP/lys/water-reaction.

TTIP pulse	TTIP purge	Lys pulse	Lys purge	Water pulse	Water purge
1 s	1 s	2 s	1 s	2 s	3 s

For the runs with no water pulse, the TTIP and lysine pulsing and purging times still remained the same. Furthermore, the cycle has been repeated 1000 times if nothing else is specified.

The reaction temperature has been one of the parameters varied in this study. However, a standard which has been used in many depositions, including the QCM runs, has been a reaction temperature of 225^{o}C. For these reactions the temperature gradient in table 4 has been used.

Table 4. This table shows the temperatures in the different zones when the reaction temperature was 225^{o}C.

Zone 1	Zone 2	Zone 3	Zone 4	Zones 5-8 (reaction zones)
110 ^{o}C	140 ^{o}C	175 ^{o}C	200 ^{o}C	225 ^{o}C

For depositions using the temperature gradient described in table 4, the precursor boat with lysine was placed in between end of zone 2 closest to the reaction chamber. The choice of placement of the precursor boat was based both on results from the precursor tester (see chapter 4.1.1) and simply trial and error. If the precursor boat was placed too close to zone 1, thinner films were obtained. On the other hand, if the precursor boat was placed too close to zone 3, the precursor experienced a dramatic color change, from white to black and brown during deposition. For depositions with other deposition temperatures than shown in table 4, it has been the aim to keep the temperature of the lysine constant. This has been achieved both with adjusting the temperature gradient itself and the placement of the precursor both, which in several runs have been in the leftmost end of zone 2 (according to Figure).

3.2 Characterization of thin films

3.2.1 Quartz crystal microbalance

The quartz crystals used were purchased from Inficon/ Maxtek. The holders for the crystals are homemade and made to fit into the reaction chamber. The crystals are connected to a PLO-10i phase lock oscillator from Maxtek, which is again connected to a TM-400 Thickness Monitor. A homemade LabVIEW program was used to log the frequency changes of the crystals with a speed of 10 Hz. In all the runs two quartz crystals were used to avoid an unsuccessful experiment if one of the sensors stopped working. The data presented in this thesis represents the average of these two plots.

3.2.2 Ellipsometry

A spectroscopic ellipsometer of the type Woolham Alpha SE was used together with the Complete Easy software to measure the film thickness and the refractive index at a wavelength of 632.8 nm on the incoming beam. The measured range of wavelengths was from 380 nm to 890 nm, and the angle between the sample and the incoming beam was 70°. A Cauchy-function optimized for transparent films on silicon wafers was used to model the data.

3.2.3 Precursor tester

The precursor tester used in this work is made at University of Oslo. Figure 22 shows a block diagram of the setup. It should be noted that this is a newly assembled piece of equipment that is still in the process of optimization.

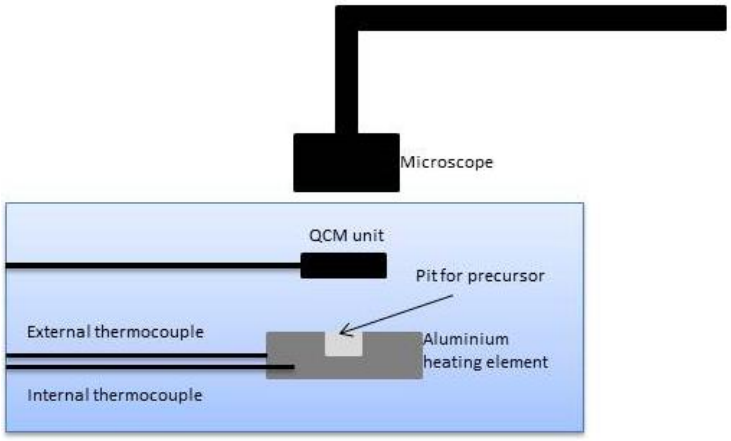

Figure 22. The setup for the precursor tester. The precursor itself is let into a pit in an aluminum heating element. The temperature of this element is controlled by the internal thermocouple. The temperature logged, however, is the one from the external thermocouple which is closer in temperature to the precursor. There is also a QCM unit just above the pit and a microscope viewing the precursor.

A limitation on this instrument is that only the aluminum block is heated. The precursor tester therefore resembles a *cold wall* reactor, which is a reactor where only the substrate is heated.

The microscope is put in a time-lapse mode where it takes pictures every 30 s. Pictures from before and after the precursor has started to sublime are shown in figure 23.

Figure 23. Pictures taken with the precursor tester before and after the sublimation of lysine started.

3.2.4 Fourier transform infrared spectroscopy

All the measurements were supposed to be done in transmittance mode using a Bruker IFS 66v/S spectrometer at a pressure of 3 mbar. The software used for the measurements was Opus 6.5 from Bruker. The measurement area, which was between 8000 and 0 cm^{-1}, was scanned 64 times for better statistics.

However, the preferred FTIR equipment became unavailable during this work, so some measurements were performed at an IRPrestige-21 instrument from SHIMADZU using the included software. For these measurements the measurement area and number of scans were kept the same. This instrument has no vacuum mode, so all the experiments were performed with air in the chamber.

3.2.5 X-ray characterization

A thin film diffractometer of the type PanAlytical Empyrian was used to conduct both GIXRD and XRR measurements. The instrument uses copper radiation and the optics used is described in table 5.

Table 5. Optics used in the XRD and XRR experiments.

	Primary beam line	Secondary beam line
XRD	Parallel beam mirror, 1/32° divergence slit	Soller-slits 0.04 rads, 0.27° parallell plate collimator
XRR	Parallel beam mirror, 1/32° divergence slit	Soller-slits 0.04 rads, XRR-slit

Moreover the XRR data was analyzed using the X'Pert Reflectivity software from PanAlytical, and the GIXRD data was analyzed using Highscore, also from PanAlytical.

3.2.6 Goniometry

The goniometer used is built at University of Oslo based on parts from Ramé-Hart Instruments. The software used was DROPimage Standard which is also the software used by Ramé-Hart. All the measurements were done by adding 2µL water stepwise until the droplet was 10µL. The contact angle was measured immediately after the last droplet was added, and for each sample, ten measurements were done right after each other, with the same droplet. The average of these measurements is the number reported in this thesis.

3.2.7 Atomic force microscopy

The AFM used in this thesis was a XE-70 microscope delivered from Park Systems. The software used for measurement and data treatment were XEP and XEI respectively. These programs are also delivered from Park Systems. In order to get better data a sound insulation box is installed around the microscope. A Non Contact High Resolution (NCHR) tip from Park Systems was used and it had a diameter of less than 10 nm. All the experiments were conducted in non-contact mode.

3.2.8 Scanning electron microscopy

A FEI Quanta 200 FEG ESEM electron microscope was used to study the structure of the cellulose membranes. The tension used was 20.0 kV and instrument was in low vacuum mode.

3.3 Cell growth

3.3.1 Sterilization and precautions

As the ALD-coating process involves heating the substrates above 200 ^{o}C in vacuum for an extended period of time (at least two hours for the shortest runs), the substrates were regarded as sterile when they were taken out from the ALD-reactor. However, the substrates needed to be transported from the Department of Chemistry at University of Oslo to Ullevål University Hospital, a stretch of approximately 1.5 km. During this transportation step the samples were carried in a closed plastic box. The box was pre-sterilized by wiping it with ethanol.

In the first experiments the substrates were also sterilized with ethanol. However, the ethanol seemed to stick to the substrates, even if it was rinsed with a balanced salt solution several times. This conclusion was drawn since all the cells seeded on these substrates died. Further experiments were done with substrates sterilized with UV-light. The sterilization was performed in the BSC and took 19 minutes.

3.3.2 Cell lines

There have been used two different types of cells in this work, one continuous and one with a limited life-span. The first are regarded as easier to handle, whereas the second may be more sensitive and therefore give better information about how the substrates will perform in the actual thought application. The continuous cell line was ARPE-19. It immortalized spontaneously and has a normal karyotype [109]. The limited life-span culture was derived from donors and passaged three times before used in this study.

3.3.3 Sub-culturing cells

The cells were examined during the different steps of sub-culturing, using a Leica DM IL LED microscope with various magnifications, usually 200x.

The medium used was Dulbecco's modified Eagle's medium:F12 (DMEM) from Sigma Aldrich. FBS from Gibco was added in a 1:10 relationship with the medium, in addition to penicillin/streptomycin (PS) in a 1:100 relationship. The latter is a combination of two antibiotics purchased from Sigma Aldrich. Hank's balances salt solution provided from Sigma Aldrich was also used in this work. The trypsin used contained 0.25 % EDTA and was provided from Life Technologies.

When sub-culturing the cells, the method described in 2.1.4 was used. The cells were seeded out from 75 cm^2 flasks made of polystyrene with vented caps. 3 mL of trypsin was used in each round, and 9 mL of DMEM was added after the trypsination. The incubator used contained 5 % CO_2.

96 welled plates pre-coated with poly-D-lysine purchased from Sigma Aldrich were also used as reference substrates.

3.3.4 Microscopy of cells

Before the cells were stained with a fluorochrome, they were fixated using methanol. The medium was aspirated and approximately 0.5 mL of methanol was pipetted into each well. The work was performed in a fume hood and not in a BSC. The methanol was left in the wells for 15 minutes. After this the methanol was aspirated and the wells with the coverslips were rinsed three times with Hank's balanced salt solution. The last round of Hank's balanced salt solution was left in the wells. It was important to have enough to properly cover the coverslips, if not the cells may have dried out and not been available for further examinations.

The fixated cells were stained with PI. The PI was provided from Sigma Aldrich with an initial concentration of 1.0 mg/mL. Before the staining was performed it was diluted with Hank's balanced salt solution in a 1:200 concentration. PI is a light sensitive compound, and unnecessary exposure to light will make the PI less intense when studying it in the microscope. Therefore, all containers with PI are wrapped in aluminum foil. After aspirating the salt solution, 0.5 mL of the PI solution was added into each well. It was left there for five minutes before the solution was aspirated and enough Hank's balanced salt solution to cover the coverslips was added into each well. The microscopy of the cells should be

performed as fast as possible after the cells are stained to minimize the fading of the samples.

This work used a Nikon Eclipse Ti fluorescence microscope. The software used was NIS-elements and the images were treated in ImageJ afterwards.

4. Results

This chapter is divided into four main subchapters. The first will present the results from the work concerning the ALD process itself and the precursor used. The next main subchapter is about further characterizations of the thin films. Thirdly there is a subchapter about coating cellulose membranes, which is a possible use for the coating process. Lastly, there is a subchapter about the cell growth experiments.

4.1 The atomic layer deposition process

4.1.1 Precursor tester

The precursor tester was used to determine the sublimation temperature of lysine.

Figure shows a plot of the resonance frequency of the QCM crystal versus the temperature of the aluminum block.

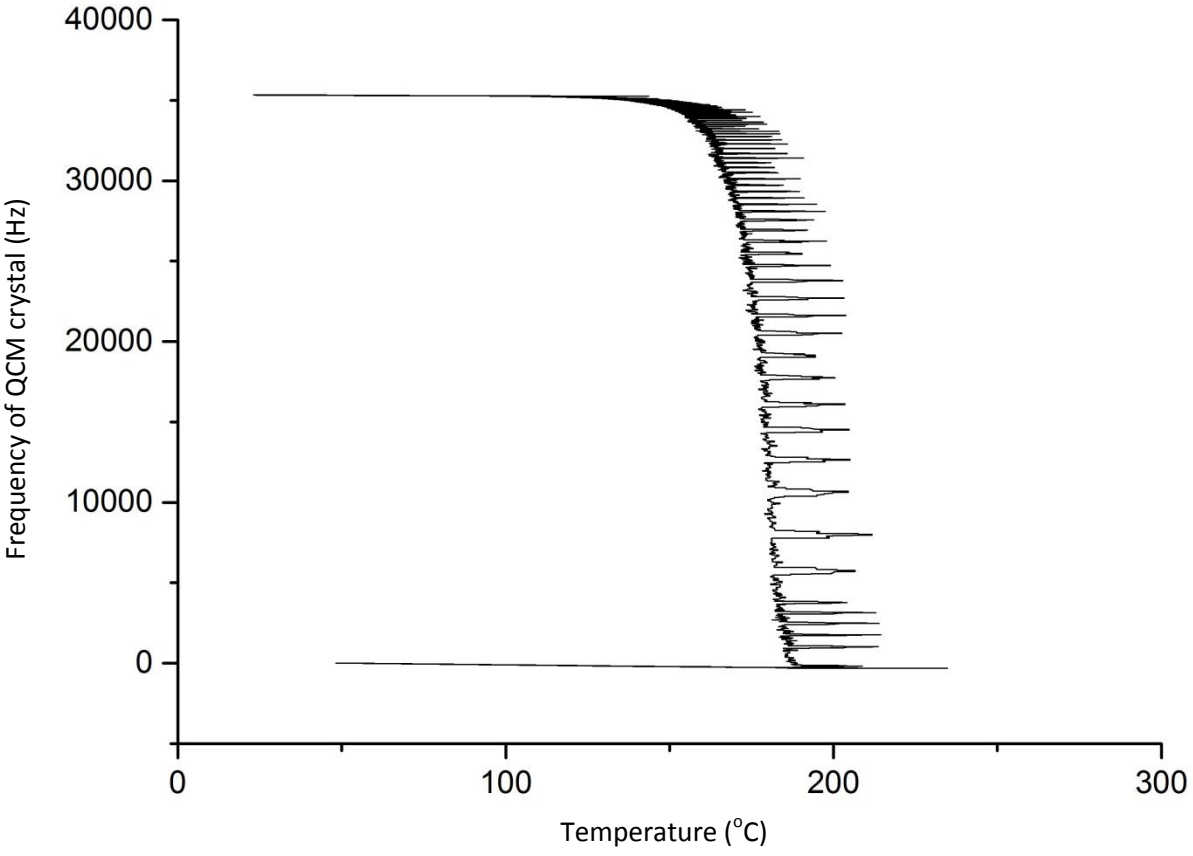

Figure 24. A graph showing the resonance frequency of the QCM crystal versus the temperature of the aluminum block.

The resonance frequency of the QCM crystal is relatively stable until the temperature reaches around 155 °C, where it starts to decrease. This is due to an increasing mass of the

quartz crystal as the precursor is condensing on its surface. The graph shows several spikes in the temperature direction during the experiment. The origin of this is somewhat unclear, and most probably related to electronic noise. The real temperature signature is taken along the low temperature line of the graph. However, the general trend is that the frequency is rapidly reduced for temperatures above 150 °C. The mass of QCM crystal remains near constant during cooling, indicating that the signal is due to a real deposit on the QCM crystal.

An alternative visual measure of when the lysine starts to sublimate can be found by studying the time-lapse pictures of the sublimation process. A picture comparing the state just before the sublimation starts with the very first sign of sublimation is shown in figure 25. The temperature is then around 152 ^{o}C.

Figure 25. Two micrographs from just before the sublimation starts and just after. The micrographs is taken with a 30s time interval in between. The particle surrounded by the blue circle is notably smaller in the right micrograph, which is the one taken last. The real diameter of the pit is 7 mm and the width of the entire initial bulk of lysine is therefore estimated to be around 4-5 mm.

The sublimation progresses slowly in the beginning, with only a small visual difference from micrograph to micrograph. These differences are mainly in the smaller particles, as in figure 25. However, as the temperature approaches 180 ^{o}C, the difference between the adjacent micrographs become very clear. This is illustrated in figure 26 with adjacent micrographs taken at a temperature of 177 ^{o}C.

Figure 26. Two micrographs from well into the sublimation process. The micrographs is taken with a 30s time interval in between. The micrograph to the right is the last picture.

Furthermore, the micrographs revealed that all the lysine sublimated, without leaving any residue behind when the temperature had reached 188 ^{o}C, as shown in figure 27.

Figure 27. A micrograph showing the empty aluminum block.

To further confirm that the sublimation process, the QCM frequencies have been plotted versus time in figure 28.

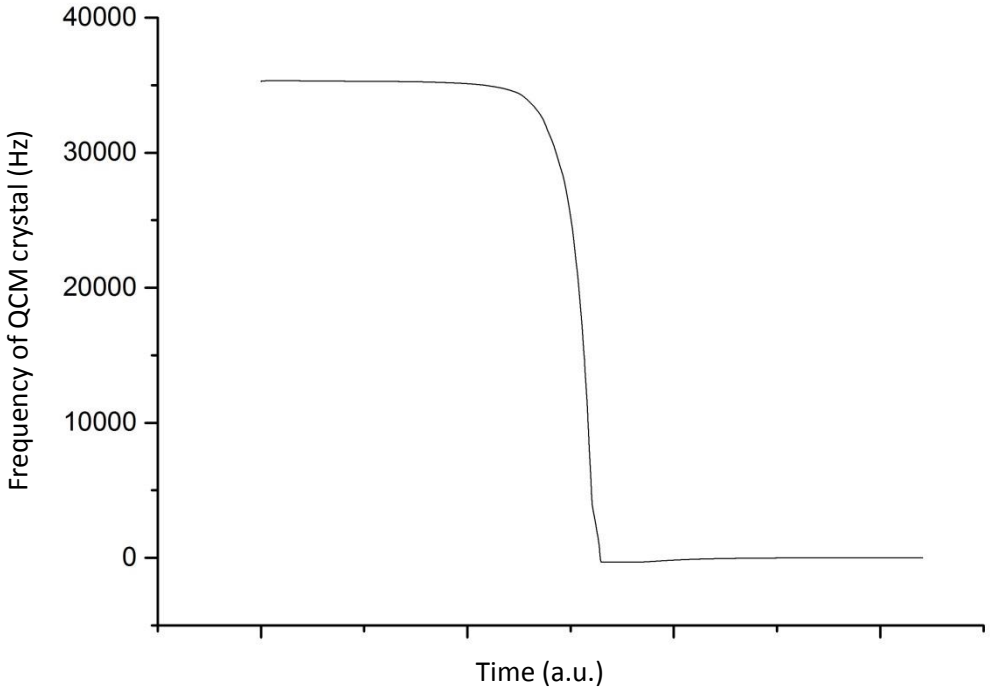

Figure 28. A plot of the QCM crystal's resonance frequency versus time.

It can be seen from figure 28 that the QCM graph gradually starts to go down, very slowly. Suddenly a lot of the lysine evaporates and the resonance frequency drops fast. After all the lysine has evaporated, the graph flattens out.

4.1.2 Quartz crystal microbalance

To determine the change of mass during deposition, and not just the frequency change, a calibration relation was made. Deposition of TiO_2 was used as reference since this is a well-known deposition system. Films of TiO_2 were deposited using pulsing parameters of 2s/ 1s/ 3s/ 5s for TTIP pulse, purge, H_2O pulse and purge, respectively. The reference film was synthesized the same temperature as the QCM measurements were performed, at 225 ^{o}C. The density and film thickness was determined by XRR analysis for the as deposited film, see chapter 9.2, Appendix B – QCM calibration. The parameters found from the QCM and XRR measurements used in the calibration relation are described in table 6.

Table 6. An overview of the values used for calculating the calibration factor, *K*.

r_{growth}, growth rate of reference film (nm/cycle)	0.0381
ρ, density of reference film (g/cm^3)	3.65
$\frac{\Delta f_{ref}}{s}$, frequency change per second of reference film (s^{-2})	0.395
t, time for one cycle (s/cycle)	7.5

The values in table 6 were plotted into equation 3 shown in chapter 2.4.1. This gave a calibration constant, *k*, equal to 0.047 $^{ng \cdot s}/_{cm^2}$. The QCM measurement of the film used for calibration is shown figure 29. Also, how this graph and the following ones are obtained must be mentioned. Firstly, two QCM crystals have been used for the measurements. Moreover, the three cycles presented for each QCM measurement are the average of the mid 16 cycles performed in the run. Hence the three presented cycles will be identical. The grey lines above and below the black ones plotted, represent the standard deviation.

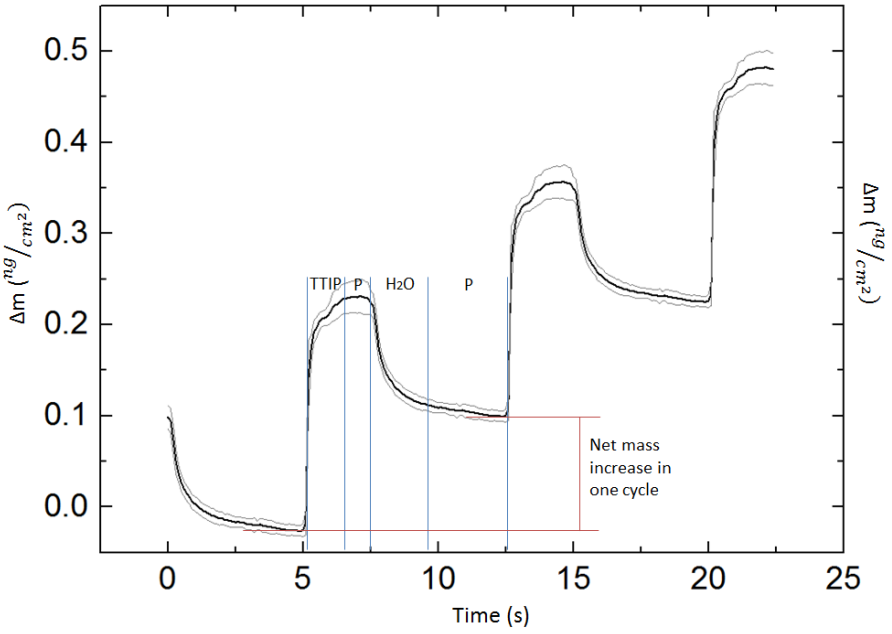

Figure 29. Mass change over time for the TTIP/water-process. The graph was obtained by QCM. This was also the reference film, making the calibration relation for the other QCM-experiments also. The TTIP pulse, purge, water pulse and purge are separated by blue lines. "P" stands for purge. The red bars show the net mass increase for one run.

From figure 29 the net mass increase for one cycle can be measured using the red bars on the graph. This method where the mass when one cycle starts is subtracted from the mass at end of the cycle, is also performed for the following graphs in this chapter. In this case the net mass increase per cycle is approximately 0.125 $^{ng}/_{cm^2}$. It can be seen that the vast part of the net mass increase comes from TTIP. In fact, when water is pulsed and purged the net mass decreases with approximately 0.123 $^{ng}/_{cm^2}$ per cycle. This can be explained by looking further into the mechanisms of chemisorption occurring at the surface. Provided that the surface is hydroxyl-terminated, the reaction scheme in equation is a possibility;

Equation 5. Suggestion of growth mechanism for TiO_2 from TTIP and water. S denotes surface species, whereas g denotes species in the gas phase.

TTIP-pulse: $(-OH)_n$ (s) + $Ti\{OCH(CH_3)_2\}_4$ (g) → $(-O-)_n$ $Ti\{OCH(CH_3)_2\}_{4-n}$ (s) + $n(CH_3)_2CHOH$(g)

Water-pulse: $(-O-)_n$ $Ti\{OCH(CH_3)_2\}_{4-n}$ (s) + 2 H_2O (g) → $(-O-)_nTi(OH)_{4-n}$ (s) +
(4-n) $(CH_3)_2CHOH$(g)

Considering Equation where it is shown that $(CH_3)_2CHOH$ is the leaving species and that the same number of H_2O molecules gets chemisorbed as the number of leaving $(CH_3)_2CHOH$ molecules, the mass decrease for the water pulse and purge is not surprising.

A QCM run was done early in the process to determine pulsing parameters for further depositions. This was performed just after it became apparent that it was actually possible to make films with TTIP and lysine as precursors. The deposition temperature for all the QCM experiments has been 225 ^{o}C.

For the TTIP/lysine system the various pulsing and purging times were investigated with QCM to establish a standard run, and the results are shown in figure 30.

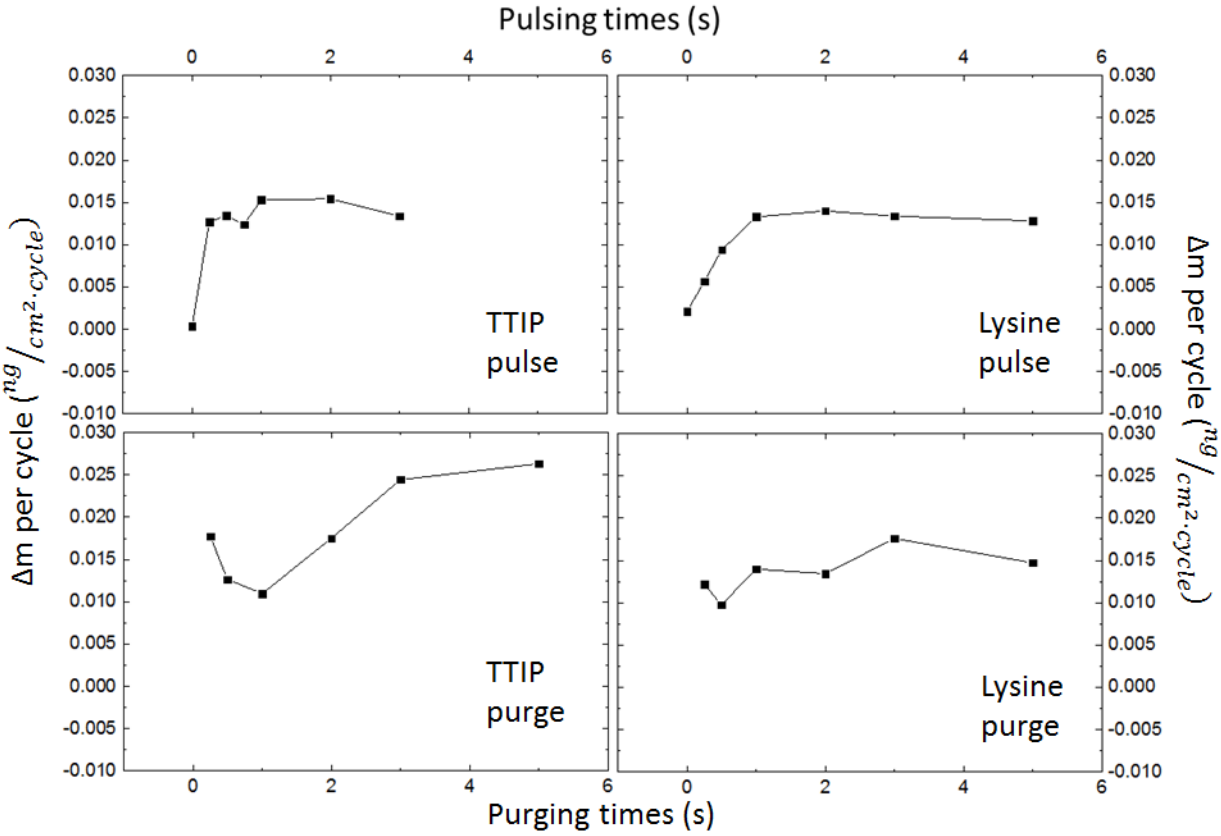

Figure 30. Pulsing and purging times versus mass increase per cycle for the TTIP/lysine system. The values not varied were held constant at 1s/2s/5s/2s for the TTIP pulse, purge, lysine pulse and purge respectively.

From figure 30 it becomes clear that the TTIP pulsing time reaches a plateau at around 0.5 s. To ensure sufficient saturation of the surface, 1 s was chosen as a standard. Similarly, lysine seems to reach the plateau at around 1 s. 2 s was therefore chosen as a standard. For the purging times 1 s looks sufficient for both precursors.

A similar experiment was conducted for the pulsing and purging times for water and the pulsing times for TTIP and lysine for the TTIP/lysine/water system. With these results the parameters for water pulsing and purging could be set. It was also of interest to study the effect of water in the system on the pulsing times of TTIP and lysine. The results of this investigation are shown in figure 31.

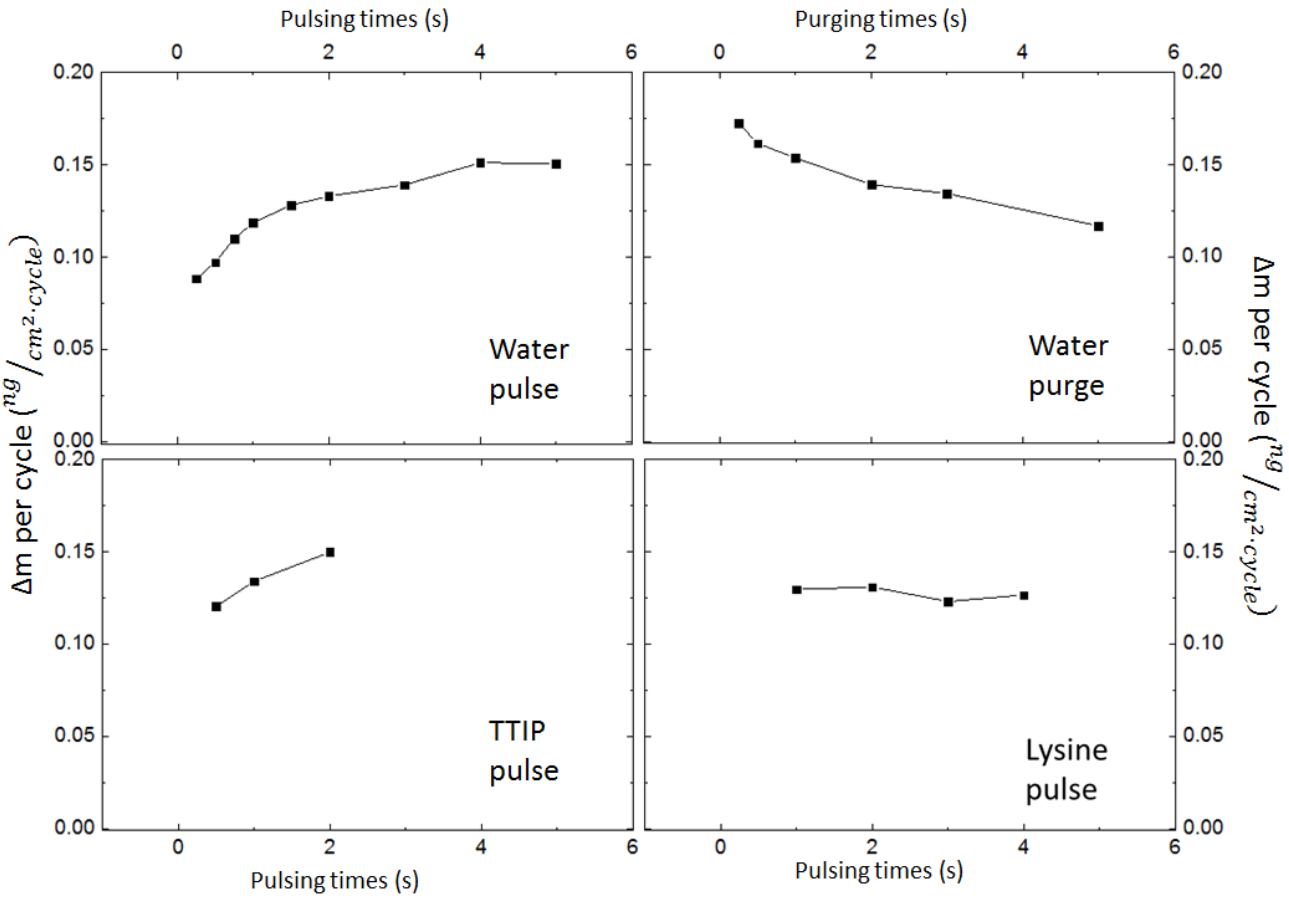

Figure 31. Pulsing and purging times versus mass increase per cycle for water and pulsing times versus mass increase per cycle for TTIP and lysine for the TTIP/lysine/water system. The values not varied were held constant at 1s/1s/2s/1s/2s/3s for the TTIP pulse, purge, lysine pulse, purge, water pulse and purge respectively.

Using Figure the pulsing and purging parameters for water were decided upon. As the pulsing graph starts to flatten out at 2s, this was set to be the standard pulsing time. Considering the graph varying the purging times for water, 3 s was thought to be sufficient.

Long-pulsing experiments have been performed for several systems investigated in this study. These QCM-measurements are used to prove the true ALD character of systems, that the growth is indeed self-limiting. The long-pulsing experiments are also used to find the net mass increases of a single cycle. These net mass increases should further be compared for the ones with standard pulsing times. Also, studying what happens when the pulsing order is altered is done with these long-pulsing experiments. In figure 32 results from long-pulsing of TTIP/lysine, TTIP/lysine/water, TTIP/(lysine + water) and TTIP/water/lysine are shown. The measured net mass increases per cycle in addition to the net mass increase per lysine pulse and purge are shown in table 8.

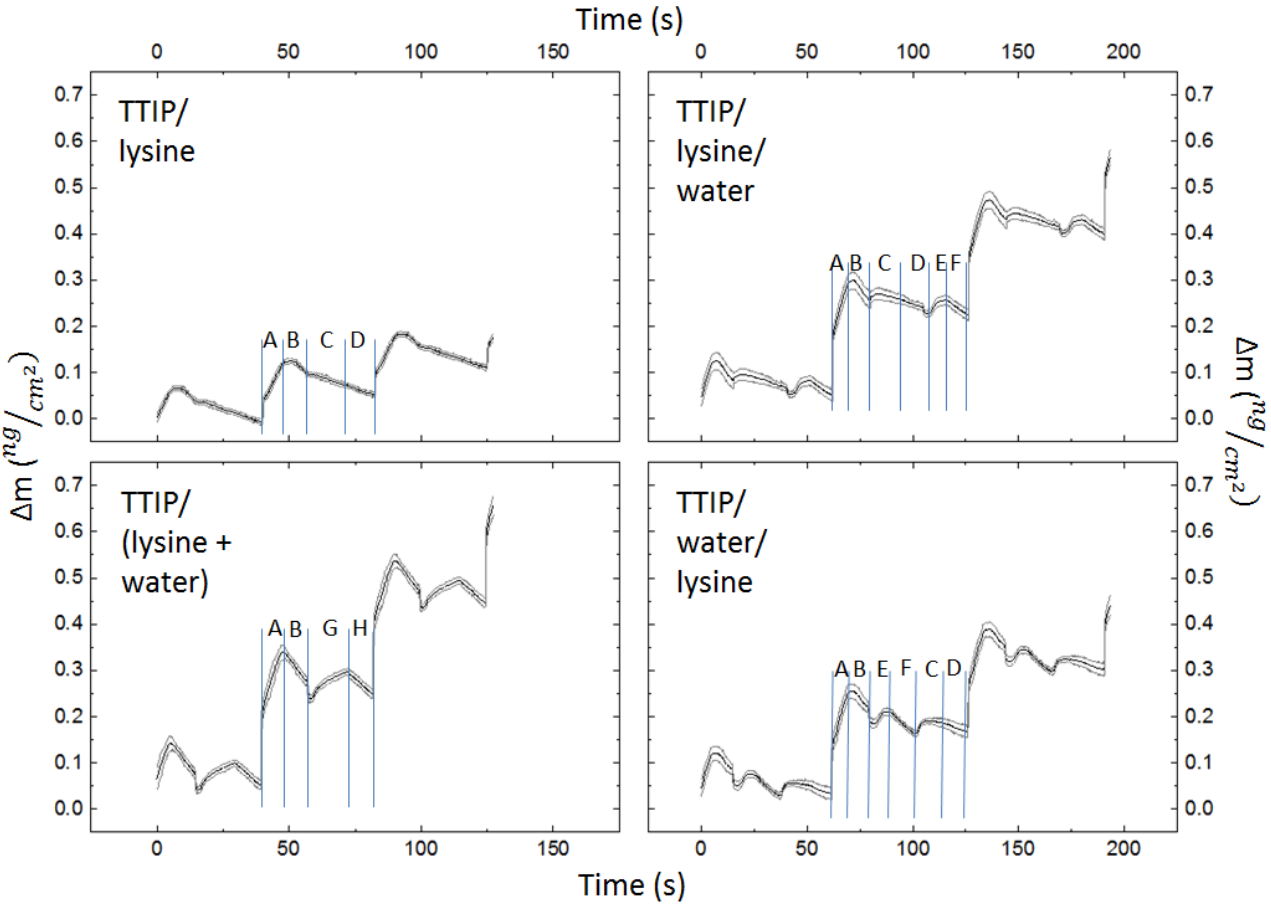

Figure 32. Long-pulsing experiments with the following pulsing parameters 7s/ 10s/ 15s/ 10s/ 7s/ 15s for the TTIP pulse, purge, lysine pulse, purge and water pulse and purge respectively. When lysine and water is pulsed simultaneously, the pulsing parameters for water are used. On the graph the various parts of the pulsing sequences are labelled in the following manner; TTIP pulse = A, TTIP purge = B, lysine pulse = C, lysine purge = D, water pulse = E, water purge = F, (lysine + water) pulse = G and (lysine + water) purge = H.

Table 8. Net mass increases per cycle for long-pulse experiments of various pulsing orders.

Pulsing order	Net mass increase per cycle ($^{ng}/_{cm^2 \cdot cycle}$)	Net mass increase per TTIP pulse and purge ($^{ng}/_{cm^2 \cdot cycle}$)	Net mass increase per lysine pulse and purge ($^{ng}/_{cm^2 \cdot cycle}$)	Net mass increase per water pulse and purge ($^{ng}/_{cm^2 \cdot cycle}$)
TTIP + lysine	0.048	0.091	-0.043	-
TTIP + lysine + water	0.184	0.200	-0.015	-0.001
TTIP + (lysine + water)	0.198	0.187	0.011*	-
TTIP + water + lysine	0.134	0.154	0.004	-0.024

*= For this sample water was pulsed simultaneously as lysine.

Figure 32 and table 8 show several differences between the systems and reveals that the order of the pulsing matters for the produced films. Firstly, it becomes clear that having water in the system increases the growth rate, as the growth rate of the TTIP/lysine system is much lower than for the other systems at 225 ^{o}C. Also, the net mass increases after a lysine pulse and purge are different between the systems. For the TTIP/water/lysine system, this net mass change is so little, it should be regarded to be within the uncertainty of the measurement, and it is anyways close to 0. A change in the order of water and lysine pulses, e.g. the TTIP/lysine/water system, makes the net mass increase after lysine pulse and purge become significantly negative. For the pure TTIP/lysine system the decrease in mass after the lysine pulse and purge is even larger. The most interesting from table 8 is perhaps the net mass increase for the simultaneously pulsed water and lysine. This is slightly positive, which is captivating when it is known that both precursors have negative net mass changes in the TTIP/water and TTIP/lysine systems. The values obtained for the TTIP/water/system, however, resemble the ones found for the TTIP/water calibration run, but relative to the net mass increase per cycle, the net mass increase after the water/pulse and purge is less negative.

A factor that may lead to misleading QCM results in this case, is whether the TTIP purging time of 10 s is sufficient to remove the entire surplus from the 7 s long pulse. For the TTIP/lys system, the negative gradient in the lysine pulse may be influenced by TTIP molecules still leaving the surface. This tendency is not seen so clearly for the TTIP/lysine/water system, but for the TTIP/water/lysine system it seems to be a lag between the start of the water pulse and the increase in mass. Similarly, is there a lag between the start of the (lysine + water) pulse in the TTIP/(lysine + water) sample.

It was also of interest to see QCM values for runs with the standard pulsing times. These are shown in figure 33 and their corresponding net mass increases per cycle are shown in table 9.

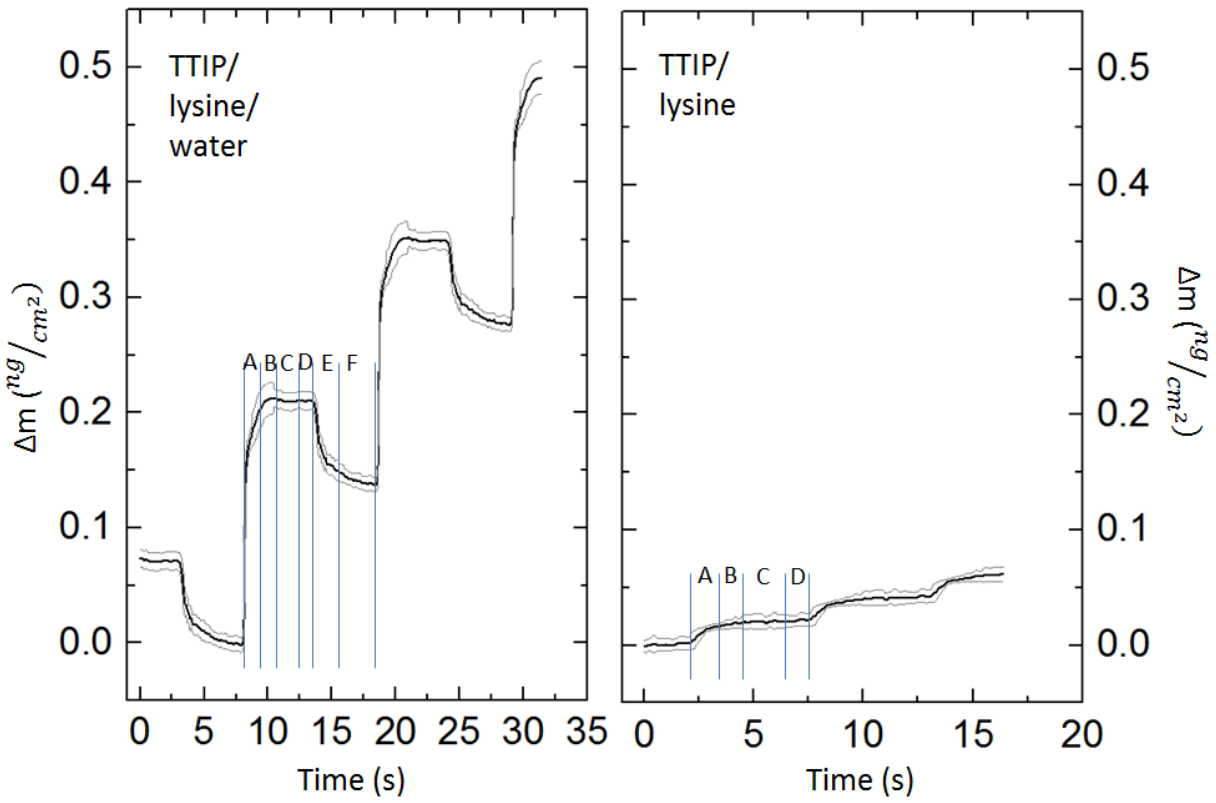

Figure 33. QCM of the standard runs with the following pulsing parameters 1s/ 1s/ 2s/ 1s/ 2s/ 3s for the TTIP pulse, purge, lysine pulse, purge and water pulse and purge respectively. On the graph the various parts of the pulsing sequences are labelled in the following manner; TTIP pulse = A, TTIP purge = B, lysine pulse = C, lysine purge = D, water pulse = E, water purge = F.

Table 9. Net mass increases per cycle for standard runs with and without water.

Pulsing order	Net mass increase per cycle ($^{ng}/_{cm^2 \cdot cycle}$)	Net mass increase per TTIP pulse and purge ($^{ng}/_{cm^2 \cdot cycle}$)	Net mass increase per lysine pulse and purge ($^{ng}/_{cm^2 \cdot cycle}$)	Net mass increase per water pulse and purge ($^{ng}/_{cm^2 \cdot cycle}$)
TTIP + lysine	0.021	0.019	0.002	-
TTIP + lysine + water	0.138	0.208	-0.002	-0.068

The first obvious observation from figure 33 and table 9 is the difference in growth rates between the systems. It seems like the surface in the TTIP/lysine/water system after the water pulse is much easier to react with for TTIP than a surface that was last exposed to lysine. This is clear from the net mass increases for the TTIP pulse and purge, which is more than 10 times higher in the TTIP/lysine/water system. Furthermore does the shape of the TTIP/lysine/water standard resemble the one found for the TTIP/water system found shown in figure 29. However, relative to the net mass increase for the system, the mass reduction after the water pulse has a lower magnitude for the TTIP/lysine/water system than for the TTIP/water system.

One thing that also becomes apparent from figure 33 and table 9 compared to the long-pulse experiments is that the mass no longer decreases after the lysine pulse. It remains constant and the values are approximately equal for both systems shown.

4.1.3 Temperature dependency

Films were deposited at temperatures ranging from 205 ^{o}C to 400 ^{o}C to characterize the effect of deposition temperature on the growth rate and also on the refractive indices. Both the film thicknesses and refractive indices were measured by ellipsometry. Results from these measurements are shown in figures 34-35. As the deposition at 400 ^{o}C for the TTIP/ lysine system probably lead to decomposition of the precursors and resolved in a lot of uncontrolled deposition in the reactor, this experiment was not reproduced for the TTIP/lysine/water system.

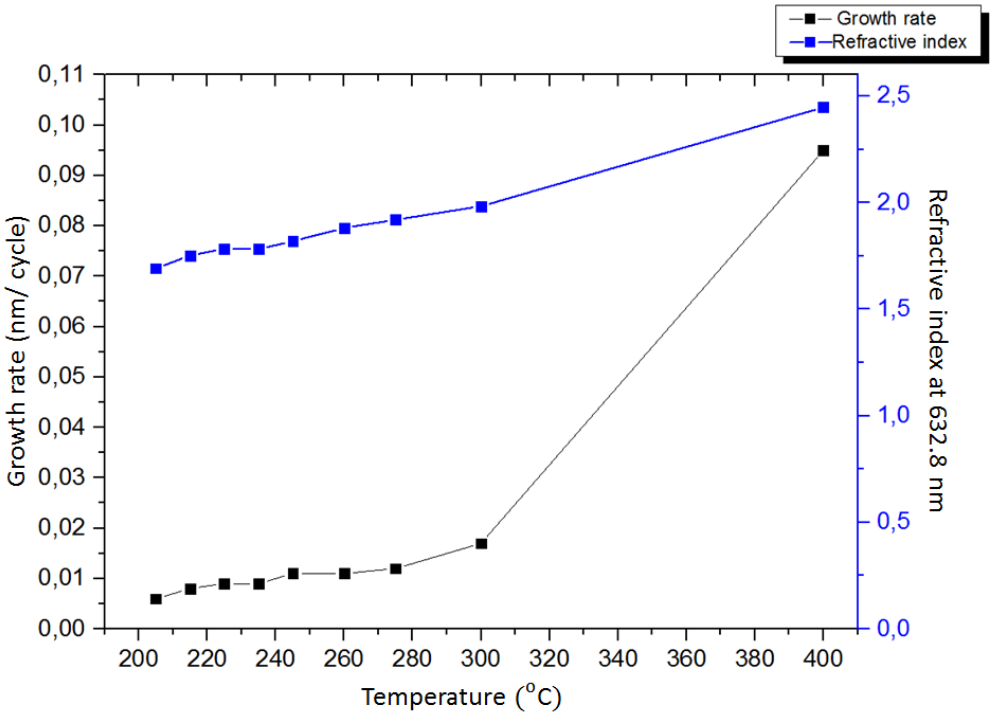

Figure 34. Growth rates and refractive indexes as functions of temperature for the TTIP/lysine system.

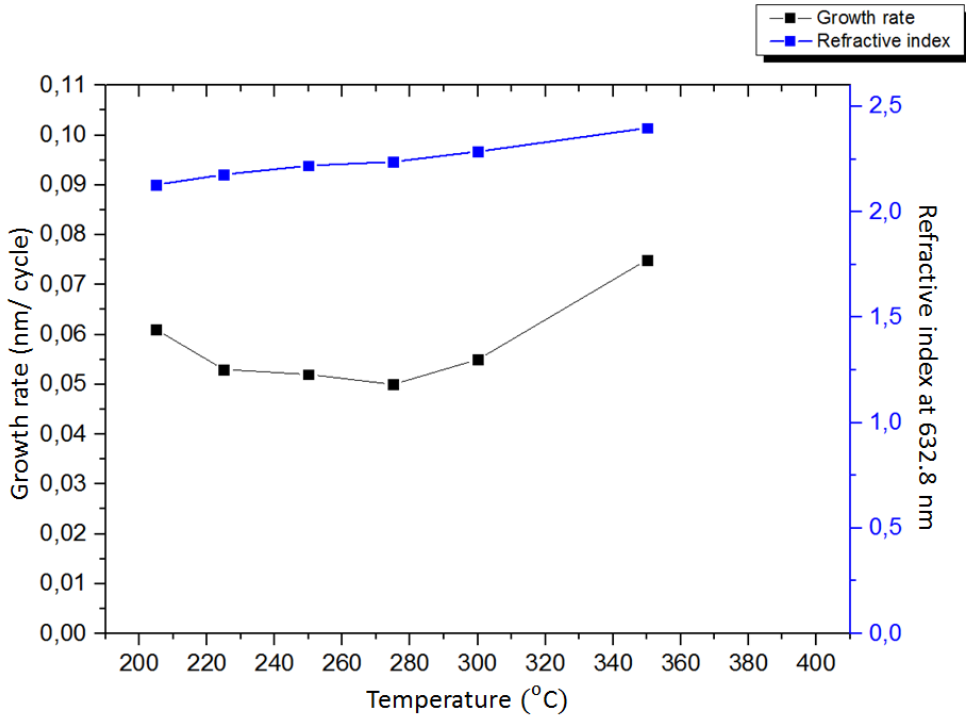

Figure 35. Growth rates and refractive indexes as functions of temperature for the TTIP/lysine/water system.

It becomes apparent from figures 34-35 that the temperature dependencies are not the same for the two systems. For the TTIP/lysine system the growth rate slowly increases with temperature up until 300 ^{o}C, before the growth rate becomes remarkably higher at 400 ^{o}C indicating a decomposition process. The slow and steady increase in growth rate over time is probably due to better kinetics. This linear tendency is not found for the TTIP/lysine/water system. Also, for lower temperatures, the growth rate increased for the TTIP/lysine/water system, which may indicate a condensation reaction happening.

For both the systems the refractive index increases with temperature. However, it should be noted that even if the increasing tendency is the same, the absolute values for the refractive indexes are higher in the TTIP/lysine/water system than in the TTIP/lysine system for the corresponding temperatures. The measured refractive index at 632.8 nm for the TTIP/water films made at 225 ^{o}C was 2.487, and the TTIP/lysine/water system shows values closer to this than the TTIP/lysine system. This may indicate the presence of more TiO_2 in the TTIP/lysine/water system.

4.1.4 Linearity of the process

For a system to show ALD growth, there should be a linear relationship between the number of cycles and the thickness of the film. To investigate if this was the case for the TTIP/lysine and the TTIP/lysine/water systems, the number of cycles were varied and the other parameters were kept constant. The results of this investigation are shown in figure 36.

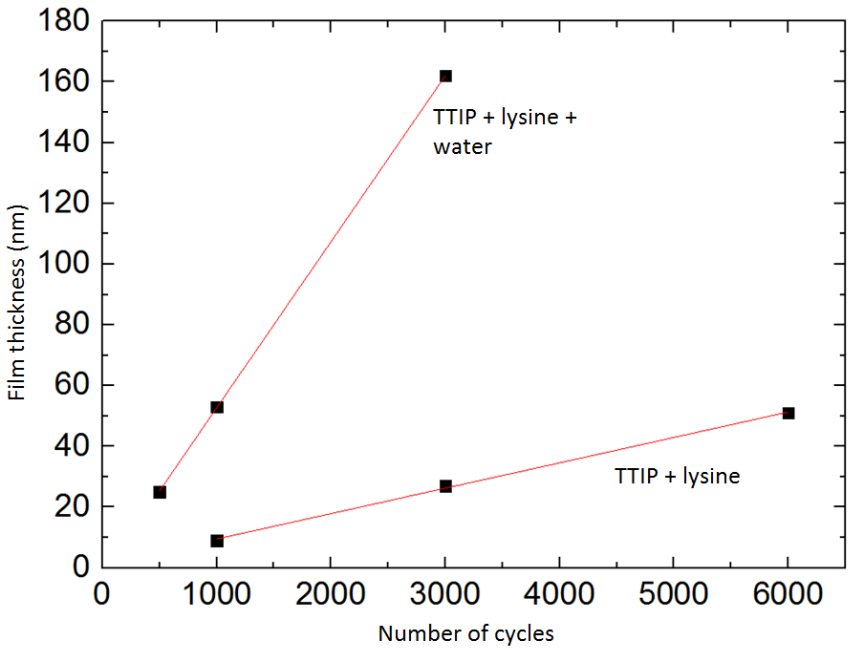

Figure 36. Graphs showing the linear relationships between number of cycles and film thickness measured with ellipsometry for the TTIP/lysine and the TTIP/lysine/water systems. All the films are made at 225 °C. The red lines are fitted with the use of Origin.

As can be seen from figure 36 both the systems showed a linear relationship between the number of cycles and the film thickness. However, depositing with lower number of cycles was not investigated here, due to the limited growth rates of the system. Such investigation might have revealed nucleation challenges in the early stages of the deposition, but this was not of a practical concern for these systems

4.1.5 Importance of pulsing order

A selection of experiments were conducted to investigate the importance of pulsing order on the films obtained, either by pulsing water before lysine or lysine and water simultaneously. Table 10 gives the film thicknesses and the refractive indices measured by ellipsometry. As can be seen from the table, the TTIP/(lysine + water) film had gradients. This is further illustrated by a picture of the film in figure 37.

Table 10. Thicknesses and refractive indexes for samples with altered pulsing orders measured with ellipsometry. For the TTIP/(lysine + water) sample two values both the thickness and refractive index are given, as there was a huge gradient from middle to the edge of the sample.

Pulsing order	Thickness (nm), 3000 cycles		Refractive index	
TTIP/lysine/water	162 nm		2.117	
TTIP/water/lysine	135 nm		2.227	
TTIP/(lysine + water)	167 nm	139 nm	2.256	2.179

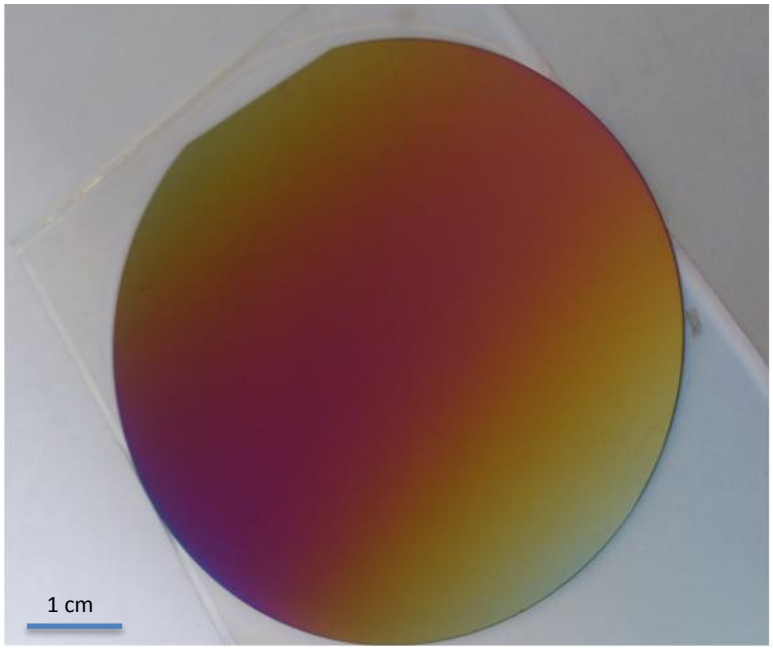

Figure 37. A picture of JNK1065, a TTIP/(lysine + water) film made at 225 °C with 3000 cycles. The color change across the film indicates a thickness gradient.

4.1.6 Film gradients

All the TTIP/ lysine and TTIP/lysine/water films further investigated in this thesis have had remarkably few gradients. Films with gradients of more than 0.5 nm in difference between the thinnest and thickest film have not been used further. Usually, the occurrence of uneven films has been due to dirty precursor tubes or substrates.

To illustrate the evenness of these films, an example of a typical run is shown in figure 38. It shows the distribution of five silicon substrates on the glass plate. The numbers on the drawing are the film thicknesses in nm measured by ellipsometry. As can be seen from the illustration, the film is very even with the front substrates being slightly thicker. This has also been the general trend for the other depositions. At most the gradient is 3.5 % / 7.5 cm.

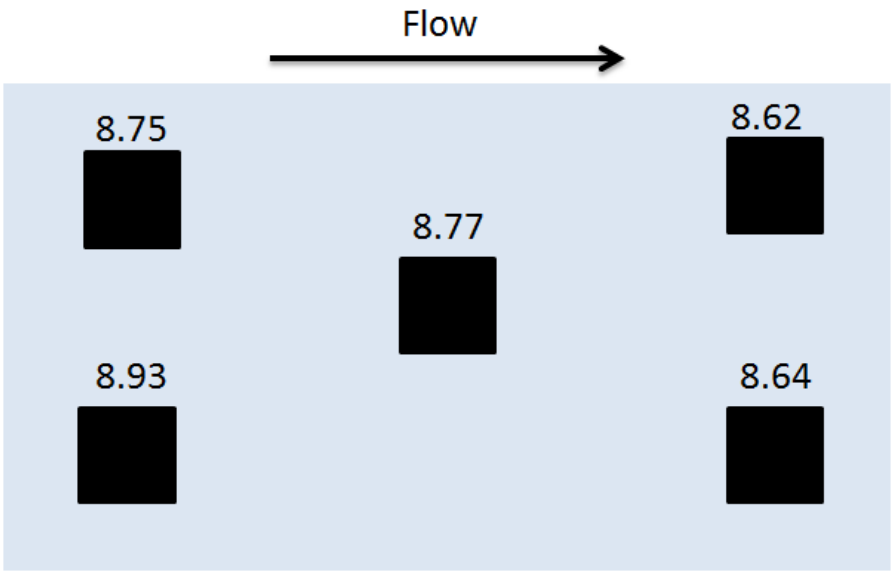

Figure 38. A drawing showing the distribution of silicon substrates on the glass plate (7.5 cm long) and their measured thicknesses in nm. This film was made at 225 °C with TTIP and lysine as precursors using standard pulsing times.

4.1.7 Stability over time

Selected samples were re measured with the ellipsometer after three and twelve months of storage to reveal the long term stability of the films. The results of these measurements are shown in table 11 which show that the TTIP + lysine and TTIP + lysine + water films are remarkably stable over time. The thicknesses of the films increase slightly over time, but not more than 10 percent or 2 nm for any of the samples. For the variation of thickness over time, there does not seem to be a difference for the samples with or without water-pulse. Neither does the deposition temperature seem to affect the long term stability. The most affected parameter is the refractive index of the films without water-pulse. It decreases remarkably, especially for the sample made at 275 °C. It was also observed a color change for this film, as the brown color on edge of the glass had faded somehow.

Table 11. An overview of the time-stability of selected films measured with ellipsometry three and twelve months after deposition.

Sample	Deposition temperature (°C)	Thickness immediately after deposition (nm)	Refractive index immediately after deposition	Thickness after three months (nm)	Refractive index after three months	Thickness after twelve months (nm)	Refractive index after twelve months
JNK1015, TTIP + lysine	225	10.5	1.931	10.8	1.902	11.1	1.866
JNK1017, TTIP + lysine	275	18.2	1.918	18.6	1.860	19.9	1.710
JNK1038, TTIP + lysine + water	225	54.6	2.170	55.0	2.165	55.5	2.178
JNK1040, TTIP + lysine + water	275	49.4	2.237	49.9	2.237	50.1	2.247

4.2 Characterization of thin films

4.2.1 Fourier transform infrared spectroscopy

The structure of L-lysine is given in figure 39 for convenience.

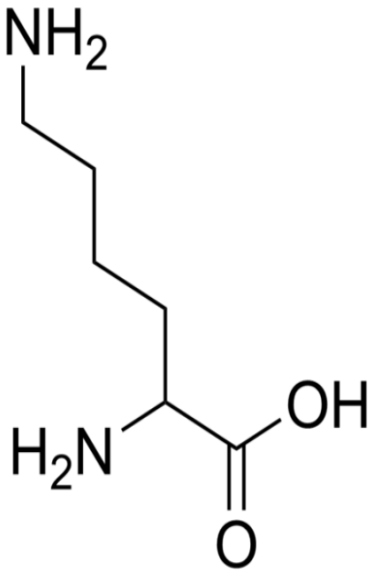

Figure 39. Structure of L-lysine.

FTIR analysis was performed on a selection of the samples to confirm that the films were indeed of a hybrid character, which means that it must contain the organic functional groups of lysine. Figures 40-41 show the FTIR spectrum of the TTIP/lysine and TTIP/lysine/water films immediately after deposition. The FTIR measurements were performed in transmission mode under vacuum. An 8-point Adjacent Averaging function is used to smooth the graphs, but all the peaks identified were present in both the smoothed spectra and the raw data.

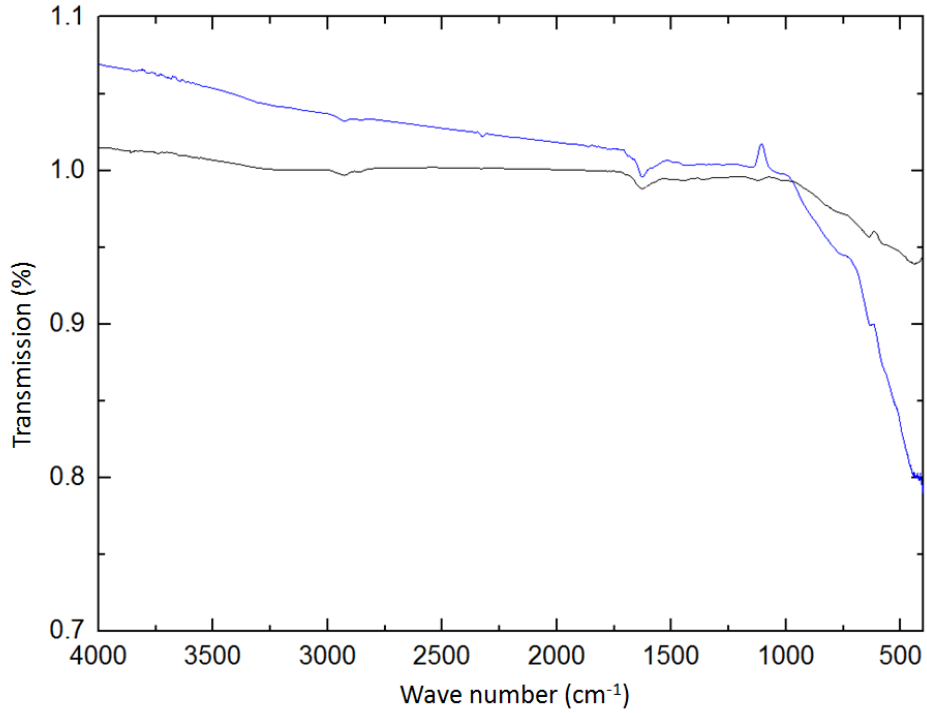

Figure 40. FTIR spectrums of JNK1044 (black lines) and JNK1046 (blue lines) right after deposition. The films were both made at 225 °C, but JNK1044 is a TTIP/lysine film whereas JNK1046 is a TTIP/lysine/water film. JNK1044 was made with 6000 cycles and had a thickness of 54 nm. JNK1046 was made with 2000 cycles and had a thickness of 105 nm.

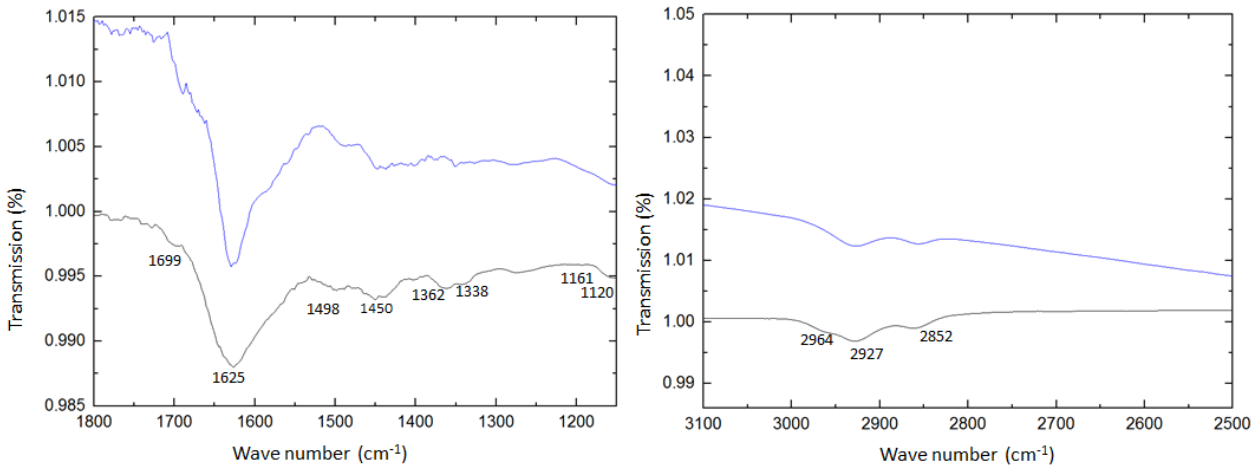

Figure 41. Enlarged parts of the FTIR spectra shown in figure 40. The numbers on the graphs refer to the most intense position of the peaks.

From figure 41, the peaks listed in table 12 were identified. The peak identification task was done in co-operation with Karina Barnholt Klepper. This was not easy, as the JNK1044 film is a bit too thin (54 nm) for FTIR analysis, where at least 70 nm of film is recommended. This is mostly due to the very poor growth rate of the system and it was unsure at the point of deposition whether the lysine precursor could actually withstand 225 °C for the time needed

to deposit 6000 cycles or not. The lysine experienced a color change during the deposition, from all white to dark brown on the top. However, as the material still showed a linear growth rate versus number of cycles relationship, it is assumed that the film studied here is representable for thinner films. Nevertheless, the peaks found in the spectrum very much resembles the expected outcome.

The wavenumbers of the peaks and interpretations of what the peaks correspond to are listed in table 12. As can be seen from the list, some of the peaks contain two overlapping signals.

Table 12. List of peak positions with interpretations for FTIR measurements performed on JNK1044 and JNK1046. The peak identification work is based on ref. [105, 106].

Peak position (cm^{-1})	Interpretation of peak
2964	NH_3^+ stretch
2927	CH_2 asymmetric stretch
2852	CH_2 symmetric stretch
1699	NH_3^+ asymmetric bend
1625 (broad)	COO^- asymmetric stretch, NH_2 deformation, NH_3^+ deformation
1498	CH_2 bending, NH_3^+ symmetric bend
1450	COO^- symmetric stretch
1438	CH_3 asymmetric deformation
1362	CH_3 symmetric deformation, CH_3 in isopropanol asymmetric deformation
1338	CH_3 in isopropanol asymmetric deformation
1161	C-C-N bend in amines
1120	C-N stretch in primary amines

Figure 40 also shows a larger gradient at lower wave numbers for the TTIP/lysine/water film than for the TTIP/lysine film. As the peaks arising from Ti-O and Ti-N bonds are expected between 550 cm^{-1} and 700 cm^{-1} [107], this increase in gradient may imply more of these bonds. More Ti-O bonds may be due to more titanium oxide in the film. Also, for the peaks in the fingerprint region, the intensities of both graphs are approximately the same. This is an interesting fact considering that the JNK1046 film is about twice the thickness of the JNK1044 film. One should be very careful to do quantitative analysis from FTIR data, as it is mainly a qualitative technique, but this may indicate that the organic component for both films are approximately equal and that the remaining part of JNK1046 thus is titanium oxide.

A careful reader may also notice a small peak, more significant for JNK1046 than for JNK1044, at around 2325 cm^{-1}. This is expected to be from an asymmetric C-O stretch from CO_2. Even though the instrument was at only 3mbar pressure, some CO_2 may still be in the chamber. If this amount is different when the sample is measured than when the background scan is taken, it will show on the spectrum.

It was also attempted to do FTIR spectrometry on JNK1044 and JNK1046 six months after deposition. However, at this time the preferred FTIR equipment had become unavailable and only an instrument with poor sensitivity was available. Measurements were attempted with the other instrument, but the signal to noise ratio was too low to get any proper information out of. It was also tried to do FTIR analysis of films were water was pulsed before or simultaneously as lysine, but these spectra are disregarded for the same reason.

4.2.3 Contact angles

As the contact angles are important for cell adhesion, these were investigated using a goniometer. The measured contact angles and the information about the corresponding samples are given in table 13. For all the samples, the substrate which had been in the middle of the reaction chamber was measured upon.

Table 13. This table presents the contact angles for the measured films and deposition temperatures and thicknesses for these films.

Sample	Deposition temperature (°C)	Contact angle(°)	Film thickness measured with ellipsometry (nm)
JNK1029, TTIP + lysine	225	58	9
JNK1031, TTIP + lysine	275	63	12
JNK1038, TTIP + lysine + water	225	63	53
JNK1040, TTIP + lysine + water	275	61	50
JNK1053, TTIP + water	250	11	40
JNK1064, TTIP + water + lysine, 3000 cycles	225	72	139
JNK1065, TTIP + (water + lysine), 3000 cycles	225	67	140

To further illustrate the vast difference in contact angles between the TiO_2 sample and the hybrid samples, pictures of JNK1029 and JNK1053 are put next to each other in figure 42.

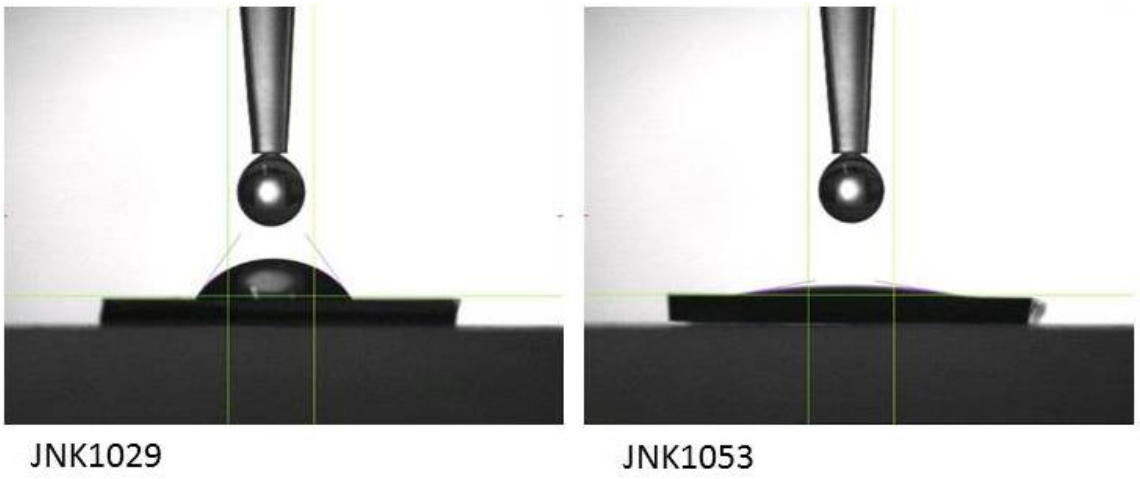

Figure 42. Differences in contact angles between the hybrid materials and the TiO_2 film. The hybrid sample is left and the oxide is at the right hand side.

As can be seen from table 13 the contact angles for all the hybrid samples are quite similar. They are all around 60° which means that they are hydrophilic, but just slightly so. The TiO_2 is however much more hydrophilic, with the contact angle only being 11°.

The uncertainties given by the goniometer should also be noted. They are reported to be in the range of $\pm 0.05^{\circ}$. As this a hundred-fold less than the results reported in table 13, the results from the goniometer should be regarded as very accurate. Also, for JNK1029 all five of the substrates were measured upon and they all gave a contact angle of 58°.

4.2.4 Crystallinity

The crystallinities of the samples were investigated with GIXRD. As the TiO_2-film deposited at 225 ^{o}C is used as a standard in this investigation, the film was characterized to see if the same results as the reported[69], were found. A comparison between a scan taken of JNK1002, a run with TTIP and water as precursors at 225 ^{o}C, and the expected scan of pure bulk anatase is shown in figure 43. Scans were made both immediately after the sample was taken out from the reactor and after a year of storage in air. The first scans were taken with a shorter program giving a poor signal-to-noise ratio, and the newest scans are therefore shown in the thesis as both of them show similar features.

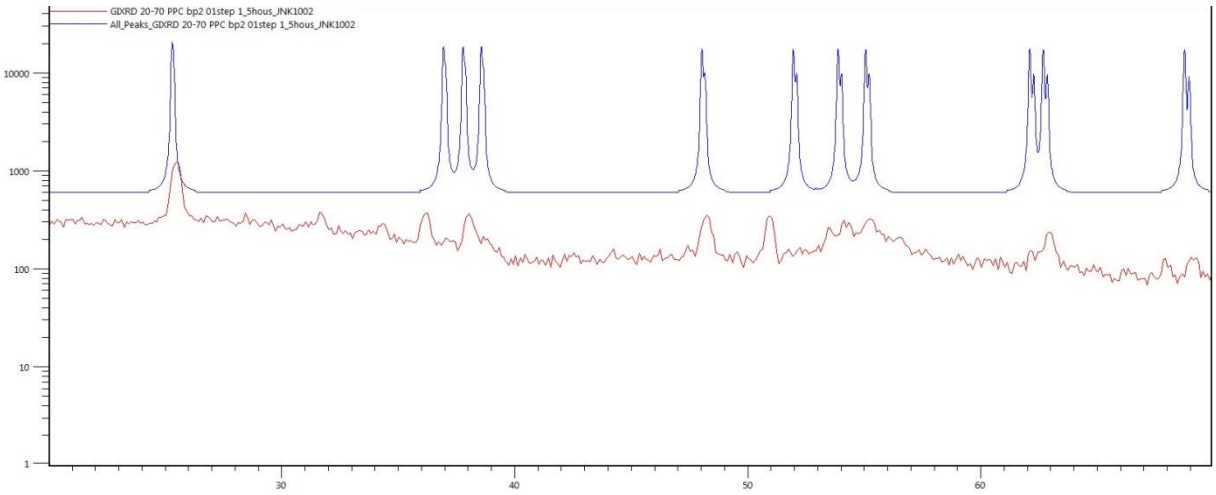

Figure 43. A diffractogram showing the measured diffraction pattern of JNK1002 (in red) and a reference diffractogram of bulk anatase (blue). The y-axis is in a logarithmic scale.

As can be seen from figure 43 the peaks of the measured scan are much less intense relative to the background than the reference pattern. Furthermore, the peaks are smeared out, which indicates that parts of the material are amorphous. Also, not all the peaks in the scan are reported for by the reference pattern. There have been problems with the instrument giving peaks at ω>60 ^{o}, where there is not supposed to be detected a signal. This is according to the person managing the instrument[108], and the reason for the phenomena is unknown. This may account for the small peaks in the far right of the diffractogram. Moreover, the silicon substrate and the native silicon oxide may give rise to signals. However, none of these spectrums gave a good match with the measured one when they were compared in Highscore.

To investigate the effect of a water-pulse together with or before the lysine-pulse, diffraction measurements were performed on such samples. Both the films tested were synthesized at 225 ^{o}C. For JNK1064 the orders of the water- and lysine-pulses were simply swapped. For JNK1065 water and lysine were pulsed simultaneously, with a pulsing time of 2 s and a purging time of 3 s. The diffractograms of both JNK1064 and JNK1065 are shown in figure 44. The diffractogram of JNK1002, the titanium oxide film, is also shown for comparison.

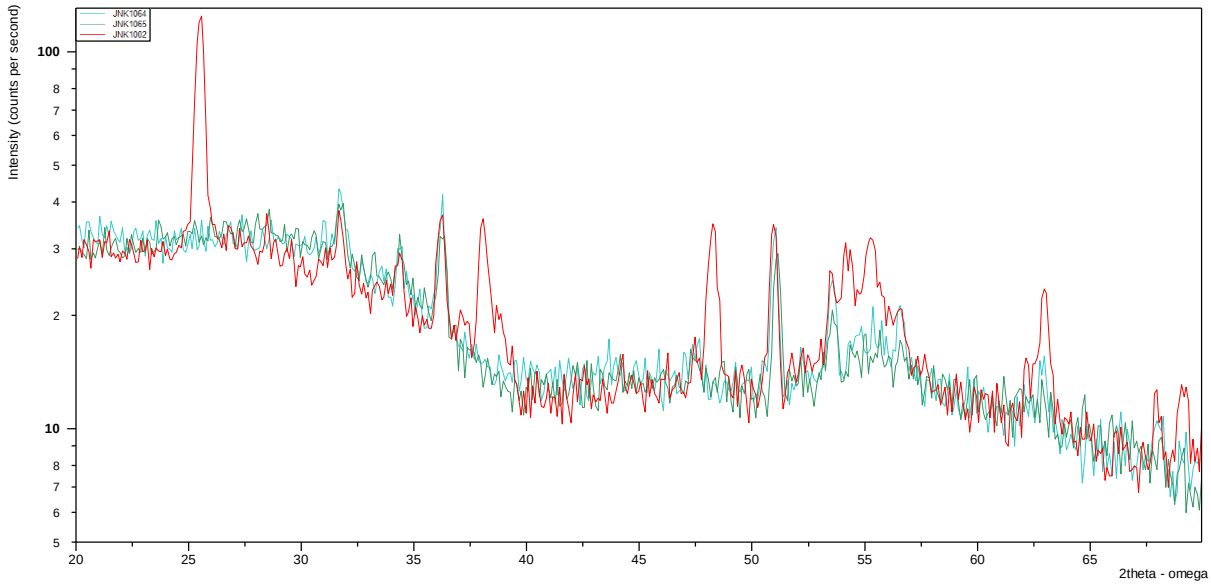

Figure 44. A diffractogram of JNK1002 (red), JNK1064 (turquoise) and JNK1065 (green). The y-axis is in a logarithmic scale.

The comparison between the diffractograms in Figure reveals that the first and most significant peak of the JNK1002-spectrum at about 25 ^{o} is absent in both the JNK1064 and JNK1065 diffractograms. This indicates an absence of anatase in JNK1064 and JNK1065. Moreover does the diffractograms of JNK1064 and JNK1065 overlap well, so it is fair to assume that they consist of the same material. The peaks in these diffractograms are so low in intensity and smeared out, that the material should be regarded as amorphous. However, there is a peak at around 51 ^{o} which is quite significant compared to the surroundings. This peak does not co-inside with any expected peaks from either silicon or titanium oxide. It does fit reasonable with a peak expected from the alpha quartz polymorph of silicon dioxide, but the rest of this spectrum is missing, so it may just be a coincidence.

Furthermore samples of hybrid films expected to be amorphous, were measured upon. The samples were both done with the standard run. JNK1014 is without the water-pulse and

JNK1038 is with a water-pulse. The diffractograms of these samples, together with JNK1002, is shown in figure 45. It should also be noted that a shorter program was used for JNK1014, as the sample anyway was expected to not show any peaks.

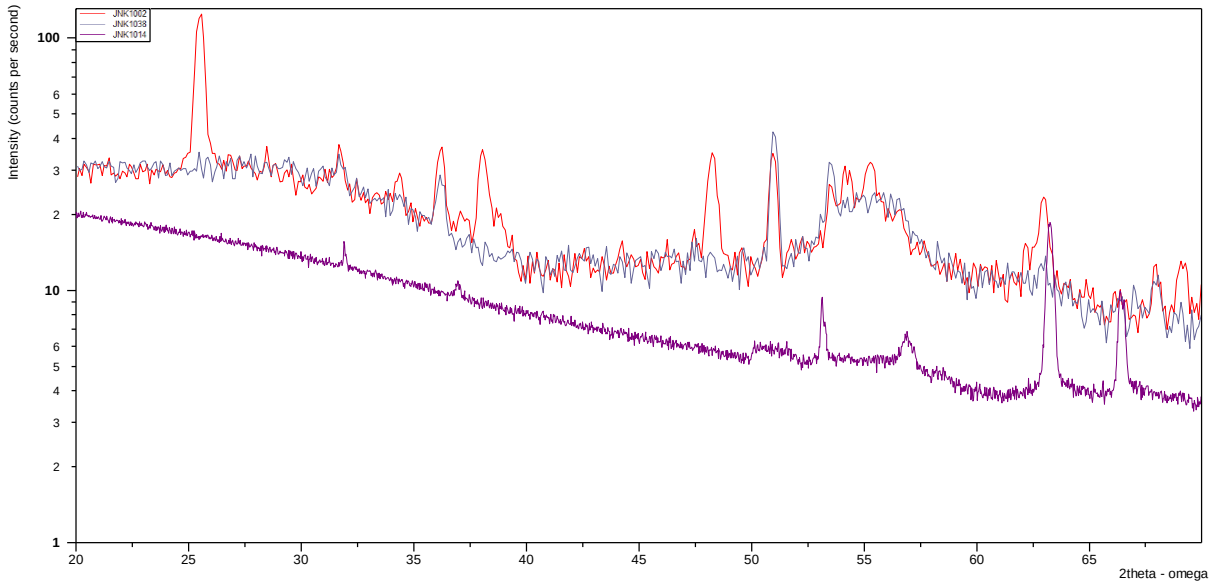

Figure 45. A diffractogram of JNK1002 (red), JNK1014 (purple) and JNK1038 (blue). The y-axis is in a logarithmic scale.

In figure 45 the diffractogram from JNK1014 clearly stands out. This is likely to be due to the fact that a shorter program was used for the scan. Also, there is some noise above 60 ^{o}, likely to be from somewhere in the instrument and definitely not from anatase, which is what this investigation aimed to see the presence of. The diffractogram of JNK1038 resembles the ones of JNK1064 and JNK1065. Both JNK1014 and JNK1038 are probably amorphous samples.

4.2.5 Surface roughness

The roughness of the surfaces of selected depositions was further characterized by atomic force microscopy. The results of these measurements are given in table 15. All measurements are based on a scanning area of 1µm^2. From table 15 it is seen that all the films with the lysine pulse before the water pulse are very flat, with roughnesses in the sub-nanometer range. It does not seem to be affected by deposition temperature or film thickness. However, it can also be observed that the films with no lysine pulse or the water pulse before the lysine pulse, are approximately a tenfold rougher.

Table 15. This table shows the different samples measured upon in the AFM and the various parameters for the deposition and the measurements.

Sample name	Deposition sequence	Deposition temperature (°C)	Roughness, Rq (nm)	Scan rate (Hz)	Film thickness measured with ellipsometry (nm)
JNK1003	TTIP + water	225	2.3	0.5	40
JNK1005	TTIP + water + lysine	225	3.6	0.5	43
JNK1016	TTIP + lysine + water	225	0.2	0.5	58
JNK1029	TTIP + lysine	225	0.3	1.0	9
JNK1033	TTIP + lysine	400	0.2	1.0	95
JNK1040	TTIP + lysine + water	275	0.3	1.0	50

Scans from a selection of hybrid films are shown in figure 46. Comparing images a and b from figure 46, the only apparent difference between them is the higher level of noise for image a. Besides that, the features seem to be similar, even though the sample in image b has a water pulse and the one in sample a does not.

Considering image c from figure 46, it looks almost identical to image b. The only difference between these two films is the deposition temperature, and from these images it does not seem to have an effect on the surface topography. Actually, looking into table 15, the roughness remains similar as the films presented in image 46 also when the temperature is 400 °C.

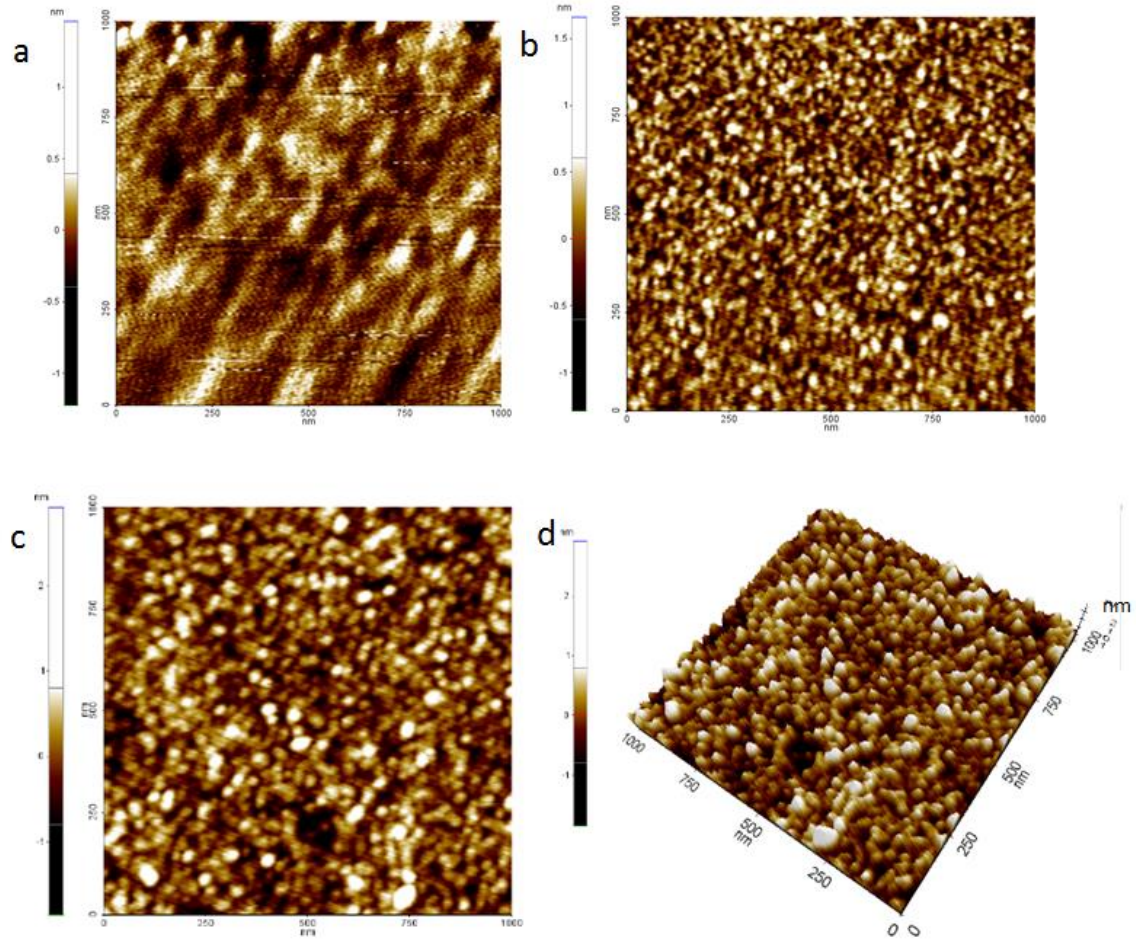

Figure 46. AFM images of hybrid films. a shows JNK1029, a TTIP/lysine film depositied at 225 °C. b shows JNK1016, a TTIP/lysine/water film deposited at 225 °C. c shows JNK1040, a TTIP/lysine film deposited at 275 °C and d shows a 3D image of JNK1040. Please note that the z-axis is enlarged on image d to make the features more visible. The scanned area is 1 µm² for each sample.

The roughest sample measured was JNK1005, which was had the water pulse before the lysine pulse. From image a shown in figure 47 it can be seen that small islands are standing out from the surface, especially in the lower right corner of the image. The measured roughness was 3.6 nm, but this number is an average over the entire area shown, and it is clear from this image that the surface topography is heterogeneous.

Also, figure 47 shows images of JNK1002, a TTIP/water sample. Image b clearly shows rounder islands standing out from the surface, but these are larger than the ones in JNK1005. An explanation for these features is that the TTIP/water film mostly consists of amorphous titanium oxide, but has some islands of anatase crystals growing out from it.

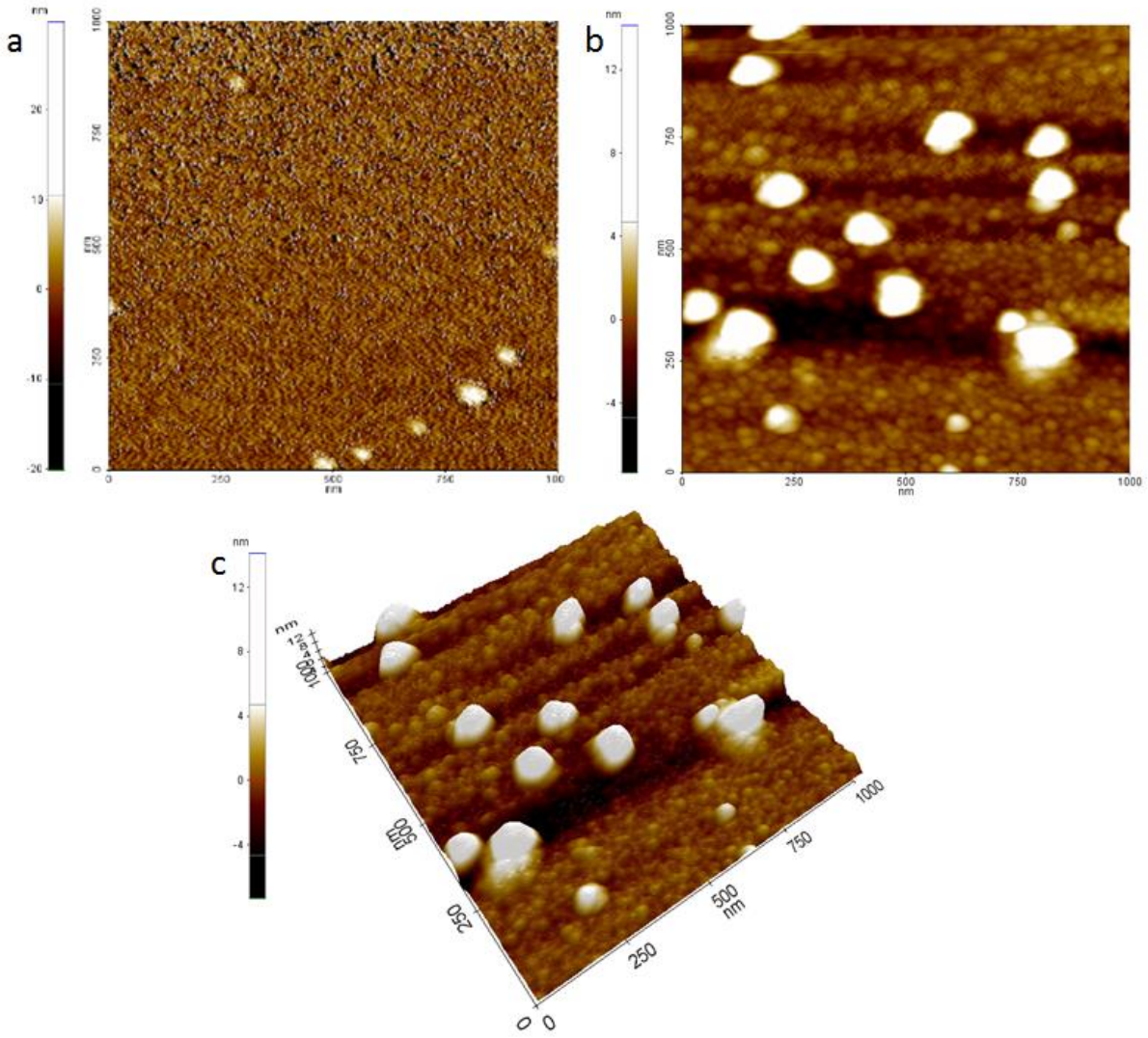

Figure 47. AFM images of film where a water pulse is directly after the TTIP pulse. a shows JNK1005, a TTIP/water/lysine film deposited at 225 °C. b shows JNK1002, a TTIP/water film deposited at 225 °C and c is a 3D image of JNK1002. Please note that the z-axis is enlarged on image c to make the features more visible. The scanned area is 1 μm² for each sample.

4.2.7 Solubility

For the hybrid films to be applicable in the cell culture laboratory, they must not be easily solvable in water or medium. Films slowly dissolving in water or medium will probably not be so dramatic, as it may give out smaller amounts of lysine to the cells.

To check if water would immediately dissolve the film, which has been the case for comparable films with $TiCl_4$ and serine as precursors[65], a droplet of water was applied on a glass plate covered with 54 nm of the hybrid material made at 225 ^{o}C with no water-pulse. The droplet was absorbed gently with a tissue paper. No mark was left in the film. Also, the droplet stayed with a relatively high contact angle on the surface. A process of dissolving the film, would probably have led to the droplet smearing out. To investigate further if the films are dissolved or detached by water, a droplet of water was applied and a tissue paper rubbed the water onto the surface, before wiping it off. The glass plate still remained the same, even after this treatment.

The same procedure was applied for a droplet of DMEM, and the results were the same as for the water droplet.

4.3 Coating cellulose membranes

To verify if the TTIP-lysine system could be coated on electrospun membranes, a cellulose membrane was attempted used as substrate. Cellulose was chosen as its melting point is higher than the temperatures required for the ALD-process. The cellulose membrane was made by PhD student Leva Momtazi. It should also be noted that the pulsing parameters were altered for these depositions. Longer pulsing and purging times were expected as the precursors have to penetrate down in the membrane. To investigate the required pulsing times, a piece of aluminum foil was clamped between two silicon substrates. The aluminum foil was shaped as shown in Figure 48. This construction produces a sample structure with a well with an aspect ratio of approximately 1:50.

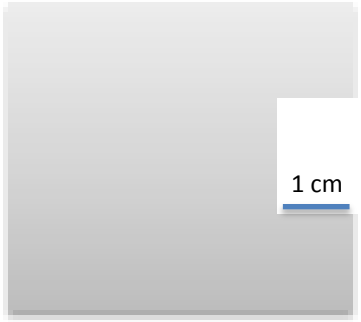

Figure 48. A drawing showing the shape of the aluminum foil used for testing how well the lysine penetrates into structures.

The pulsing times shown in table 16 were used for the test with the aluminum foil. The test showed that the film penetrated well in between the silicon wafers, and the same pulsing times were therefore used when the cellulose membranes were coated.

Table 16. A table showing the pulsing times used for coating electrospun membranes.

TTIP pulse	TTIP purge	Lys pulse	Lys purge	Water pulse	Water purge
4 s	4 s	8 s	4 s	8 s	12 s

Two runs of coating cellulose membranes were done, one with water-pulse and one without. Both the experiments were conducted at 225 ^{o}C using 1000 cycles. Silicon substrates were also added in addition to the membranes to verify the film thickness using ellipsometry.

A color change was observed for the membrane after deposition. The uncoated membranes were white as paper, whereas they turned brown during deposition. SEM analysis was conducted on coated and uncoated membranes to observe the structural integrity of the membranes during deposition.

Micrographs showing an overview of the uncoated cellulose membrane, the membrane at a higher magnification and two various coatings are shown in figure 49.

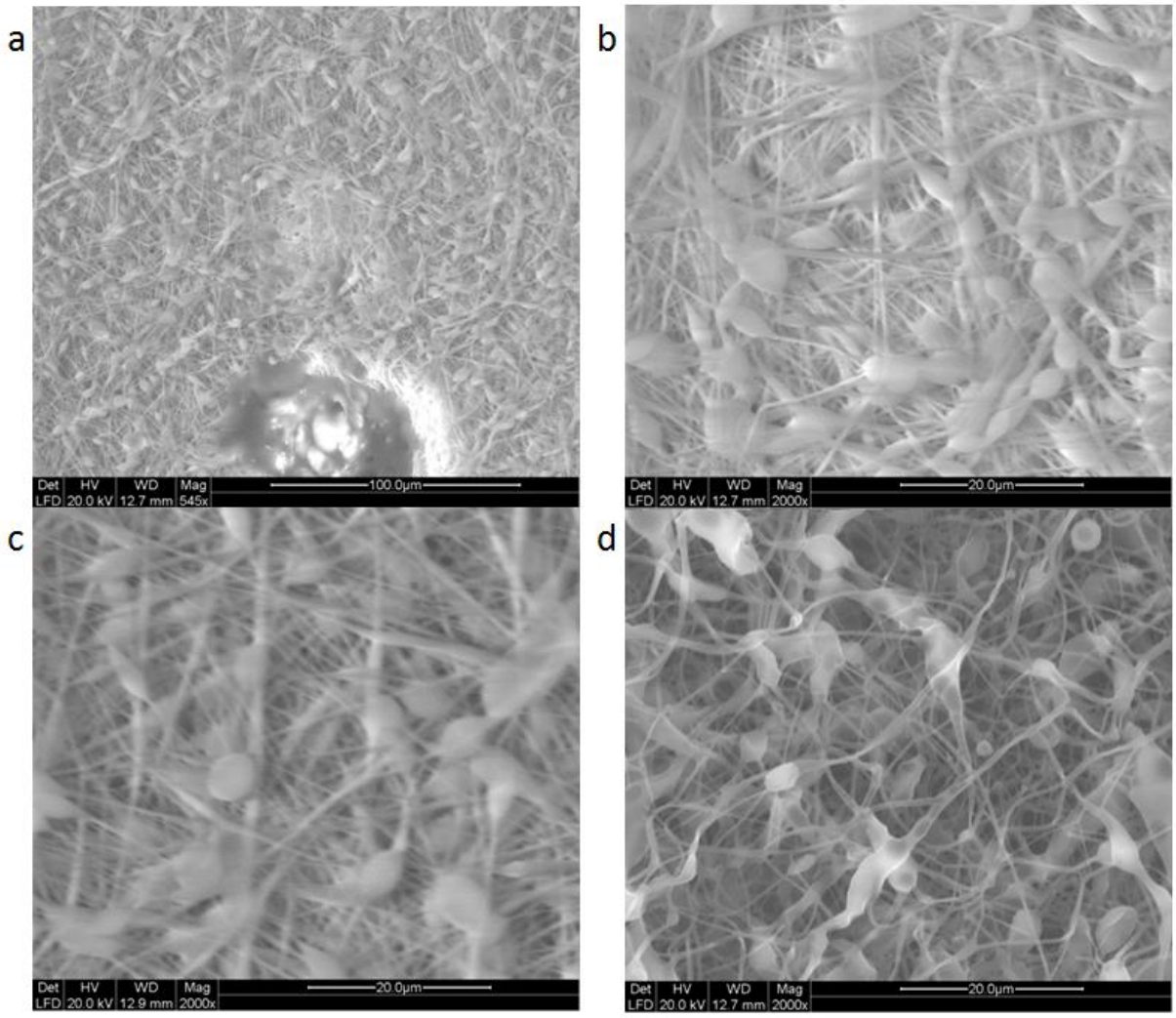

Figure 49. SEM micrographs of coated and uncoated membranes. a is an overview of the uncoated cellulose membrane, b is the cellulose membrane with a higher magnification, c is JNK1062, a cellulose membrane coated with TTIP + lysine at 225 °C and d is JNK1063, a cellulose membrane coated with TTIP + lysine + water at 225 °C.

From figure 49 it becomes apparent that the uncoated cellulose membrane does not purely consist of thin fibers. Beads were observed on many of the fibers, which is a feature often observed for electrospun fibers for non-optimal spinning conditions. Also, in the lower part of micrograph a, some of the membrane is molten or damaged. This is most likely due to heating from the electron beam during acquisition of the SEM images. Micrograph b shows even more clearly the beaded character of the fibers. It also seems like some of the fibers are thicker for tens of micrometers and does not only have a “thread with beads”-like appearance.

The coated membrane in micrograph c seems to mostly consist of thin fibers with some round beams. Some of the elongated, thicker parts of the fibers are also found here and there is no visual difference between the membrane with this coating and the uncoated membrane.

Micrograph d, however, does not look like b and c as the beaded character is less resembled here. Rather, it seems like the membrane has started melting into more odd shapes and less proper fibers remain. A reason for this may be that the run coating micrograph d lasted for approximately 5.5 h longer than the one without water pulse. This may indicate that the fiber cannot take 225 ^{o}C for an extended period of time.

4.4 Cell growth

The results given in this chapter are based on counting cells on images taken with fluorescence microscopy. To illustrate the difference between a light microscopy micrograph and a fluorescence microscopy micrograph, one of each type from the same sample are shown in figure 50.

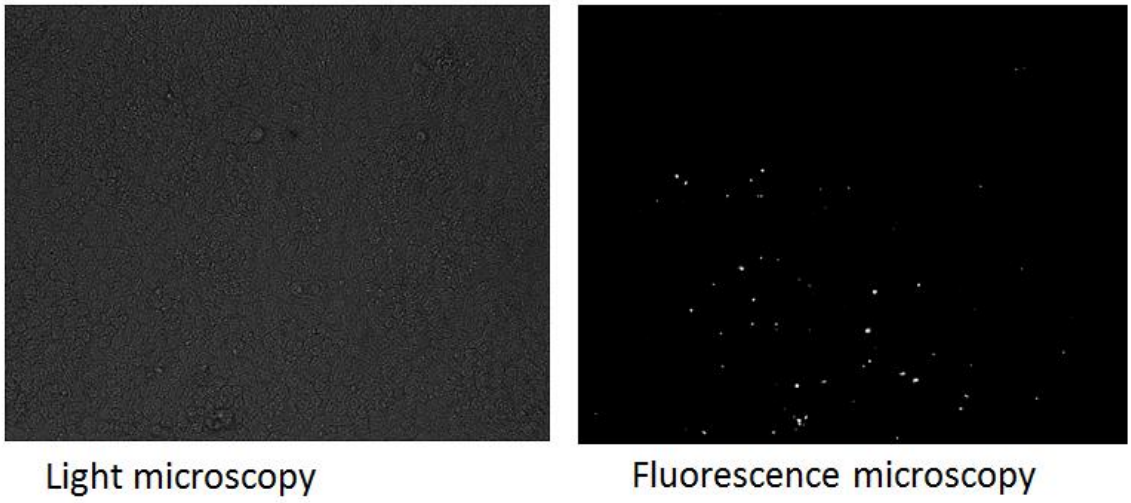

Figure 50. Light microscopy and fluorescence microscopy micrographs of the same sample. For the fluorescence micrograph the white dots are the light emitting nuclei of the cells.

The micrograph obtained by light microscopy clearly shows that the cells are completely confluent, but the fluorescence micrograph does not confirm that. One reason for this is that PI only stains the nucleus of the cell. Even though two cells may be completely close

together, their nuclei are not, and hence the cells may not appear confluent on a fluorescence micrograph. Another factor is the success rate of the staining itself. It will never be so that all the cells get stained, however, when performing cell quantification experiments using the same protocol for all the samples, there is no apparent reason why the staining should be more successful for one sample than the other. The mean cell count of the studied sample compared to the reference sample should therefore be viewed as independent of the staining process.

In spite of this, the signal from the dyed samples may be influenced during the microscopy process itself. As mentioned, the samples are very light sensitive and only emit a limited number of times. If one sample is studied for an extended period of time in the microscope, the staining might fade for this sample. Also, perhaps more serious if these are not already studied, the staining of the neighboring may fade, giving errors.

Another point to be aware of before considering the results from the cell growth experiments, is that PI will stain the nucleus of both dead and living cells. This means that some of the counted cells may be dead. However, there is no reason why a larger proportion of the cells should be dead on one sample than the other if the same protocol is followed. This is yet another reason why it is important to only compare cell growth experiments where the cells are seeded out simultaneously; implying that the age of the cell culture and the number of seeded cells are the same.

For the cell growth experiments, both the time between seeding and fixating the cells and the cell type itself were varied. Bar charts of the mean cell count for three wells for various experiments are shown in figure 51. As can be seen from figure 51, the cells thrive equally well on the coated substrates as on the reference plastic, except for the titanium oxide sample, where they do not proliferate.

In addition to these results, it was tried to culture the transformed cell line on coated substrates for longer timespans, but these experiments were not successful. This cell line was old already before being used in this thesis. This became clear immediately after the initial seeding of the cells, where it took the cells a week to become confluctant, which is much longer than normally anticipated. The age of the transformed cell line may be why further experiments with them were not possible. It was also tried to seed cells on poly-D-

lysine coated wells. However, this was the last experiment conducted and the cells did not proliferate here either.

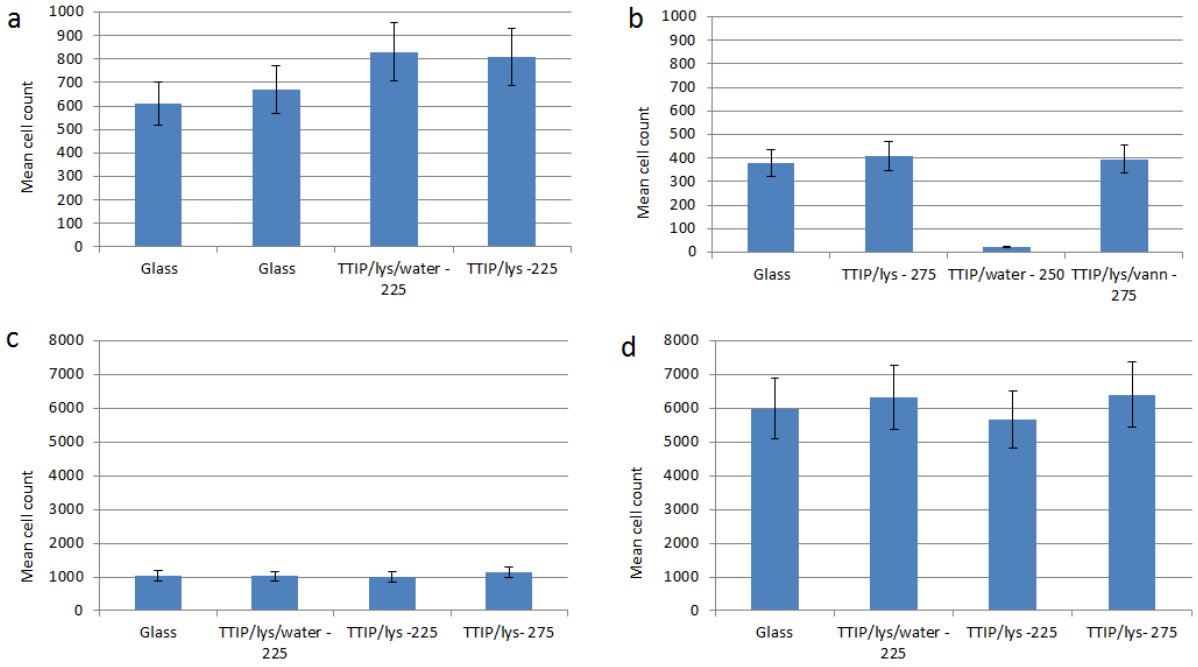

Figure 51. Bar charts showing the mean cell counts for cells seeded out on various substrates. The number after the pulsing sequence refers to the deposition temperature. Experiment a had 22.000 cells seeded in each well and were cultured for 2 hours using transformed cells. Experiment b had 17.000 cells seeded in each well and were cultured for 2 hours using transformed cells. Experiment c had 32.000 cells seeded in each well and were cultured for 2 hours using normal cells. Experiment d had 33.000 cells seeded in each well and were cultured for 3 days using normal cells. The experiments were performed consecutively in time, meaning that the transformed cell line has been passaged once more in b than in a, and that the normal cell line has been passaged once more in d than c.

5. Discussion

This chapter will first propose and discuss some growth mechanisms for the ALD process in view of the results found and other published work, then discuss the films with altered pulsing order, the temperature dependencies of the depositions, the stability of the films and lastly the cell growth experiments.

5.1 Growth mechanisms

Both the TTIP/lysine and TTIP/lysine/water systems have given even films, however, with a much higher growth rate for the latter. Even if the films from TTIP/lysine and TTIP/lysine/water systems have different refractive indices and vary in growth rate, the materials have been very similar in most other aspects. The AFM images showed almost equal surface topographies. Moreover, the goniometer method resulted in similar contact angles around 60 ^{o}, and the cells seemed to have the same affinity to both types of surfaces.

The FTIR measurements clearly show that the produced films are of a hybrid character, as expected for films of these systems. The FTIR spectrum of pure L-lysine is given in figure 52 for comparison with figure 41 found in chapter 4.2.1.

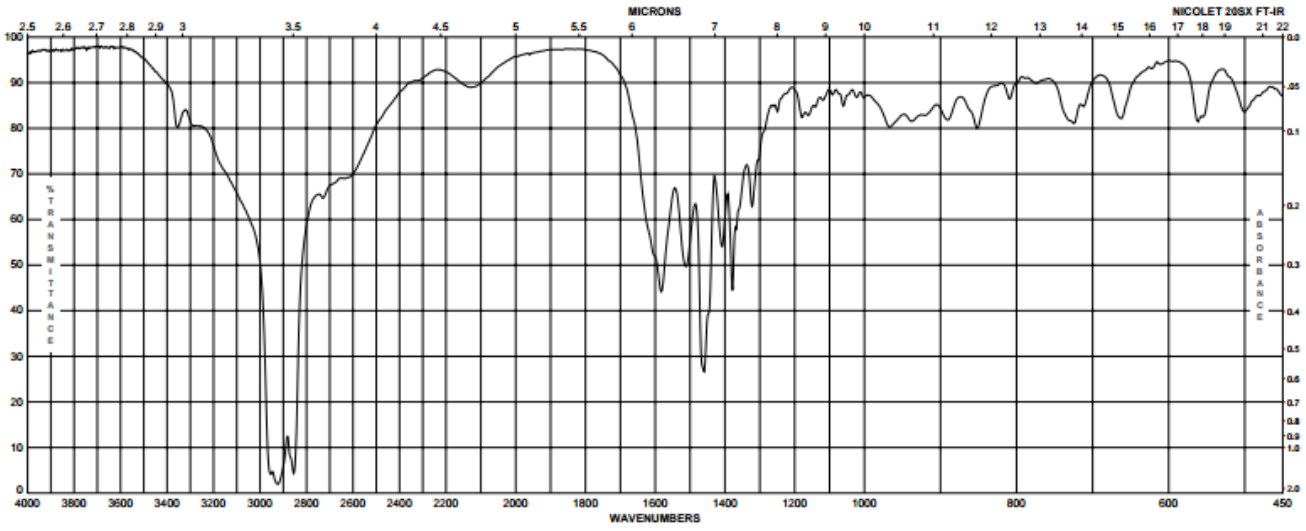

Figure 52[109]. FTIR spectrum of pure L-lysine powder.

As can be seen from figure 52, the most intense peaks on the spectrum are located around 2900 cm^{-1}. A broad and intense absorption band in this area often corresponds to O-H stretching[105, 106]. This absorption band also has several less intense, superimposed absorption bands on each side. These bands may be related to the CH_2 and NH_3^+ stretching

modes already identified for the hybrid films (see chapter 4.2.1). A difference between the spectrum for pure lysine and the hybrid is that the position of the most intense absorption band in the cluster of bands around 1600 cm^{-1} to 1400 cm^{-1} is shifted. For the pure lysine this is around 1475 cm^{-1}, whereas it is at 1625 cm^{-1} for the hybrids. Since the shift between these peaks is quite large, it may be that the reason for the peak is in fact different, i.e. various bonds in the samples.

Absorption bands related to C-OH bending are typically found in this area. The presence of the O-H stretching and C-O-H bending vibrational modes in the pure lysine spectrum and the lack of such in the hybrid film spectra indicate that the acid group of the lysine takes part in the film formation.

However, even if it is certain that lysine and TTIP has bonded together, it is not evident *how* this happens. Furthermore, it is not clear which role water plays when it is added to the system, and why this increases the growth rate so dramatically. Therefore are growth mechanisms and which materials these various mechanisms will lead to discussed further in this chapter.

In the following two pages, two growth schemes for the TTIP/lysine system are presented in figure 53 and figure 54. The first is a simple linear scheme, where one TTIP binds to one lysine and so on. Since carboxylate groups are normally more reactive than amine groups, it is assumed that this functional group will dominate the initial attachment between the amino acid and the TTIP-saturated surface. This leaves two amine groups for the next sequence of TTIP precursor. As one amine group is very close to the already formed carboxylate group, it is further assumed that it bonds to the amine group in the other end of the molecule due to steric hindrance.

For the second mechanism, the assumptions about reactivities for the functional groups are kept. However, this mechanism is not a linear one, as it suggests that there is a double reaction of the lysine in between two TTIPs. In this mechanism, both the carboxylate and one of the amine groups take place in the reaction simultaneously. Since lysine has three functional groups, this will still leave the last amine group available for the next TTIP. Steric hindrance will most likely be significant in this reaction scheme. This may be a reason for the poor growth rate of the material.

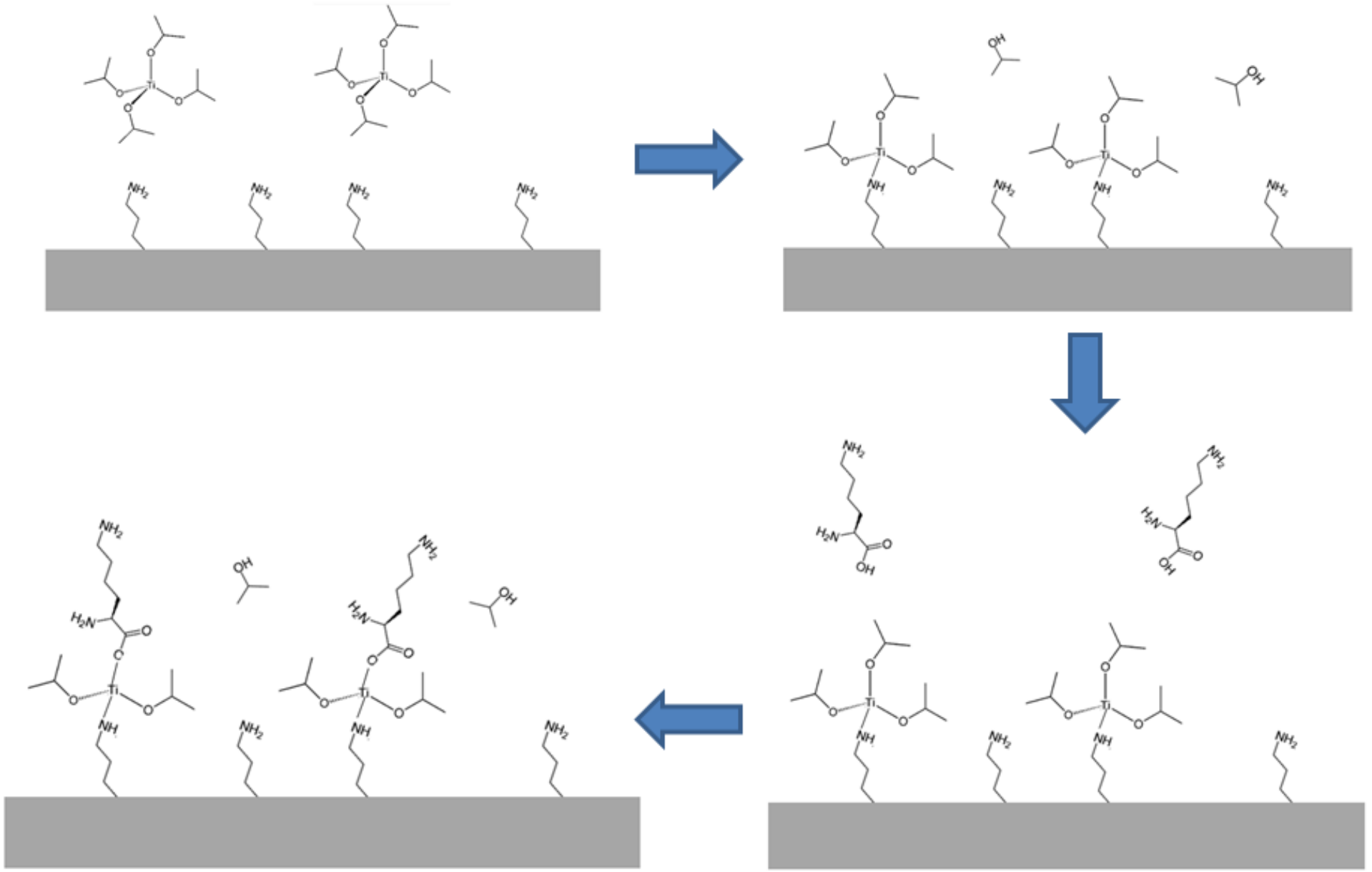

Figure 53. Proposal for a linear growth mechanism for the TTIP/lysine system.

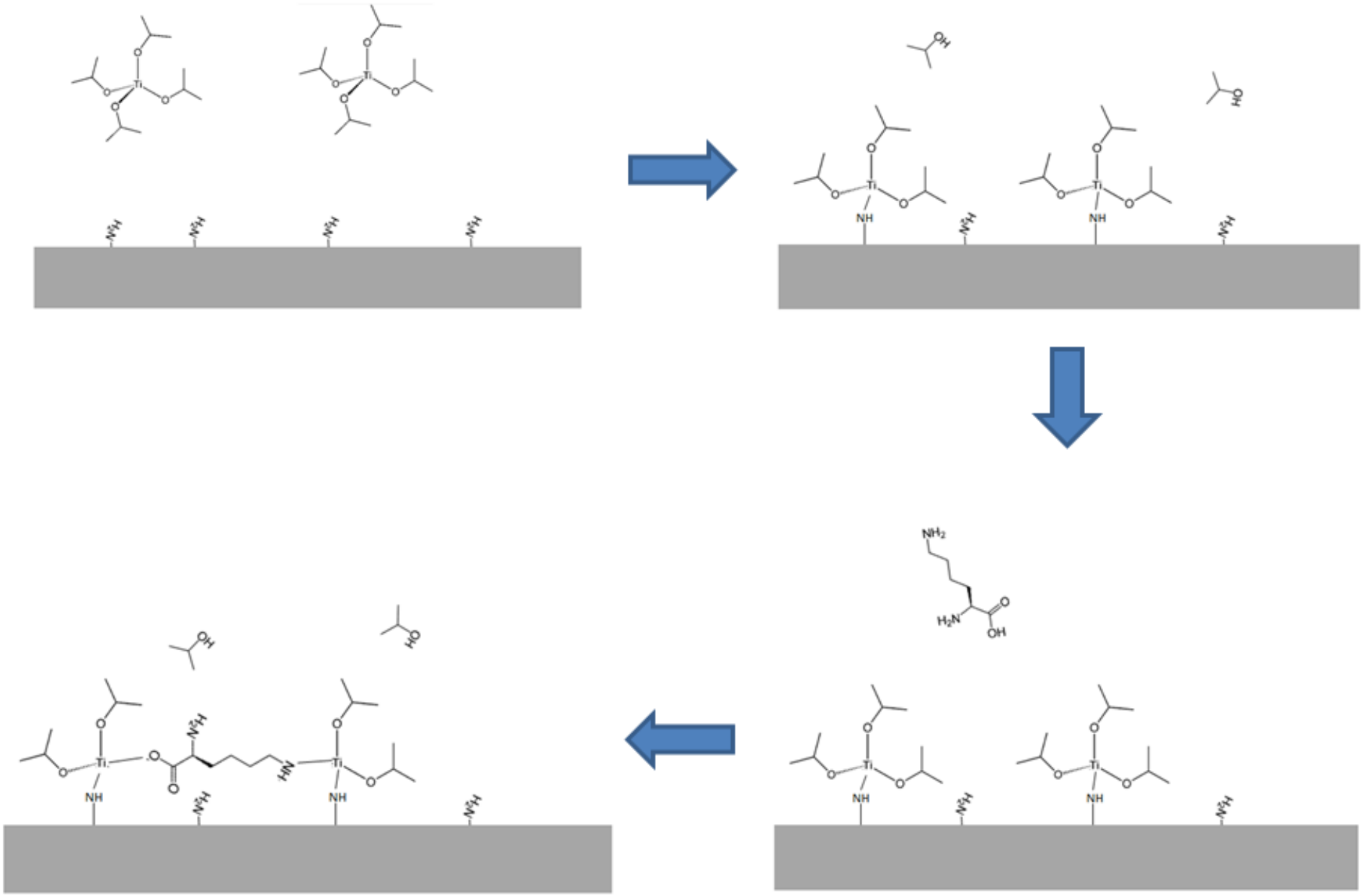

Figure 54. Proposal for a double-reaction mechanism for the TTIP/lysine system.

From the QCM data for the long pulsing experiments of the TTIP/lysine shown in figure 32 (in chapter 4.1.2), it is seen, that after the lysine pulse and purge the mass decreases. In comparison, it remains approximately zero for the standard runs shown in figure 33 (in chapter 4.1.2). The uncertainty in the measurements should be taken into consideration in this case, but the decrease in mass for the long-pulsing experiment is so large that it is significant. The slight increase in the standard run, however, is not, which means that a slight decrease or a slight increase in mass is equally likely to be correct. Evaluating how realistic the first and second growth mechanism are based solely on the QCM data is close to impossible. Nevertheless, the decrease in mass, or at least the absence of a huge increase in mass after the lysine pulse, may suggest that the overall mass change between the reaction of lysine and the loss of possible leaving groups is not large. The molecular mass of lysine is 146.19 g/mol, whereas the molecular mass of isopropanol is 60.10 g/mol. A possible reaction mechanism resulting in near mass equality is the loss of two or a bit more than two isopropanol molecules for one lysine molecule. This is coherent with the double reaction growth mechanism shown in figure 54. In fact, a triple-reaction may take place sometimes and as this will stop any further growth of the material, it may be a reason for the low growth rate.

The double reaction mechanism does not, however, account for the decrease in mass after the lysine pulse and purge in the long-pulsing experiments. The results presented in this thesis may suggest that an etching reaction involving lysine may take place on the surface, when the surface is exposed to it for longer pulsing times. These kinds of effects have been reported for the TMA/ glutaric acid system previously, where pulsing times longer than 4 s for glutaric acid led to a mass decrease in the QCM measurements[110]. The structure of glutaric acid is shown in figure 55.

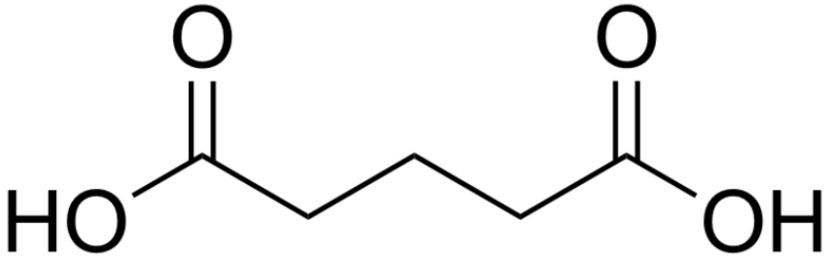

Figure 55[111]. The structure of glutaric acid.

As can be seen from figure 55, the glutaric acid has five carbons arranged in a linear manner, similar to lysine's six. It was suggested that glutaric acid forms volatile complexes with components from the surface. This may also be the case for lysine.

One huge difference between the TTIP/lysine system studied in this work and the other hybrid materials made previously, such as the TMA/glutaric acid films, are the very low growth rates for the TTIP/lysine system. In fact, the growth rates for the TTIP/lysine system are more than one order of magnitude lower than the growth rates for the TMA/glutaric acid system[110] at 225 ^{o}C, which incidentally is not particularly high for this type of materials. Using the software Chem3D Pro.14, the length of lysine between the carboxylate group and the amine group on the first carbon is estimated to be about 6.701 Å. Recalling the that growth rate for the TTIP/lysine system at 225^{o}C is approximately 0.09 Å/ cycle, it is obvious that one complete layer of lysine molecules does not attach each time if the material grows in a linear manner. One reason for this may be shielding effects. The isopropoxide groups in TTIP may hide the central titanium from the lysine. Likewise, lysine may bond in such a way that the remaining functional groups point downwards. This would make them unavailable for the next incoming TTIP. To see how extensive the shielding is, it is interesting to compare the growth rates for the TTIP/lysine system to the growth rates for the $TiCl_4$/lysine system. The latter system has growth rates at 2.5 Å/cycle at 225 ^{o}C. At temperatures ranging from 250 ^{o}C to 300 ^{o}C, the growth rates are fairly constant, and at 275 ^{o}C it is 1.5 Å/cycle[66]. In other words, the growth rate decreases a tenfold when changing from $TiCl_4$ to TTIP as the titanium precursor. This is a much larger difference than in the case of $TiCl_4$/water compared to TTIP/water, where the growth rate is halved for the latter[69]. The low growth rates for the TTIP/lysine system may therefore be a combination of shielding effects from both precursors.

Another thing to consider is that even if the system grows linearly, the lysine may still bind in various ways. As the illustration in figure 53 shows, the carboxylate group of lysine forms one bond to titanium in a unidentate complex. It may be that both the oxygen atoms in one carboxylate group bind to the same titanium atom forming a bidentate complex. If the carboxylate group bonds to two titanium atoms, a bridging complex is formed. Information about this can be deducted from the splitting of the carboxylate asymmetric and symmetric stretching, Δ, in the FTIR spectra. Δ=175 cm^{-1} is found for the TTIP/lysine films and the

TTIP/lysine/water films. According to literature[112], unidentate carboxylate complexes is dominating if $\Delta \approx 200\ cm^{-1}$, bidentate carboxylate complexes are found in the range $50\ cm^{-1} < \Delta < 150 cm^{-1}$, and bridging carboxylate complexes are found in the range $130\ cm^{-1} < \Delta < 200 cm^{-1}$. Assuming that the labelling of the absorption bands in the FTIR spectra were done correctly, this indicates that the carboxylate group enter into a bridging complex formation between to titanium atoms.

This study has also shown that adding a water pulse after the lysine pulse increases the growth rate of the material dramatically. The question is then what role water plays in the system. There are two general proposals on what might be occurring. The first is that water somehow activates the lysine. This can for example occur by protonation of the amine group, making it more reactive for the next incoming TTIP molecule. The FTIR spectra support this to some extent, as some peaks are interpreted as originating from NH_3^+. However, there is one major problem with this suggestion. If water protonates the amine group, there will be an OH^- ion left. This ion has to end up somewhere. Categorically speaking, this can be one of two places, either in the film or in the exhaust. FTIR measurements show no clear absorption bands related to OH-stretching in the film, while OH-stretching is clearly visible in the pure lysine reference spectrum. Assuming that the leftover OH group is a part of the exhaust, the question is what by-products are being formed. One possible solution is that water protonates the amine group, and that water and acetone leaves as by-products after reaction with the next TTIP.

The second proposal on which role water might play, is that it reacts with the titanium containing surface species. This will form an OH group bonded to the titanium atom and an isopropanol molecule in the gaseous phase. This OH will in turn be available for a TTIP molecule. This TTIP may react with the next lysine molecule. Since the water molecules are much smaller than lysine, they may be able to find titanium seats unavailable to lysine and hence use more of the reaction seats on TTIP. An implication of this growth mechanism is that a part of the film will be TiO_2. The resulting film is therefore a hybrid oxide composite material. This suggestion of a composite film is supported by the refractive indexes at 632.8 nm wavelength light for the various materials. For the true hybrid films of the TTIP/lysine system, the refractive indices are below 2.0 within the ALD window. For the TTIP/lysine/water films, however, the refractive indices are in the range of 2.2 to 2.4,

indicating a significant increase in optical density. Recalling that the refractive index for amorphous TiO_2 is 2.493[113], it is a clear indication of TiO_2 in the TTIP/lysine/water films.

The number of reacting seats on each TTIP in the TTIP/lysine/water system assuming it reacts like pure TTIP/water may also give information about what is going on. This type of estimation has been done for the TTIP/D_2O system previously[114] and the same method will be employed here. The basis of the estimation is a relation between the obtained QCM data and the various reaction mechanisms, shown in equation 6.

Equation 6

$$\frac{\Delta m_{total}}{\Delta m_{TTIP}} = \frac{M(TiO_2)}{M(Ti\{(OCH(CH_3)_2\}_4) - n\,M((CH_3)_2CHOH)}$$

where Δm_{total} is the net mass change for the system per cycle, Δm_{TTIP} is the net mass change for the TTIP pulse and purge per cycle, $M(TiO_2)$ is the molar mass of titanium oxide, $M(Ti\{(OCH(CH_3)_2\}_4)$ is the molar mass of TTIP, $M((CH_3)_2CHOH)$ is the molar mass of isopropanol and n is the number of reacting seats on TTIP.

As TTIP has four possible seats for a reaction with water, n will be varied between 0 and 4. Only considering the integers, this gives rise to table 17. The reaction mechanisms are based on equation 5 found in chapter 4.2.1.

Table 17. Estimated $\Delta m_{total}/\Delta m_{TTIP}$ ratios for variable numbers of reacting seats on TTIP for the TTIP/water system and the corresponding reaction mechanism.

n	Proposed reaction mechanism	$\Delta m_{total}/\Delta m_{TTIP}$
0	$Ti\{OCH(CH_3)_2\}_4\,(g) \rightarrow Ti\{OCH(CH_3)_2\}_4\,(s)$ $Ti\{OCH(CH_3)_2\}_4\,(s) + 2\,H_2O\,(g) \rightarrow TiO_2\,(s) + 4\,(CH_3)_2CHOH\,(g)$	0.28
1	$(-OH)\,(s) + Ti\{OCH(CH_3)_2\}_4\,(g) \rightarrow (-O-)Ti\{OCH(CH_3)_2\}_3\,(s) + (CH_3)_2CHOH\,(g)$ $(-O-)\,Ti\{OCH(CH_3)_2\}_3\,(s) + 2\,H_2O\,(g) \rightarrow (-O-)_2Ti(OH)_2\,(s) + 3\,(CH_3)_2CHOH\,(g)$	0.36
2	$2(-OH)\,(s) + Ti\{OCH(CH_3)_2\}_4\,(g) \rightarrow (-O-)_2\,Ti\{OCH(CH_3)_2\}_2\,(s) + 2\,(CH_3)_2CHOH\,(g)$ $(-O-)_2\,Ti\{OCH(CH_3)_2\}_2\,(s) + 2H_2O\,(g) \rightarrow (-O-)_2Ti(OH)_2\,(s) + 2\,(CH_3)_2CHOH\,(g)$	0.49
3	$3(-OH)\,(s) + Ti\{OCH(CH_3)_2\}_4\,(g) \rightarrow (-O-)_3\,Ti\{OCH(CH_3)_2\}\,(s) + 3\,(CH_3)_2CHOH\,(g)$ $(-O-)_3\,Ti\{OCH(CH_3)_2\}\,(s) + 2\,H_2O\,(g) \rightarrow (-O-)_2Ti(OH)\,(s) + (CH_3)_2CHOH\,(g)$	0.77
4	$4(-OH)\,(s) + Ti\{OCH(CH_3)_2\}_4\,(g) \rightarrow (-O-)_4\,Ti\,(s) + 4(CH_3)_2CHOH\,(g)$ $(-O-)_4\,Ti\,(s) + 2\,H_2O\,(g) \rightarrow (-O-)_2Ti(OH)_4(s)$	1.82

The actual $\Delta m_{total}/\Delta m_{TTIP}$ ratios have been calculated from the QCM data. Except for the TTIP/water system, the values are based on the long pulse experiments. The obtained ratios are shown in table 18.

Table 18. $\Delta m_{total}/\Delta m_{TTIP}$ ratios for various reactions.

Pulsing order	Observed $\Delta m_{total}/\Delta m_{TTIP}$ from QCM measurements
TTIP/water	0.50
TTIP/water/lysine	0.94
TTIP/lysine/water	0.92
TTIP/(lysine + water)	1.15

As can be seen from tables 17 and 18, the $\Delta m_{total}/\Delta m_{TTIP}$ ratio for TTIP/water system is close to what expected if n=2. This is also what was found for the TTIP/D_2O system[114]. However, the values for the TTIP/water/lysine, TTIP/lysine/water, TTIP/(lysine + water) systems indicate a higher number of reacting seats for each system. This is counterintuitive to the fact that lysine should make it more difficult for the TTIP and water to react. It therefore seems like the reaction mechanisms shown in table 17 are not applicable for any of the films having a lysine pulse.

The fact that equation 6 is a simplified equation should also be taken into consideration. The proper way to consider this is to look at the mass change after the TTIP pulse and purge and dividing it by the mass change after the water pulse and purge. It is then related to n as shown in equation 7 below.

Equation 7

$$\frac{\Delta m_{TTIP}}{\Delta m_{water}} = \frac{M(Ti\{(OCH(CH_3)_2\}_4) - nM((CH_3)_2CHOH)}{2M(H_2O) - (4-n)\,M((CH_3)_2CHOH)}$$

where Δm_{TTIP} is the net mass change for the system per cycle, Δm_{water} is the net mass change for the TTIP pulse and purge per cycle, $M(H_2O)$ is the molar mass of water, $M(Ti\{(OCH(CH_3)_2\}_4)$ is the molar mass of TTIP, $M((CH_3)_2CHOH)$ is the molar mass of isopropanol and n is the number of reacting seats on TTIP.

The observed values for the $\frac{\Delta m_{TTIP}}{\Delta m_{water}}$ ratios are shown in table 19. Using the relation in equation 7 and an excel sheet, the best fit for n were also decided. These are also shown in table 19. However, best fit n values were not possible to find for TTIP/lysine/water and

TTIP/(lysine + water). This indicates that the assumed reaction mechanism is not taking place. It is also noticeable that the best fit value for n increases when a lysine pulse is added after the water.

Table 19. Observed $\Delta m_{TTIP}/\Delta m_{water}$ ratios for various reactions and their estimated best fit for n.

Pulsing order	Observed $\Delta m_{TTIP}/\Delta m_{water}$ from QCM measurements	n for best fit
TTIP/water	-2.01	2.095
TTIP/water/lysine	-6.42	3.156
TTIP/lysine/water	-200	-
TTIP/(lysine + water)	14*	-

*This value is based on the net mass increase after the combined lysine and water pulse.

Similar calculations were tried for the TTIP/lysine and TTIP/lysine/water systems to find $\Delta m_{TTIP}/\Delta m_{lysine}$ ratio. However, no realistic combinations of parameters were found. This is an indication of some other mechanisms happening other than the ones shown in figures 53 and 54.

5.2 Films with altered pulsing orders

The results shown in table 19 indicates that a possibility of the TTIP/water/lysine leading to titanium oxide films. Even though it was not possible to estimate a n-value for the TTIP/(lysine + water) system, this may also be connected to the lysine being pulsed simultaneously.

Moreover, the refractive index is 2.227, which is just slightly lower than for the oxide, but higher than for the TTIP/lysine/water films made at the same temperature. This may be an indication of the presence of some lysine in the TTIP/water/lysine film.

Also, the contact angle measurements show vastly different results from the TTIP/water system to the TTIP/water/lysine system, where the first had a contact angle of 11^{o} and the second of 72^{o}. This is in turn a slightly higher contact angle than for the hybrid films. Two various theories may explain this. First, TTIP/water/lysine may mostly be a hybrid film, and therefore has similar contact angles as the other hybrid films measured in this work. An alternative to this is to consider when the contact angle measurements were performed relative to the depositions. The TTIP/water film was measured directly after deposition whereas the TTIP/water/lysine and TTIP/(water + lysine) films were measured after seven and six days of storage in air, respectively. It has previously been overserved in our group

that even if TiO_2 are very hydrophilic directly after deposition, the contact angles increase with time when they are stored in air, for time spans as short as hours and a few days[115]. The comparable contact angles for the TTIP/water/lysine system and the other hybrid films, does therefore not unambiguously mean that the TTIP/water/lysine system results in hybrid material.

The GIXRD measurements performed on this sample are also ambiguous. The clear anatase reflection in the TTIP/water diffractogram, is absent in the TTIP/water/lysine sample. This indicates that the TTIP/water/lysine film does not contain anatase. However, the absence of anatase says nothing about whether the film is amorphous titanium oxide or a hybrid film.

Furthermore, the topography of the TTIP/water/lysine film suggests that it is not the same material as for the TTIP/lysine and TTIP/lysine/water systems, as the AFM results show that the TTIP/water/lysine film is a tenfold rougher than the TTIP/lysine/water film made at the same temperature.

An experiment was performed with lysine and water being pulsed simultaneously. For all the films made in the work of this thesis, this was the only film with large gradients. Interestingly, the refractive index also showed gradients, with 2.256 at the thicker part of the film and 2.179 at the thinner part of the film. A possible explanation for this is to view water and lysine as two competitors over the available spots to react with the titanium containing surface species. As water is more reactive than lysine in this sample, reactions with water will dominate the first part of the film, giving a thicker and denser film. However, on the back end of the substrate the concentration of lysine in the gas phase is higher than the water, as much of this water has already reacted. This will lead to more lysine reacting with the film. This lysine will also give rise to steric hindrance for the next TTIP, and lysine richer parts of the film are therefore thinner. Also, this thesis has shown that the TTIP/lysine system has lower refractive indices than TTIP/water, and lysine rich parts of the TTIP/(lysine + water) films also should therefore have lower refractive indices than the rest of the film.

GIXRD and contact angle measurements for the films with co-pulsing of water and lysine revealed no new information when compared to the TTIP/water/lysine-system. This indicates that the bulk- and surface structure of the films does not depend on whether water is introduced before or simultaneously as lysine.

5.3 Temperature dependency

It is difficult to say from the results found in this work whether or not the produced films remain the same material when the deposition temperature is altered within the ALD window. From AFM and goniometry measurements, it seems like the material remains the same. However, the refractive indices increase with temperature for both systems. This indicates that the material gets denser, either by a larger part of the structure being TiO_2 or perhaps by rearranging the packing of the material into a denser fashion.

5.4 Stability

The films produced in this work have generally been remarkably stable. “Growth” after the sample is taken out from the reactor, is often referred to as “fluffing” of the films. For example, $TiCl_4$/lysine films made at 325 ^{o}C, with an initial thickness of 82 nm, were reported to be approximately 90 nm just one hour after deposition[66]. This fluffing is in fact quite moderate, but extreme compared to the small changes found in this work. Currently, research is conducted on the TMA/cyanoric acid and TMA/melamin systems at NAFUMA[116], and these fluff to a much larger extent. The TMA/cyanoric film increased in thickness from 485 nm to 778 nm in a week; whereas the TMA/melamin system is so sensitive to air that the films increase with 10 nm from each consecutive ellipsometer measurement for approximately 600 nm thick films. These measurements really put the stability of TTIP/lysine into perspective.

The films also differ from other hybrid films when it comes to solubility, for example from $TiCl_4$/serine films which have been soluble in water[65]. Experiments in this thesis have shown that the TTIP/lysine films were not soluble in water or DMEM, which is important if the films are to be used for cell growth. Furthermore, lysine powder is readably soluble in water[117]. The fact that these films are not, supports that the hybrid films have unique characteristics compared to their oxidic counterparts or the pure organic precursors.

5.5 Cell growth

For the cell growth experiments there were no significant differences between the proliferation of the cells between the reference glass plates and the various coated substrates except for the titanium oxide sample. It is known the titanium oxide becomes antibacterial when UV-light is irradiated onto it, and also that it may be less biocompatible

after irradiation[118]. This may be just what happens for the titanium oxide films in this sample.

It is further interesting to see how the cells proliferate equally well independent of deposition temperature of the ALD films and the presence of a water pulse in the system. This may be yet another indication of that TTIP/lysine and TTIP/lysine/water films have similar surfaces. It is at least sure that the cells do not experience the TTIP/lysine/water and the TTIP/water surfaces differently.

6. Conclusion

In this thesis hybrid films of TTIP/lysine and TTIP/lysine/water have been deposited successfully by ALD. The films obtained have been smooth, amorphous and slightly hydrophilic with contact angles around 60 ^{o}. FTIR confirmed the hybrid character of the films.

The growth rates at 225 ^{o}C were 0.09 Å/cycle and 0.53 Å/cycle for the TTIP/lysine and TTIP/lysine/water systems respectively. These two systems did not experience the same variation of growth rates versus deposition temperatures. For the TTIP/lysine system the growth rate increased slightly over temperature within the range from 205 ^{o}C to 300 ^{o}C, and there was a remarkable increase in growth rate at 400 ^{o}C. However, TTIP/lysine/water system also experienced an increased growth rate at 205 ^{o}C. The refractive indices also increased with deposition temperature. Even though the temperature dependencies for the refractive indices were the same for both the TTIP/lysine and TTIP/lysine/water systems, the values were higher for the TTIP/lysine/water system than for the TTIP/lysine system. For example, at 225 ^{o}C, these were 2.177 and 1.784 respectively.

The effect of moving the water pulse before or simultaneously as the lysine pulse was also investigated. The TTIP/water/lysine system gave even films with a comparable growth rate to the TTIP/water system, but a slightly lower refractive index. The TTIP/(lysine + water) system, however, gave a thickness gradient of 20 %/ 2.5 cm, and it also had a gradient in the refractive index. Both of these films were GIXRD amorphous.

Initial experiments of coating cellulose membranes for cell growth applications were performed. This seemed to be successful for the TTIP/lysine system, but the membrane coated with TTIP/lysine/water did not keep its structural integrity properly during the coating process, probably due to a longer reaction time.

Both normal and transformed cells were seeded on TTIP/lysine and TTIP/lysine/water coated coverslips. The cells proliferated equally well on the coated coverslips as on the reference glass slips and the deposited material is therefore at least biocompatible. The exception was the TTIP/water coated coverslips, where the cells did not proliferate. Experiments with growing transformed cells for longer time spans were unsuccessful, but this is probably due to old cells.

7. Future directions

Even if this study has gone in depth with the TTIP/lysine and TTIP/lysine/water systems, further investigation can be done on these types of materials. Firstly, it would of course have beneficial with more FTIR measurements of good quality. Modelling of the various ALD growth modes and their respective expected FTIR spectrums, would also be beneficial. These types of modellings are already done today[119], but not at NAFUMA. Other useful measurements can be in-situ IR measurements, which may give information about the bonding in various parts of the ALD cycle. Also, studying the exhaust from the ALD reactor may give interesting information. For example, whether the by product is actually isopropanol or not, can be confirmed with mass spectroscopy (MS) on the exhaust tube. Both in-situ FTIR and MS on the exhaust are employed in at least one ALD research group already[120]. Another method that can be used to study the structure of the hybrid-oxide composite further, is to use cross-sectional transmission electron microscopy (TEM).

Furthermore, it would be interesting to study the thermal properties of the hybrid films in order to clarify the stability, and the types of end-products which would form. If the coatings made in this thesis are ever to be used in a cell culture laboratory they should be sufficiently thermally stable to withstand sterilization procedures. The stability of the film towards water should also be investigated in a more thorough manner. One way this may be done is to cover the film with water for a period of time and then study the water with nuclear magnetic resonance (NMR). If the film dissolves, lysine should be found in the NMR measurements.

A simple coating experiment of a cellulose membrane was conducted in this thesis. However, for this combination a lot of work remains. Firstly, a membrane with finer fibers without the beads would be preferable for the final product. Also, cells must be seeded out on the membrane. The fact that the membrane is not transparent complicates this process, and the cells must be investigated with a SEM. As cellulose is not a well-known material for cell growth, it may also be beneficial to coat other polymeric membranes for similar investigations.

Another thing to look into is whether it is possible to coat other types of 3D structures besides the electrospun ones. In this research group surfaces have been structured simply by using soot from a candle, and this should be a readily available surface to coat.

A natural step forward from this investigation, is of course to try the same with other amino acids as precursors. Serine has been tried in the group together with $TiCl_4$, but is should be investigated paired with TTIP as well. Currently, hybrid films of glycine and TTIP are deposited in the group. As glycine is a part of RGD, it is the first step to deposit this. However, there are large steps between depositing a hybrid TTIP/ glycine film and a pure organic film of RGD. Also, there are many ways the three amino acids in RGD may combine, so achieving this is a hard task. Also, if a film was indeed obtained by pulsing arginine/glycine/ aspartic acid, it is next to impossible to know how it is actually bonded. FTIR will be a useful tool, but the exact bonding will still be hard to know, and it may not even be homogeneous throughout the sample.

It should also be questioned whether RPE cells are actually the ones that benefit the most from growing inside 3D membranes. As they naturally occur as monolayers, 3D scaffolds are not likely to be used for this kind of cells. Using RPE cells will of course give a general measure on how cells thrive on the samples, but a cell type that natively stratifies should also be tried on the membranes.

Regarding the cells, in this study only the number of cells adhering to the samples has been studied. Further examinations of the cells may include studying the morphology and differentiation of the cells, especially for the limited lifespan cultures. Fresher cell lines that grow faster and adhere easier should also be tried on the TTIP/lysine substrates. Also, experiments with a higher number of substrates used each time will most likely limit the errors in the experiments.

8. References

1. Greco, Prinz, and Smith, *Nanoscale Technology in Biological Systems*. 2004, Boka Raton, USA: Taylor & Francis.
2. Wigley, *The cell culture laboratory*, in *Basic Cell Culture - A Practical Approach*, Davis, Editor. 2002, Oxford University Press: Oxford, UK.
3. Carrel and Burrows, *Cultivation of adult tissues and organs outside of the body.* The Journal of the American Medical Association, 1910. **55**(16): p. 1379-8.
4. Cartwright and Shah, *Culture media*, in *Basic Cell Culture - A Practical Approach*, Davis, Editor. 2002, Oxford University Press: Oxford, UK.
5. http://www.sigmaaldrich.com/life-science/cell-culture/cell-culture-products.html?TablePage=9628642. 15/9-2014.
6. *Tissue engineering.* Nature Biotechnology, 2000. **18**(10s): p. IT56-IT58.
7. Atala, *Tissue engineering of reproductive tissues and organs.* Fertility and Sterility, 2012. **98**(1): p. 21-29.
8. http://ed.ted.com/lessons/printing-a-human-kidney-anthony-atala. 27/10-14.
9. Maher, *Tissue engineering: How to build a heart.* Nature, 2013. **499**(7456): p. 20-22.
10. Hosseinkhani, Mehrabani, Karimfar, Bakhtiyari, Manafi, and Shirazi, *Tissue Engineered Scaffolds in Regenerative Medicine.* World Journal of Plastic Surgery, 2014. **3**(1): p. 3-7.
11. Lackner and Waldhauser, *Inorganic PVD and CVD Coatings in Medicine - A Review of Protein and Cell Adhesion on Coated Surfaces.* Journal of Adhesion Science and Technology, 2010. **24**(5): p. 925-961.
12. Healy, Rezania, and Stile, *Designing Biomaterials to Direct Biological Responses.* Annals of the New York Academy of Sciences, 1999. **875**: p. 24-35.
13. Li, Zhang, Guo, Dong, Liu, and Mamdouh, *Collagen coated tantalum substrate for cell proliferation.* Colloids and Surfaces B: Biointerfaces, 2012. **95**(1): p. 10-15.
14. Stamova and Pompe, *Structure and function of ECM-inspired composite collagen type I scaffolds.* Soft matter, 2012. **8**: p. 10200–10212.
15. Noiset, Schneider, and Marchand-Brynaert, *Adhesion and growth of CaCo2 cells on surface-modified PEEK substrata.* Journal of Biomaterials Science, Polymer Edition, 2000. **11**(7): p. 767-786.
16. Nojehdehian, Moztarzadeh, Baharvand, Mehrjerdi, Nazarian, and Tahriri, *Effect of poly-L-lysine coating on retinoic acid-loaded PLGA microspheres in the differentiation of carcinoma stem cells into neural cells* International Journal of Artificial Organs, 2010. **33**(10): p. 721-730.
17. http://www.neuvitro.com/index.htm. 20/1-15.
18. Lien, Ko, and Huang, *Effect of pore size on ECM secretion and cell growth in gelatin scaffold for articular cartilage tissue engineering.* Acta Biomaterialia, 2009. **5**(2): p. 670-679.
19. Timpl, Rohde, Risteli, Ott, Robey, and Martin, *Laminin.* Methods in Ezmyology, 1982. **82**: p. 831-838.
20. http://www.stemcell.com/en/Products/All-Products/Vitronectin-XF.aspx. 24/3-15.
21. Eid, Chen, Griffith, and Glowacki, *Effect of RGD coating on osteocompatibility of PLGA-polymer disks in a rat tibial wound.* Journal of Biomedical Materials Research, 2001. **57**(2): p. 224-231.
22. Ruoslahti and Pierschbacher, *Arg-Gly=Asp: A Versatile Cell Recognition Signal* Cell, 1986. **44**: p. 517-518.
23. Elias and Meirelles, *Improving osseointegration of dental implants.* Expert Review of Medical Devices, 2010. **7**(2): p. 241-256.
24. Hong, Azens, Ekdahl, Granqvist, and Nilsson, *Material-specific thrombin generation following contact between metal surfaces and whole blood.* Biomaterials, 2005. **26**(12): p. 1397-1403.
25. Wälivaara, Aronsson, Rodahl, Lausmaa, and Tengvall, *Titanium with different oxides: in V&U studies of protein adsorption and contact activation* Biomaterials, 1994. **15**(10): p. 827–834.

26. Manso, Ogueta, Pérez-Rigueiro, García, and Martínez-Duart, *Testing biomaterials by the in-situ evaluation of cell response.* Biomolecular Engineering, 2002. **19**(2-6): p. 239–242.
27. *hydroxyapatite*, in *Gale Encyclopedia of Medicine*. 2008, The Gale Group, Inc.
28. Paital, Bunce, Nandwana, Honrao, and Nag, *Laser surface modification for synthesis of textured bioactive and biocompatible Ca-P coatings on Ti-6Al-4V.* Journal of Materials Science: Materials in Medicine, 2011. **22**(6): p. 1393-1406.
29. Ji, Ponton, and Marquis, *Microstructural characterization of hydroxyapatite coating on titanium.* Journal of Materials Science: Materials in Medicine, 1992. **3**(4): p. 283-287.
30. Boyd, Meenan, and Leyland, *Surface characterisation of the evolving nature of radio frequency (RF) magnetron sputter deposited calcium phosphate thin films after exposure to physiological solution.* Surface and Coatings Technology, 2006. **200**(20-21): p. 6002-6013.
31. Metikoš-Huković, Tkalacec, Kwokal, Piljac, and Tkalacec, *An in vitro study of Ti and Ti-alloys coated with sol-gel derived hydroxyapatite coatings.* Surface and Coatings Technology, 2003. **165**(1): p. 40-50.
32. Nelea, Iliescu, and Mihailescu, *Hydroxyapatite thin films grown by pulsed laser deposition and radio-frequency magnetron sputtering: Comparative study.* Applied Surface Science, 2004. **228**(1-4): p. 346-356.
33. Shirkhanzadeh, *Bioactive calcium phosphate coatings prepared by electrodeposition.* Journal of Materials Science Letters, 1991. **10**(23): p. 1415-1417.
34. Majewski and Allidi, *Synthesis of hydroxyapatite on titanium coated with organic self-assembled monolayers.* Materials Science and Engineering: A, 2006. **420**(1-2): p. 13-20.
35. Dunn, Aotaki-Keen, Putkey, and Hjelmeland, *ARPE-19, A Human Retinal Pigment Epithelial Cell Line with Differentiated Properties.* Experimental Eye Research, 1996. **62**(2): p. 155–170.
36. Tezcaner, Bugra, and Hasırcı, *Retinal pigment epithelium cell culture on surface modified poly(hydroxybutyrate-co-hydroxyvalerate) thin films.* Biomaterials, 2003. **24**(25): p. 4573–4583.
37. Lu, Garcia, and Mikos, *Retinal pigment epithelium cell culture on thin biodegradable poly(DL-lactic-co-glycolic acid) films.* Journal of Biomaterials Science, Polymer Edition, 1998. **9**(11): p. 1187-1205.
38. Thomson, Giordano, Collier, Ishaug, Mikos, Lahiri-Munir, and Garcia, *Manufacture and characterization of poly(α-hydroxy ester) thin films as temporary substrates for retinal pigment epithelium cells.* Biomaterials, 1996. **17**(3): p. 321–327.
39. Lu, Nyalakonda, Kam, Bizios, Göpferich, and Mikos, *Retinal pigment epithelial cell adhesion on novel micropatterned surfaces fabricated from synthetic biodegradable polymers.* Biomaterials, 2001. **22**(3): p. 291–297.
40. Lu, Yaszemski, and Mikos, *Retinal pigment epithelium engineering using synthetic biodegradable polymers.* Biomaterials, 2001. **22**(24): p. 3345–3355.
41. Lu, Kam, Hasenbein, Nyalakonda, Bizios, Göpferich, Antonios, and Mikos, *Retinal pigment epithelial cell function on substrates with chemically micropatterned surfaces.* Biomaterials, 1999. **20**(23-24): p. 2351–2361.
42. Wagner, Benson, Rennie, and MacNeil, *Effects of pharmacological modulation of intracellular signalling systems on retinal pigment epithelial cell attachment to extracellular matrix proteins* Current Eye Research, 1995. **14**(5): p. 373-384.
43. Kubota, Nishida, Yamato, Yang, Kikuchi, Okano, and Tanoa, *Transplantable retinal pigment epithelial cell sheets for tissue engineering.* Biomaterials, 2006. **27**(19): p. 3639–3644.
44. Okano, Yamada, Sakai, and Sakurai, *A novel recovery system for cultured cells using plasma-treated polystyrene dishes grafted with poly(N-isopropylacrylamide).* Journal of Biomedical Materials Research, 1993. **27**(10): p. 1243–1251.
45. http://www.theglobeandmail.com/life/health-and-fitness/health/successful-retina-transplant-sparks-hope/article21270294/. 24/3-15.

46. Hirami, Osakada, Takahashi, Okita, Yamanaka, Ikeda, Yoshimura, and Takahashi, *Generation of retinal cells from mouse and human induced pluripotent stem cells.* Neuroscience letters, 2009. **458**(3): p. 126–131.
47. http://en.wikipedia.org/wiki/Shinya_Yamanaka. 24/3-15.
48. George, *Atomic Layer Deposition: An Overview.* Chemical reviews, 2010. **110**(1): p. 111-113.
49. Puurunen, *Surface chemistry of atomic layer deposition: A case study for the trimethylaluminum/water process.* Journal of Applied Physics, 2005. **97**(12).
50. Kääriänen, Cameron, Kääriänen, and Sherman, *Atomic Layer Deposition; Principles, Characteristics and Nanotechnology Applications*. 2013, Beverly, Massachusetts, USA/ Hoboken, New York, USA: Scrivener Publishing/ Wiley.
51. Yoshimura, Tatsuura, and Sotoyama, *Polymer films formed with monolayer growth steps by molecular layer deposition.* Applied Physics Letters, 1991. **59**(4): p. 482-483.
52. Nilsen and Fjellvåg, *Thin films prepared with gas deposition technique.* World intellectual property organization, 2006(PCT/NO2005/000488).
53. Dameron, Seghete, Burton, Davidson, Cavanagh, Bertrand, and George, *Molecular Layer Deposition of Alucone Polymer Films Using Trimethylaluminum and Ethylene Glycol.* Chemistry of Materials, 2008. **20**(10): p. 3315–3326.
54. Yoon, O'Patchen, Seghete, Cavanagh, and George, *Molecular Layer Deposition of Hybrid Organic-Inorganic Polymer Films using Diethylzinc and Ethylene Glycol†.* Chemical Vapour Deposition, 2009. **15**(4-6): p. 112-121.
55. Nilsen, Klepper, Nielsen, and Fjellvåg, *Deposition of Organic- Inorganic Hybrid Materials by Atomic Layer Deposition.* Emerging ALD Applications I, 2008. **16**(4): p. 3-14.
56. Sundberg and Karppinen, *Organic and inorganic–organic thin film structures by molecular layer deposition: A review.* Beilstein Journal of Nanotechnology, 2014. **2014**(5): p. 1104–1136.
57. Thoresen, *Syntese av porøse filmer av TiO2 med ALD*, in *Department of Chemistry*. 2012, University of Oslo: Oslo, Norway.
58. Abdulagatov, Hall, Sutherland, Lee, Cavanagh, and George, *Molecular Layer Deposition of Titanicone Films using TiCl4 and Ethylene Glycol or Glycerol: Growth and Properties.* Chemistry of Materials, 2012. **24**(15): p. 2854-2863.
59. Nilsen, Haug, Finstad, and Fjellvåg, *Molecular Hybrid Structures by Atomic Layer Deposition – Deposition of Alq3, Znq2 and Tiq4 (q = 8-hydroxyquinoline).* Chemical Vapour Deposition, 2013. **19**(4-6): p. 174-179.
60. Yoon, Han, and Sung, *Fabrication of a new type of organic-inorganic hybrid superlattice films combined with titanium oxide and polydiacetylene.* Nanoscale Research Letters, 2012. **7**(71).
61. Sundberg and Karppinen, *Organic–Inorganic Thin Films from TiCl4 and 4-Aminophenol Precursors: A Model Case of ALD/MLD Hybrid-Material Growth?* European Journal of Inorganic Chemistry, 2014. **2014**(6): p. 968-974.
62. Chen, Li, Wang, Yu, Duan, Chen, Song, Qin, and Knez, *Nanoporous Nitrogen-Doped Titanium Dioxide with Excellent Photocatalytic Activity under Visible Light Irradiation Produced by Molecular Layer Deposition.* Angewandte Chemie International Edition, 2013. **52**(35): p. 9196-9200.
63. Sood, Sundberg, Malm, and Karppinen, *Layer-by-layer deposition of Ti‐4,4′-oxydianiline hybrid thin films.* Applied Surface Science, 2011. **257**(15): p. 6435-6439.
64. Klepper, Nilsen, Hansen, and Fjellvåg, *Atomic layer deposition of organic–inorganic hybrid materials based on saturated linear carboxylic acids.* Dalton Transactions, 2011. **40**(17): p. 4337–4748.
65. Muri, *Syntese av hybridfilmer med TiCl4 og serin med ALD-egenskaper til filmer med aminosyrer og titan*, in *Department of Chemistry*. 2012, University of Oslo: Oslo, Norway.
66. Weiby, *Hybrid films of TiCl4 and lysine*, in *Department of Chemistry*. 2012, University of Oslo: Oslo, Norway.
67. Klepper, *ALD of TiCl4 and glycine, not yet published*. 2014.
68. http://www.sigmaaldrich.com/catalog/product/fluka/89545?lang=en&region=NO. 3/3-15.

69. Ritala, Leskelä, Niinistö, and Haussalo, *Titanium Isopropoxide as a Precursor in Atomic Layer Epitaxy of Titanium Dioxide Thin Films* Chemistry of Materials, 1993. **5**(8): p. 1174-1181.
70. Lee, Ryu, Choi, Lee, Im, and Sung, *Rapid Vapor-Phase Fabrication of Organic–Inorganic Hybrid Superlattices with Monolayer Precision.* Journal of the American Chemical Society, 2007. **129**(51): p. 16034–16041.
71. Xie, Jiang, Detavernier, Deduytsche, Meirhaeghe, Ru, Li, and Qu, *Atomic layer deposition of TiO2 from tetrakis-dimethyl-amido titanium or Ti isopropoxide precursors and H2O.* Journal of Applied Physics, 2007. **102**(8).
72 http://www.praxair.com/~/media/North%20America/US/Documents/SDS/Praxair%20TDMAT%20C8H24N4Ti%20Safety%20Data%20Sheet%20SDS%20P6331.pdf. 12/3-15.
73. Roberts, *Sterilization*, in *Basic Cell Culture - A Practical Approach*, Davis, Editor. 2002, Oxford University Press: Oxford, UK.
74. http://www.tuttnauer.com/laboratory-autoclaves?gclid=CjwKEAjwucmoBRDmysGsgbDr5j0SJAAxL9absRw--nXhNaUWguTBN0eJhC8Q_JU3IidfQ2V7rhG_YhoCugjw_wcB. 25/3-15.
75. http://www.crebs.org/dustless-16006-review/. 26/3-15.
76. http://www.ars.usda.gov/News/docs.htm?docid=14605&page=3. 26/3-15.
77. McAteer and Davis, *Basic cell culture technique and the maintenance of cell lines*, in *Basic Cell Culture - A Practical Approach*, Davis, Editor. 2002, Oxford University Press: Oxford, UK.
78. Stathopoulos and Elliott, *Formation of mouse or sheep redblood-cell rosettes by lymphocytes from normal and leukæmic individuals.* The Lancet, 1974. **303**(7858): p. 600–601.
79. Anselme, Ploux, and Ponche, *Cell/ Material Interfaces: Influences of Surface Chemistry and Surface Topography on Cell Adhesion.* Journal of Adhesion Science and Technology, 2010. **24**(5): p. 831-852.
80. Carré and Lacarrière, *How Substrate Properties Control Cell Adhesion. A Physical–Chemical Approach.* Journal of Adhesion Science and Technology, 2010. **24**(5): p. 815–830.
81. García, *Get a grip: integrins in cell–biomaterial interactions.* Biomaterials, 2005. **26**(36): p. 7525–7529.
82. Burridge, Fath, Kelly, Nuckolls, and Turner, *FOCAL ADHESIONS: Transmembrane Junctions Between the Extracellular Matrix and the Cytoskeleton* Annual Review of Cell and Developmental Biology, 1988. **1988**(4): p. 487-525.
83. Askari, Tynan, Webb, Martin-Fernandez, Ballestrem, and Humphries, *Focal adhesions are sites of integrin extension.* The Journal of Cell Biology, 2010. **188**(6): p. 891-903.
84. Bigerellea, Anselmec, Noëlc, Rudermana, Hardouinc, and Iosta, *Improvement in the morphology of Ti-based surfaces: a new process to increase in vitro human osteoblast response.* Biomaterials, 2002. **23**(7): p. 1563–1577.
85. MacDonald, *Primary culture and the establishment of cell lines*, in *Basic Cell Culture - A practical Approach*, Davis, Editor. 2002, Oxford University Press: Oxford, UK.
86. Brooker, Widmaier, Graham, and Stiling, *Biology*. Second Edition ed. 2011, New York, USA: McGraw-Hill.
87. http://www.nnds.no/down-syndrom/info-down-syndrom/. 26/3-15.
88. O'Neill and Hsie, *Phenotypic expression time of mutagen-induced 6-thioguanine resistance in Chinese hamster ovary cells (CHO/HGPRT system).* Mutation Research/Fundamental and Molecular Mechanisms of Mutagenesis, 1979. **59**(1): p. 109-118.
89. Dobbie and Zicha, *Microscopy of living cells*, in *Basic Cell Culture - A Practical Approach*, Davis, Editor. 2002, Oxford University Press: Oxford, UK.
90. http://www.nobelprize.org/nobel_prizes/chemistry/laureates/2014/. 16/4-15.
91. Mao and Mullins, *Conjugation of Fluorochromes to Antibodies*, in *Immunocytochemical Methods and Protocols*, Oliver and Jamur, Editors. 2010, Humana Press: New York City, US.
92. http://flowbook.denovosoftware.com/index.php?title=Flow_Book/Chapter_3:_Fluorescence_%26_Fluorochromes. 16/4-15.

93. Sauerbrey, *Verwendung von Schwingquarzen zur Wägung dünner Schichten und zur Mikrowägung.* Zeitschrift für Physik, 1959. **155**(2): p. 206-222.
94. Pavia, Lampman, Kriz, and Vyvyan, *Introduction to Spectroscopy*. Fourth edition ed. 2009, Belmont, California, USA: Brooks/ Cole.
95. Griffiths and Haseth, *Fourier Transform Infrared Spectroscopy*. 2007, Hoboken, New Jersey, USA: Wiley.
96. Albergotti, *Fourier Transform Spectroscopy Using a Michelson Interferometer.* American Journal of Physics, 1972. **40**: p. 1070-1078.
97. http://commons.wikimedia.org/wiki/Category:Michelson_interferometer#mediaviewer/File:FTIR_Interferometer.png. 12/2-15.
98. Bragg and Bragg, *The Reflection of X-rays by Crystals.* Royal Society of London Proceedings A, 1913. **88**(605): p. 428-38.
99. http://commons.wikimedia.org/wiki/File:BraggPlaneDiffraction.svg. 17/2-15.
100. http://ia.physik.rwth-aachen.de/methods/xray/www-xray-eng.pdf. 26/2-15.
101. Kiessing, *Interferenz von Röntgenstrahlen an dünnen Schichten.* Annalen der Physik, 1931. **402**(7): p. 769-788.
102. Tompkins and McGahan, *Spectroscopic Ellipsometry and Reflectometry: A User's Guide*. 1999, Hoboken, New Jersey, USA: Wiley.
103. https://commons.wikimedia.org/wiki/File:Pear_interaction_SEM_english.svg. 24/5-15.
104. Klepper, *Deposition of organic-inorganic hybrid materials by atomic layer deposition*, in *Department of Chemistry, Centre for Materials Science and Nanotechnology*. 2011, University of Oslo: Oslo, Norway.
105. Silverstein, Webster, and Kiemle, *Spectrometric Identification of Organic Compounds*. Seventh edition ed. 2005, Hoboken, New Jersey, USA: Wiley.
106. Shurvell, *Sample Characterisation and Spectral Data Processing*, in *Handbook of Vibrational Spectroscopy*, Chalmers and Griffiths, Editors. 2002, Wiley: Chichester, UK.
107. Siebert, *Anwendung der Schwingungsspektroskopie in der Anorganishen Chemie*. Third edition ed. 1966, Berlin, Germany: Spring Verlag.
108. Fjellvåg, *Noice from the GIXRD Instrument*, Kvalvik, Editor. 2015.
109. http://www.sigmaaldrich.com/spectra/ftir/FTIR001809.PDF. 26/5-15.
110. Klepper, Nilsen, Francis, and Fjellvåg, *Guidance of growth mode and structural character in organic–inorganic hybrid materials – a comparative study.* Dalton Transactions, 2014. **43**(9): p. 3492-3500.
111. https://commons.wikimedia.org/wiki/File:Glutaric_acid.png. 22/5-15.
112. Verpoort, Haemers, Roose, and Maes, *Characterization of a Surface Coating formed from Carboxylic Acid-Based Coolants.* Applied Spectroscopy, 1999. **53**(12): p. 1528-1534.
113. http://www.filmetrics.com/refractive-index-database/TiO2+-+Amorphous/Titanium-Dioxide. 22/5-15.
114. Rahtu and Ritala, *Reaction Mechanism Studies on Titanium Isopropoxide–Water Atomic Layer Deposition Process.* Chemical Vapour Deposition, 2002. **8**(1): p. 21-28.
115. Louison, *Kontroll av overflatefukting gjennom strukturering og kjemisk modifisering av overflater*, in *Department of Chemistry*. 2015, University of Oslo: Oslo, Norway.
116. Grosås, *Hybrid ALD with TMA and cyanoric acid/ melamin*. 2015, University of Oslo.
117. http://www.sigmaaldrich.com/catalog/product/sigma/l5501?lang=en&region=NO. 26/5-15.
118. Verdier, Coutand, Bertron, and Roques, *Antibacterial Activity of TiO2 Photocatalyst Alone or in Coatings on E. coli: The Influence of Methodological Aspects.* Coatings, 2014. **2014**(4): p. 670-686.
119. http://www.tyndall.ie/users/simonelliott. 22/5-15.
120. Goldstein, McCormick, and George, *Al2O3 Atomic Layer Deposition with Trimethylaluminum and Ozone Studied by in Situ Transmission FTIR Spectroscopy and Quadrupole Mass Spectrometry.* Journal of Physical Chemistry, 2008. **112**(49): p. 19530–19539.

9. Appendix

9.1 Appendix A – HSE data

In this appendix SJAs (safe job analysis) for handling the chemicals used in this thesis are shown. Cells are excludes from this list, as the handling of cell cultures is well described in chapters 2.1 and 3.3.

Chemical to be handled	Potential hazard	Precautions	Recommended first aid and fire-fighting response
TTIP	Flammable liquid and vapor, may be fatal in contact with skin, toxic to inhale, serious eye irritant, may cause damages on the central nervous system	Work in fume hood, keep away from open flames, goggles, lab coat and gloves must be used, eye wash bottles should be nearby	Move to fresh air after inhalation, eyes must be flushed after contact, skin must be flushed with water and rinsed with soap after contact, medical attention must be seeked if any contact with substance All extinguishing media are suitable, but vapors may form explosive mixtures with air
Lysine	Harmless	-	-
Methanol	Flammable, toxic to inhale, swallow and absorbs through the skin, eye irritant, may harm the unborn child	Work in fume hood, keep away from open flames, goggles, lab coat and gloves must be used, eye wash bottles should be nearby, must not be handled by pregnant women	Move to fresh air after inhalation, eyes or skin must be flushed after contact, medical attention must be seeked if contact with the eye or ingestion, never give anything by mouth after ingestion All extinguishing media are suitable, but the flame may be invisible during the day
Trypsin-EDTA	Toxic to inhale and swallow, eye irritant, skin irritant, mutagenic	Goggles, lab coat and gloves should be used, eye wash bottles should be nearby	Move to fresh air after inhalation, eyes or skin must be flushed after

			contact, medical attention must be seeked if contact with the eye or ingestion
PI	Toxicity not fully evaluated, but may be irritating to the eye, skin and harmful to inhale	Goggles, lab coat and gloves should be used, eye wash bottles should be nearby	Move to fresh air after inhalation, eyes or skin should be flushed after contact, medical attention must be seeked if contact with the eye or ingestion

9.2 Appendix B – QCM calibration

In this appendix the raw data from the XRR measurement used for the QCM calibration is shown.